Nodal Staging in Head and Neck Squamous Cell Carcinoma by Combining Different Imaging Techniques

Petra K. de Koekkoek-Doll

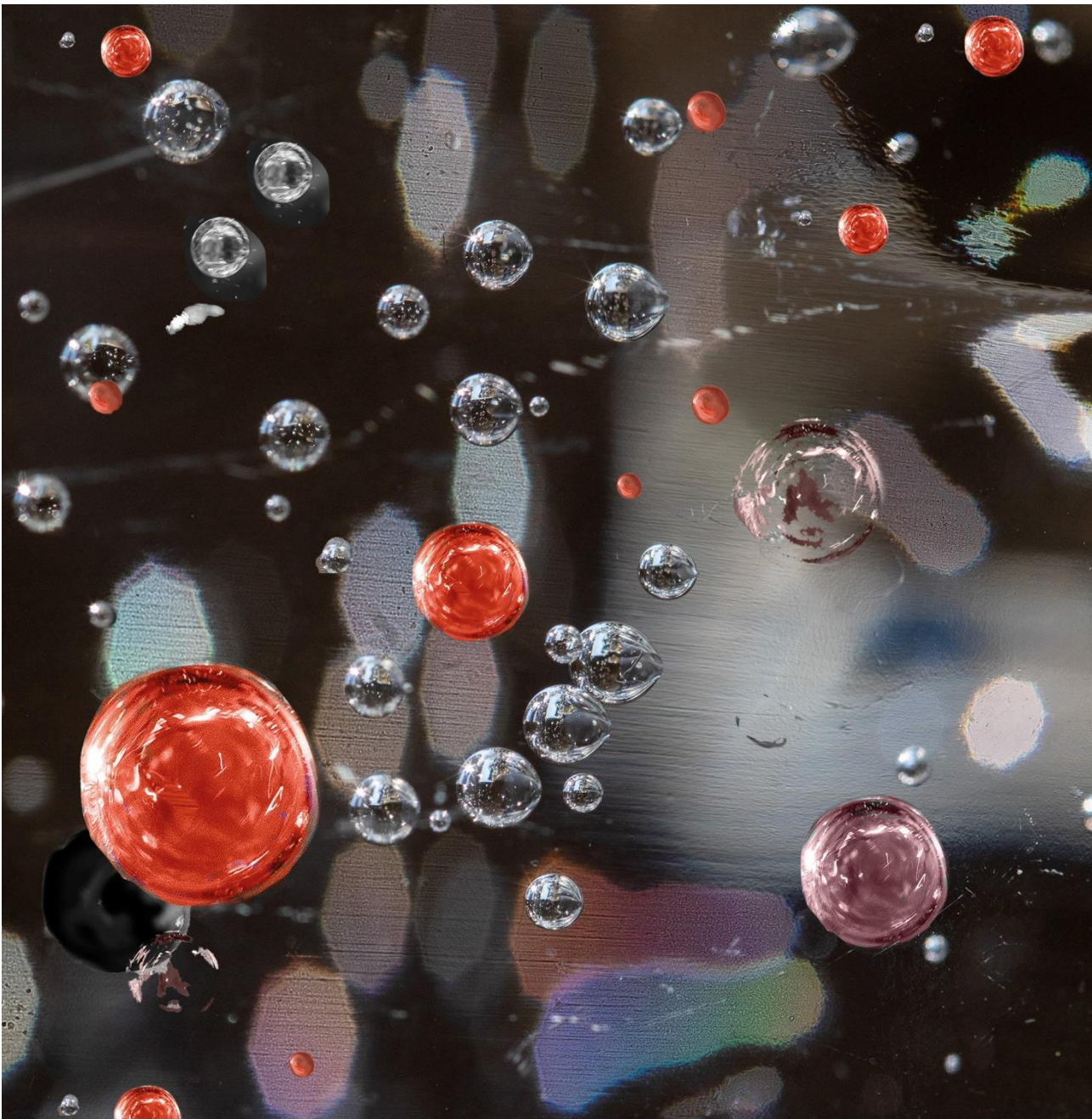

Nodal Staging in Head and Neck Squamous Cell Carcinoma by Combining Different Imaging Techniques

Petra K. de Koekkoek-Doll

The research in this thesis was performed in the Netherlands Cancer Institute, Amsterdam, Department of Radiology

The author would like to acknowledge Pedro Sanches, PhD and Frans Gleuwink (Philips Benelux, Boschdijk 525, 5621JG Eindhoven) for providing knowledge and training on Percunav image fusion (MR, CT, PET and gratefully acknowledges the financial support provided by the Netherlands Cancer Institute, Department of Radiology

The publication of this thesis was financially supported by the Netherlands Cancer Institute and the Maastricht University

Nodal Staging in Head and Neck Squamous Cell Carcinoma by Combining Different Imaging Techniques

ISBN-978-94-6458-967-2

Art work Cover design and lay out: Petra K. de Koekkoek-Doll
Printing: Ridderprint; www.ridderprind.nl

Nodal Staging in Head and Neck Squamous Cell Carcinoma by Combining Different Imaging Techniques

PROEFSCHRIFT

ter verkrijging van de graad van doctor

aan de Universiteit van Maastricht

op gezag van de Rector Magnificus

Prof. dr. Pamela Habibović

Volgens het besluit van het College van Decanen

in het openbare te verdedigen

Op maandag 3 april 2023 om 16.00 uur

door

Petra Katharina de Koekkoek-Doll

Geboren 28 december 1960 te Breitenwang, Oostenrijk

Promotores:
Prof. dr. R. G.H. Beets-Tan
Prof. dr. J. A. Castelijns, Vrije Universiteit Amsterdam
Prof. dr. M. W. van den Brekel, Universiteit van Amsterdam

Beoordelingscommissie:

Prof. dr. Bernd Kremer, voorzitter
Dr. Pim de Graaf, Amsterdam Universitair Medisch Centrum
Dr. Frank Hoebers
Prof. dr. Aad van der Lugt, Erasmus MC Rotterdam
Prof. dr. Axel Zur Hausen

Voor mijn geliefde mama en papa

Contents

Abbreviations

HNC = head and neck cancer
HNSCC = head and neck squamous cell carcinoma
N-stage = nodal stage
N-staging = Nodal staging
N0 = Node negative neck
FNAC = Fine needle aspiration cytology
US= ultrasound
USgFNAC = Ultrasound guided fine needle aspiration cytology
Fused-USgFNAC= Real time fused image guided fine needle aspiration cytology
SNB = Sentinel node biopsy
ND = Neck dissection
END = Elective neck dissection
SND = Selective neck dissection
CT = Computed tomography
PET = positron emission tomography
18-F FDG = ^{18}F-fluordeoxyglucose
SUV = standardized uptake value
SUVmax = maximal standardized uptake value
MRI = Magnetic resonance imaging
DWI = Diffusion weighted imaging
ADC = Apparent diffusion coefficient
DW-MRI = diffusion weighted magnetic resonance imaging
PDI = Power Doppler imaging
PDUS = Power Doppler ultrasound
MFI = Micro flow imaging
RT = Radio therapy
CRT = chemo-radiation therapy

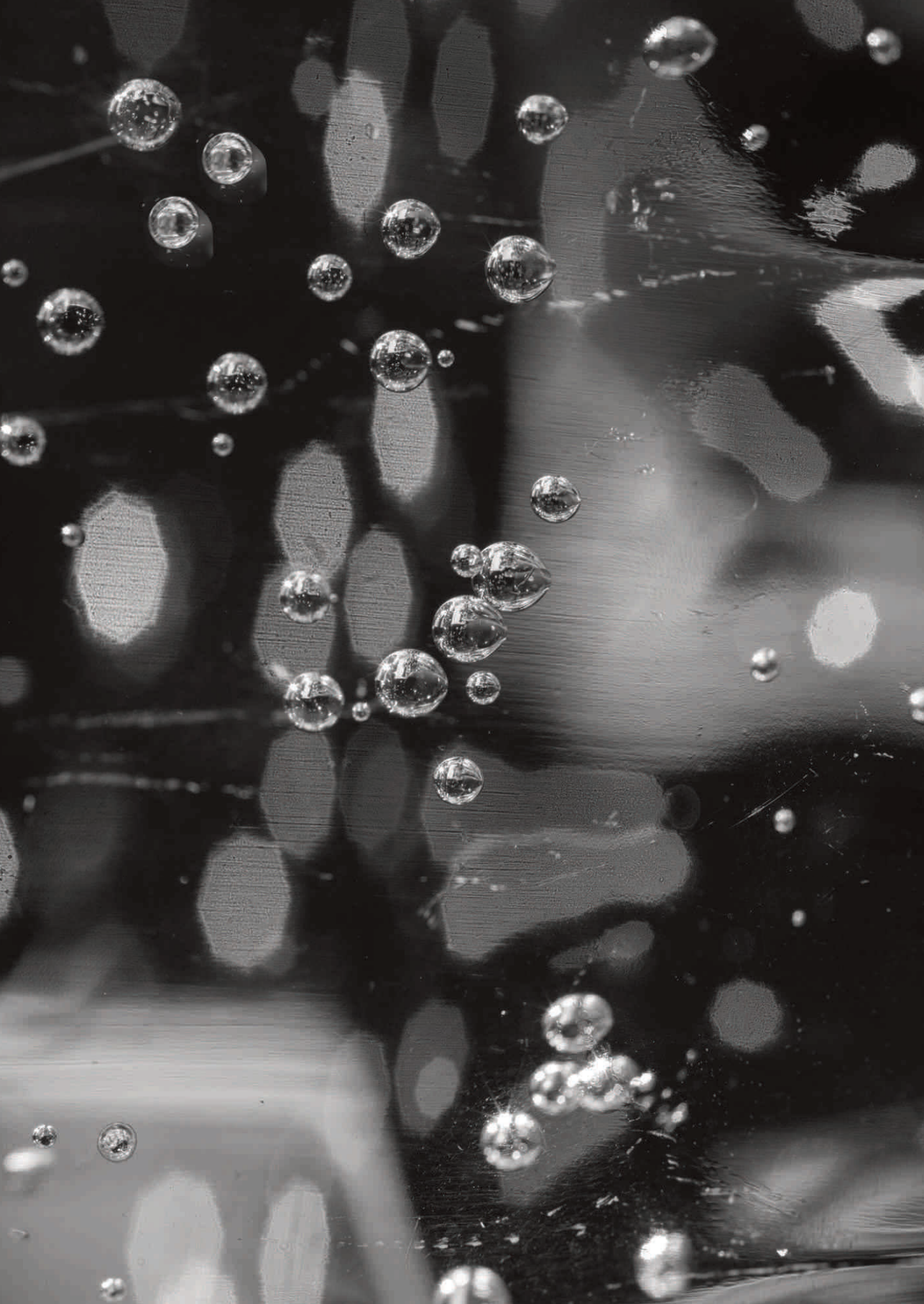

CHAPTER 1

General introduction and outline of the thesis

General Introduction

Squamous cell carcinoma (SCC) of the mucosal linings of the head and neck (HN) globally is the seventh most common malignancy and accounts for around 4% of all malignancies. [1] [2] [3] The presence of cervical lymph node metastases will reduce expected survival with approximately 50% [4]. Therefore it is, next to tumor volume, one of the most important predictors for survival. [5]

Managing of HNSCC often includes neck dissection (ND), radiotherapy (RT) or chemo-radiation therapy (CRT). ND and RT might well have a high impact of neck functionality. To provide an optimal personalized treatment with minimized treatment morbidity accurate cervical nodal staging (N-staging) is most important. [6] [7]

The neck is divided into neck levels which are used to describe the position of the nodes. (Fig.1)

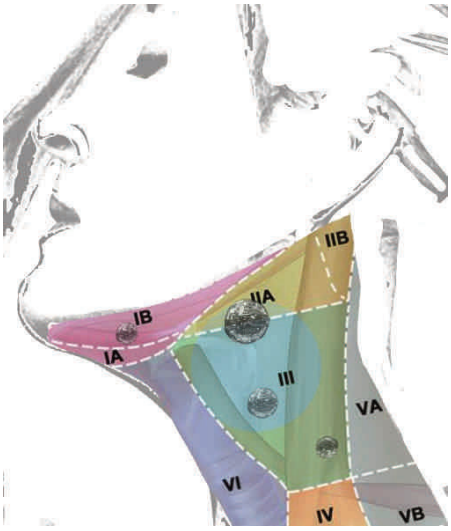

Figure 1: lymph node levels in head and neck

This figure demonstrates the levels of the neck which are used to describe the position of the lymph nodes at palpation or imaging

Depending on the location of the primary tumor, metastatic spread can be expected in the first “nodes at risk” in corresponding drainage levels. Knowledge about neck level involvement will lead to precise treatment planning with either

selective neck dissection (SND) of involved levels only or level based radiation therapy planning.

N-staging of HNSSC refers to assessment of the lymph node metastases for primary HNSSC. N-Staging is categorized by location, number, lateralization, size, presence of extra nodal extension (ENE) and is different for human papilloma virus related HNSCC (HPV-related).

Regional node metastases can be evaluated clinically (cN) or pathologically (pN). cN-staging includes information about palpation of the neck, imaging and fine needle aspiration and pN-Staging about histopathological results of neck dissection (ND).

Exact N-staging is essential for predicting survival and individualized treatment planning which is a balancing act between sufficient radical treatment and preservation of functional structures. If the probability of occult metastases is less than 20% watchful-waiting policy instead of elective neck dissection can be considered [8], although there is a tendency to perform elective neck treatment or Sentinel node biopsy also in these cases.

Next to physical examination, imaging plays a crucial role in assessing tumor volume and lymph node metastases.[9][10]
Palpation of the neck for lymph nodes has an overall sensitivity of around 60-70%. [11] That means that around 30-40% of lymph node metastases are at palpation clinically occult (cN0).

To detect these palpatory occult metastases Ultrasound (guided-fine-needle-aspiration-cytology) (US(gFNAC), computed tomography (CT), magnetic resonance imaging (MRI) and ^{18}F-fluordeoxyglucose (FDG) positron emission tomography(PET)-CT are widely used for neck nodal staging.

Imaging can be divided in anatomical and functional imaging.

Anatomical imaging:

Mean anatomical criteria's to determinate the presence of malignancy in lymph nodes are size, shape, fatty hilum sign, central necrosis and extra nodal spread. Anatomical modalities using these criteria are CT ,MRI and US.

Functional and molecular imaging:

Molecular imaging techniques such as PET , using different tracers, and functional imaging such as perfusion and diffusion weighted (DW)-MRI techniques enable detection of metabolic alterations or specific protein expressions and tumor micro vascularization and cellularity and are therefore important modalities for oncological imaging. With Doppler sonography and micro-flow imaging (MFI) vascularization can be detected.

CT and conventional MRI: Although resolution of conventional MRI and CT has increased, it remains challenging to differentiate between reactive and metastatic lymph nodes. Apart from nodal size and shape criteria, irregular enhancement patterns, based on differences in vascularization and necrosis, play a major role. Unfortunately, these criteria are only useful in case of larger metastases (i.e. > 5mm), and do not the frequently occur small metastases. Consequently, both imaging techniques have a moderate sensitivity (74-78%) and specificity (76-80%). [12]

Positron emission tomography: PET is a very sensitive functional imaging technique to assess metabolism in oncology [13]. Different radioactive tracers are used to measure changes in the metabolic process. Flourodeoxyglucose (F18, 18-F FDG or FDG) is an important tracer used in oncological imaging. The FDG uptake by the tissue is a marker of glucose uptake which is closely correlated to the tissue metabolic. PET enables imaging of several metabolic processes. It is an important diagnostic modality but also important assessor for risk prediction and to monitor therapy response and to detect tumor recurrence. In head and neck cancer FDG PET-CT is an important imaging tool to assess the primary tumor and nodal staging.[14] PET has a significantly higher accuracy in node-staging than MRI and CT [15] with a pooled sensitivity and specificity to detect metastatic lymph nodes in the neck of 84% and 96%, respectively. [16] Nevertheless in patients with cT1-T2N0 oral cavity SCC sensitivity drops to 50-58%. [17] [18] Reactive nodes are difficult to distinguish from small metastatic nodes. To distinguish between reactive and malignant nodes selection of nodes with low cut of SUVmax values is necessary but it will result in a low specificity with a high rate of unnecessary punctures.[19]

Diffusion weighted MR imaging: DW-MRI or DWI is a method of signal contrast generation based on the differences in Brownian motion of water protons in biological tissue. Brownian motion is the random motion of particles in a medium

(liquid or gas). In tissue with a higher cellularity, such as tumor, random motion will be restricted. By performing DWI using different b values quantitative analyses by apparent diffusion coefficient (ADC) map are possible. This analysis is usually performed automatically. In neuroradiology DW imaging is most important and in stroke imaging it is the modality of choice. [20] In oncological imaging it is an important imaging tool and widely used. [21][22][23] In head and neck radiology DW-MR imaging has an increasing importance in diagnostic imaging, predicting and monitoring of therapy and detecting of tumor recurrence. [24] It has been shown that DW-MR imaging had a better diagnostic performance to detect lymph node metastases in HNSCC than turbo spin-echo MRI with a higher sensitivity (76% vs 7%) but a slightly lower specificity (94% vs 99.5%) in detecting sub-centimeter nodal metastases.[25]

As the sum of tumor cell growth is associated with the glucose metabolism an inverse correlation between FDG-uptake and ADC-values should be expected. Study results are contra dictionary. Buelbuel et al found a significant association between PET, dynamic contrast enhanced MRI (DCE-MRI) and DWI parameters which indicates a relationship between glucose metabolism, tumor cellularity and vascular permeability in HNSCC. They also found an inverse correlation between SUVmax and ADC but this was statistically not significant. [26] In another study a significant negative correlation between SUVmax and ADC was demonstrated. [27] However, in some other studies no correlation between SUVmax and ADC was found. [28][29]

Assessing pretreatment DWI and FDG-PET in the tumor and largest lymph nodes showed that combining DWI and FDG PET-CT resulted in a better prediction of treatment failure compared to each single parameter assessment separately. [30]

Ultrasound and ultrasound guided fine needle aspiration cytology (USgFNAC):

With high resolution gray scale ultrasound morphological node criteria such as size, nodal boundary and fatty hilum sign, cystic transformation or infiltration of the surrounding tissue might well be detected. [31][32][33] It was shown that tumor positive elective neck dissection contain a high incidence of micro metastases and in 25% of all tumor positive elective neck dissections, only micro metastases smaller than 3 mm were found. [34] UsgFNAC sensitivity is very much dependent on the ultra-sonographer, the selection of lymph nodes to aspirate as well as the

aspiration technique. To obtain a high sensitivity lymph nodes with a minimal diameter of 5mm or more in level 2 and of 4 mm in the rest of the neck should be aspirated [35], which means that a large number of node aspirations is required to obtain a high sensitivity. To avoid unnecessary aspirations and to minimize false-negativity the biggest challenge is to select the right nodes to puncture and to obtain the right sampling within the node. [36]

In previous research, it has been tried to increase the sensitivity of USgFNAC by specifically aspirating the sentinel node. In this technique, after scintigraphy, the SN was aspirated and confirmation of the correct lymph node selection was obtained by measuring radio-activity of the aspirate. [37] [38]

Power Doppler Imaging: Tumors have a higher metabolism, for which oxygen and nutrients are delivered by blood vessels. Tumor vascularization is closely related to tumor grow. Macro-vascular pattern of this angiogenesis can be detected by Power Doppler imaging (PDI). It has been shown that metastatic lymph nodes can have a peripheral vascularization or a mixed hilar and peripheral visualization. [39][40] It also enables assessment of the vascular resistive index (RI) which is reported to be higher in malignant than in benign nodes. [41]

Micro flow Imaging: Micro flow Imaging (MFI) is a new Doppler technology designed to detect slow blood flow signals without using contrast agents. It enables detection of small vessel blood flow with high resolution and low number of artefacts. It has been shown that the sensitivity of MFI to detect tumor vascularity was higher than those of Color Doppler Imaging (CDI) or PDI. [42][43]

Elastography: Elastography is an US imaging technique to assess the elasticity of tissue. Malignant tissue is in common stiffer than normal tissue [44]. Stiff tissue shows less deformation (strain) than soft tissue. There are two types of Elastography Strain Elastography (SE) and Shear wave Elastography (SWE). SE is a qualitative technique using the transducer for tissue palpation and demonstrate the relative stiffness of tissue while SWE uses acoustic radiation force impulses (ARFI) to measure tissue displacement which is a promising technique in the assessment of malignant cervical nodes. [45] [46]

Although new developments in functional US imaging techniques , such DPI and Elastography have slightly increased the accuracy, US guided FNAC still is the standard as it has almost no false positives and specificity is almost 100%. [47]

Image fusion

Real time image fusion and needle navigation: New fusion image technologies with electronic tracking system enable multimodality real time image fusion (MRI, CT or PET-CT) with live ultrasound. [48] The system contains a magnetic field generator, a patient and ultrasound tacker and a needle tracker.

The Percunav solution (Philips Epic 7) has been developed to provide image fusion between real-time US imaging and other imaging modalities such as MRI, CT or PET-CT.
It also allows real-time tracking of needle navigation for percutaneous intervention procedures.
Data of MRI, CT or PET-CT are transported into the ultrasound system. Corresponding images of MRI, CT or PET-CT on one hand and ultrasound on the other hand can be fused in real time. Initial fusion can be performed automatically or manually by anatomically or external makers. After fusion real time US images and corresponding CT,MRI or PET-CT images are arranged side by side and in an overlay in the US monitor and they move synchronically together.

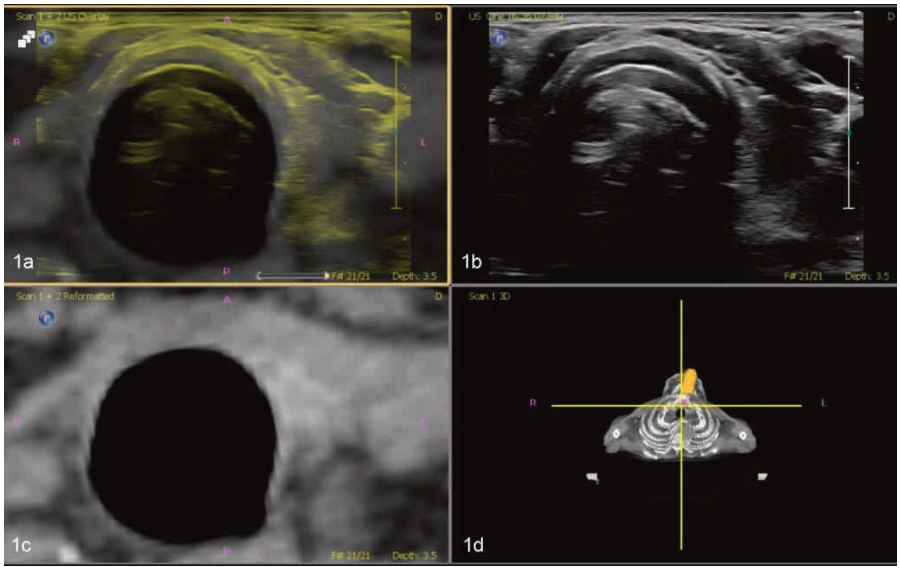

1a: overlay US (yellow) and CT (grey); 1b: US image; 1c: reformatted CT image; 1d: volume representation of CT image and probe location

After initial fusion the integrated target planning tool can be used to mark CT, MRI or PET-CT findings as targets. Real time image fusion helps to detect the location of these marked targets on ultrasound and provides the possibility to indicate the needle route for percutaneous interventional procedures. It appears to be a promising image technique in liver, kidney and pancreatic pathologies. [49]

Until now, research on feasibility of real time image fusion of head and neck lymph nodes are not available. We hypothesize that real time image fusion of ultrasound and PET-CT is feasible and can identify small PET-positive nodes on ultrasound with more confidence and real time image fused guided-FNAC could be performed.

Aim of this thesis

The aim of this thesis was to investigate the use of modern multimodality imaging technologies to optimize the selection of nodes for fine needle aspiration and to improve nodal staging in HNSCC-patients.

The following study questions will be addressed:

1. Is real time imaging fusion of PET-CT and ultrasound feasible?
2. Will real time image fused guided fine needle aspiration improve the detection rate of malignant nodes ?
3. Can we optimize selection criteria for nodes to be punctured?

Outline of this thesis

In the first study, **Chapter 2**, we aimed to evaluate the feasibility of real time image fusion of ultrasound and FDG PET positive lymph nodes of the neck. We aimed to investigate the added value of fine needle aspiration in PET positive neck nodes identified by and guided by real time image fusion.

In Chapter 3 we defined SUVmax cut off values to predict malignancy in real time image fused fine needle aspiration of lymph nodes in HNSCC-patients. Aim of the

study was to improve node selection by defining SUVmax cut off values for nodes to aspirate and to improve the sensitivity of USgFNAC in (borderline) PET-positive neck nodes of HNSCC patients.

In **Chapter 4** we evaluated ADC values in PET-positive nodes compared to PET-negative nodes and we tried to point out if we can find a correlation between ADC values and SUVmax values in benign and malignant PET-positive nodes. Aim was to correlate ADC values of nodes identified on MR-DWI with PET- positive lymph nodes identified on PET-CT and to investigate the possible improvement of predicting malignancy in small lymph nodes by combining both imaging tools.

In **Chapter 5** we investigated the additional value of the new micro-flow imaging technology to visualize peripheral vascularization of neck nodes . Aim of the study was to evaluate the predictive value of malignancy in nodes with present peripheral vascularization compared to morphological features and the value of additional used selection criteria for nodes to puncture.

REFERENCES

1. Singh P, Contente M, Bennett B, Hall J, Bailey H, Bailey A, Zarrelli L, Polanco Sanchez C. Real-World Treatment Patterns and Outcomes in Patients with Head and Neck Cancer: Point-in-Time Survey of Oncologists in Italy and Spain. Adv Ther 2021; 38:4722–4735.

2. Ferlay J, Shin HR, Bray F, Forman D, Mathers C, Parkin DM. Estimates of worldwide burden of cancer in 2008: GLOBOCAN 2008. Int J Cancer 2010; 127:2893–2917.

3. Jemal A, Bray F, Center MM, Ferlay J, Ward E, Forman D. Global cancer statistics. CA Cancer J Clin 2011; 61:69–90.

4. Kelly HR, Curtin HD. Chapter 2 Squamous Cell Carcinoma of the Head and Neck—Imaging Evaluation of Regional Lymph Nodes and Implications for Management. Semin Ultrasound, CT MRI 2017; 38:466–478.

5. Hanahan D, Weinberg RA. The Hallmarks of Cancer Review evolve progressively from normalcy via a series of pre. Cell 2000; 100:.

6. Nieuwenhuis EJC, Castelijns JA, Pijpers R, van den Brekel MWM, Brakenhoff RH, van der Waal I, Snow GB, Leemans CR. Wait-and-see policy for the N0 neck in early-stage oral and oropharyngeal squamous cell carcinoma using ultrasonography-guided cytology: is there a role for identification of the sentinel node? Head Neck 2002; 24:282–9.

7. Al-Mamgani A, Verheij M, van den Brekel MWM. Elective unilateral nodal irradiation in head and neck squamous cell carcinoma: A paradigm shift. Eur J Cancer 2017; 82:1–5.

8. Weiss MH, Harrison LB, Isaacs RS. Use of decision analysis in planning a management strategy for the stage N0 neck. Arch Otolaryngol Head Neck Surg 1994; 120:699–702.

9. Lodder Frank A Pameijer Coen RN Rasch Michiel W M van den Brekel Alfons JM Balm WL. Prognostic signifi cance of radiologically determined neck node volume: a systematic review. Oncology 2012; 48:.

10. Godény M. Prognostic factors in advanced pharyngeal and oral cavity cancer; Significance of multimodality imaging in terms of 7th edition of TNM. Cancer Imaging 2014; 14:1–13.

11. van den Brekel MWM, Castelijns JA. What the clinician wants to know: surgical perspective and ultrasound for lymph node imaging of the neck. Cancer Imaging 2005; 5 Spec No:0–16.

12. Kyzas PA, Evangelou E, Denaxa-Kyza D, Ioannidis JPA. 18F-Fluorodeoxyglucose Positron Emission Tomography to Evaluate Cervical Node Metastases in Patients With Head and Neck Squamous Cell Carcinoma: A Meta-analysis. JNCI J Natl Cancer Inst 2008; 100:712–720.

13. Abrantes AM, Pires AS, Monteiro L, Teixo R, Neves AR, Tavares NT, Marques IA, Botelho MF. Tumour functional imaging by PET. Biochim Biophys Acta - Mol Basis Dis 2020; 1866:165717.

14. Goel R, Moore W, Sumer B, Khan S, Sher D, Subramaniam RM. Clinical Practice in PET/CT for the Management of Head and Neck Squamous Cell Cancer. Am J Roentgenol 2017; 209:289–303.

15. Roh JL, Yeo NK, Kim JS, Lee JH, Cho KJ, Choi SH, Nam SY, Kim SY. Utility of 2-[18F] fluoro-2-deoxy-D-glucose positron emission tomography and positron emission tomography/computed tomography imaging in the preoperative staging of head and neck squamous cell carcinoma. Oral Oncol 2007; 43:887–893.

16. Sun R, Tang X, Yang Y, Zhang C. 18FDG-PET/CT for the detection of regional nodal metastasis in patients with head and neck cancer: A meta-analysis. Oral Oncol 2015; 51:314–320.

17. Kyzas PA, Evangelou E, Denaxa-Kyza D, Ioannidis JPA. 18F-Fluorodeoxyglucose Positron Emission Tomography to Evaluate Cervical Node Metastases in Patients With Head and Neck Squamous Cell Carcinoma: A Meta-analysis. JNCI J Natl Cancer Inst 2008; 100:712–720.

18. Kim SJ, Pak K, Kim K. Diagnostic accuracy of F-18 FDG PET or PET/CT for detection of lymph node metastasis in clinically node negative head and neck cancer patients; A systematic review and meta-analysis. Am J Otolaryngol - Head Neck Med Surg 2019; 40:297–305.

19. Van Den Brekel MWM, Castelijns JA, Snow GB. The Size of Lymph Nodes in the Neck on Sonograms as a Radiologic Criterion for Metastasis: How Reliable Is It? American Journal of Neuroradiology 19(4):695-700

20. Chalela JA, Kidwell CS, Nentwich LM, Luby M, Butman JA, Demchuk AM, Hill MD, Patronas N, Latour L, Warach S. Magnetic resonance imaging and computed tomography in emergency assessment of patients with suspected acute stroke: a prospective comparison. Lancet (London, England) 2007; 369:293–298.

21. van ’t Sant I, van Eden WJ, Engbersen MP, Kok NFM, Woensdregt K, Lambregts DMJ, Shanmuganathan S, Beets-Tan RGH, Aalbers AGJ, Lahaye

MJ. Diffusion-weighted MRI assessment of the peritoneal cancer index before cytoreductive surgery. Br J Surg 2019; 106:491–498.

22. Beets-Tan RGH, Beets GL. MRI for assessing and predicting response to neoadjuvant treatment in rectal cancer. Nat Rev Gastroenterol Hepatol 2014 118 2014; 11:480–488.

23. Messina C, Bignone R, Bruno A, Bruno A, Bruno F, Calandri M, Caruso D, Coppolino P, De Robertis R, Gentili F, Grazzini I, Natella R, Scalise P, Barile A, Grassi R, Albano D. Diffusion-Weighted Imaging in Oncology: An Update. Cancers (Basel) 2020; 12:1–28.

24. Thoeny HC, De Keyzer F, King AD. Diffusion-weighted MR imaging in the head and neck. Radiology 2012; 263:19–32.

25. Vandecaveye V, De Keyzer F, Vander Poorten V, Dirix P, Verbeken E, Nuyts S, Hermans R. Head and neck squamous cell carcinoma: value of diffusion-weighted MR imaging for nodal staging. Radiology 2009; 251:134–146.

26. Bülbül HM, Bülbül O, Sarıoğlu S, Özdoğan Ö, Doğan E, Karabay N. Relationships Between DCE-MRI, DWI, and 18 F-FDG PET/CT Parameters with Tumor Grade and Stage in Patients with Head and Neck Squamous Cell Carcinoma. Mol Imaging Radionucl Ther 2021; 30:177–186.

27. Nakajo M, Nakajo M, Kajiya Y, Tani A, Kamiyama T, Yonekura R, Fukukura Y, Matsuzaki T, Nishimoto K, Nomoto M, Koriyama C. FDG PET/CT and diffusion-weighted imaging of head and neck squamous cell carcinoma: Comparison of prognostic significance between primary tumor standardized uptake value and apparent diffusion coefficient. Clin Nucl Med 2012; 37:475–480.

28. Zhang L, Song T, Meng Z, Huang C, Chen X, Lu J, Xian J. Correlation between apparent diffusion coefficients and metabolic parameters in hypopharyngeal squamous cell carcinoma: A prospective study with integrated PET/MRI. Eur J Radiol 2020; 129:109070.

29. Fruehwald-Pallamar J, Czerny C, Mayerhoefer ME, Halpern BS, Eder-Czembirek C, Brunner M, Schuetz M, Weber M, Fruehwald L, Herneth AM. Functional imaging in head and neck squamous cell carcinoma: correlation of PET/CT and diffusion-weighted imaging at 3 Tesla. Eur J Nucl Med Mol Imaging 2011; 38:1009–1019.

30. Martens RM, Noij DP, Koopman T, Zwezerijnen B, Heymans M, de Jong MC, Hoekstra OS, Vergeer MR, de Bree R, Leemans CR, de Graaf P, Boellaard R, Castelijns JA. Predictive value of quantitative diffusion-weighted imaging

and 18-F-FDG-PET in head and neck squamous cell carcinoma treated by (chemo)radiotherapy. Eur J Radiol 2019; 113:39–50.

31. Ahuja AT, Ying M, Ho SY, Antonio G, Lee YP, King AD, Wong KT. Ultrasound of malignant cervical lymph nodes. Cancer Imaging 2008; 8:48–56.

32. Khanna R, Sharma AD, Khanna S, Kumar M, Shukla RC. Usefulness of ultrasonography for the evaluation of cervical lymphadenopathy. World J Surg Oncol 2011; 9:29.

33. Hohlweg-Majert B, Metzger MC, Voss PJ, Hölzle F, Wolff K-D, Schulze D. Preoperative cervical lymph node size evaluation in patients with malignant head/neck tumors: comparison between ultrasound and computer tomography. J Cancer Res Clin Oncol 2009; 135:753–759.

34. van den Brekel MW, van der Waal I, Meijer CJ, Freeman JL, Castelijns JA, Snow GB. The incidence of micrometastases in neck dissection specimens obtained from elective neck dissections. Laryngoscope 1996; 106:987–91.

35. Van den Brekel MW, Leemans CR, Snow GB. Assessment and management of lymph node metastases in the neck in head and neck cancer patients. Crit Rev Oncol Hematol 1996; 22:175–82.

36. Borgemeester MC, van den Brekel MWM, van Tinteren H, Smeele LE, Pameijer FA, van Velthuysen M-LF, Balm AJM. Ultrasound-guided aspiration cytology for the assessment of the clinically N0 neck: Factors influencing its accuracy. Head Neck 2008; 30:1505–1513.

37. Colnot DR, Nieuwenhuis EJC, Van den Brekel MWM, Pijpers R, Brakenhoff RH, Snow GB, Castelijns JA. Head and neck squamous cell carcinoma: Us-guided fine-needle aspiration of sentinel lymph nodes for improved staging - Initial experience. Radiology 2001; 218:289–293.

38. Nieuwenhuis EJC, Castelijns JA, Pijpers R, Van Den Brekel MWM, Brakenhoff RH, Van Der Waal I, Snow GB, Leemans CR. Wait-and-SEE Policy for the N0 Neck in Early-Stage Oral and Oropharyngeal Squamous Cell Carcinoma Using Ultrasonography-Guided Cytology: Is there a Role for Identification of the Sentinel Node? Head Neck 24 282-289, 2002; .

39. Marouzi; MIMDMLMA, Davachi B, Mostaan LV, Langaroodi AJ, Memar B, Azimi SA, Marouzi P. Evaluation of the Sonographic Features of Metastatic Cervical Lymph Nodes in Patients With Head and Neck Malignancy. J Craniofac Surg 2011; 22:2179–2184.

40. Gupta A, Rahman K, Shahid M, Kumar A, Qaseem SMD, Hassan SA, Siddiqui FA. Sonographic assessment of cervical lymphadenopathy: Role of high-

resolution and color Doppler imaging. Head Neck 2010; 33:n/a-n/a.

41. JD M, A L, JW O. Contrast-enhanced color Doppler sonography for evaluation of enlarged cervical lymph nodes in head and neck tumors. AJR Am J Roentgenol 2000; 174:1279–1284.

42. Bae JS, Lee JM, Jeon SK, Jang S. Comparison of MicroFlow Imaging with color and power Doppler imaging for detecting and characterizing blood flow signals in hepatocellular carcinoma. Ultrasonography 2020; 39:.

43. Bartolotta TV, Orlando AAM, Schillaci MI, Spatafora L, Marco M Di, Matranga D, Firenze A, Cirino A, Ienzi R. Ultrasonographic Detection of Vascularity of Focal Breast Lesions: Microvascular Imaging Versus Conventional Color and Power Doppler Imaging. Ultrason Imaging 2021; 43:273–281.

44. Barr RG. Elastography in Clinical Practice. Radiol Clin North Am 2014; 52:1145–1162.

45. Suh CH, Choi YJ, Baek JH, Lee JH. The diagnostic performance of shear wave elastography for malignant cervical lymph nodes: A systematic review and meta-analysis. Eur Radiol 2017; 27:222–230.

46. Wang B, Guo Q, Wang JY, Yu Y, Yi AJ, Cui XW, Dietrich CF. Ultrasound Elastography for the Evaluation of Lymph Nodes. Front Oncol 2021; 11:3133.

47. Souren C, Kloss-Brandstätter A, Stadler A, Kross K, Yamauchi K, Ketelsen D, Kessler P, Lethaus B. Ultrasound-guided fine-needle aspiration cytology as a diagnostic tool in comparison to ultrasound and MRI for staging in oral- and oropharyngeal squamous cell tumors. J Cranio-Maxillofacial Surg 2016; 44:197–201.

48. Maybody M, Stevenson C, Solomon SB. Overview of navigation systems in image-guided interventions. Tech Vasc Interv Radiol 2013; 16:136–143.

49. Schwarze V, Rübenthaler J, Marschner C, Fabritius MP, Rueckel J, Fink N, Puhr-Westerheide D, Gresser E, Froelich MF, Schnitzer ML, Hokamp NG, Afat S, Staehler M, Geyer T, Clevert D-A. Advanced Fusion Imaging and Contrast-Enhanced Imaging (CT/MRI-CEUS) in Oncology. Cancers (Basel) 2020; 12:.

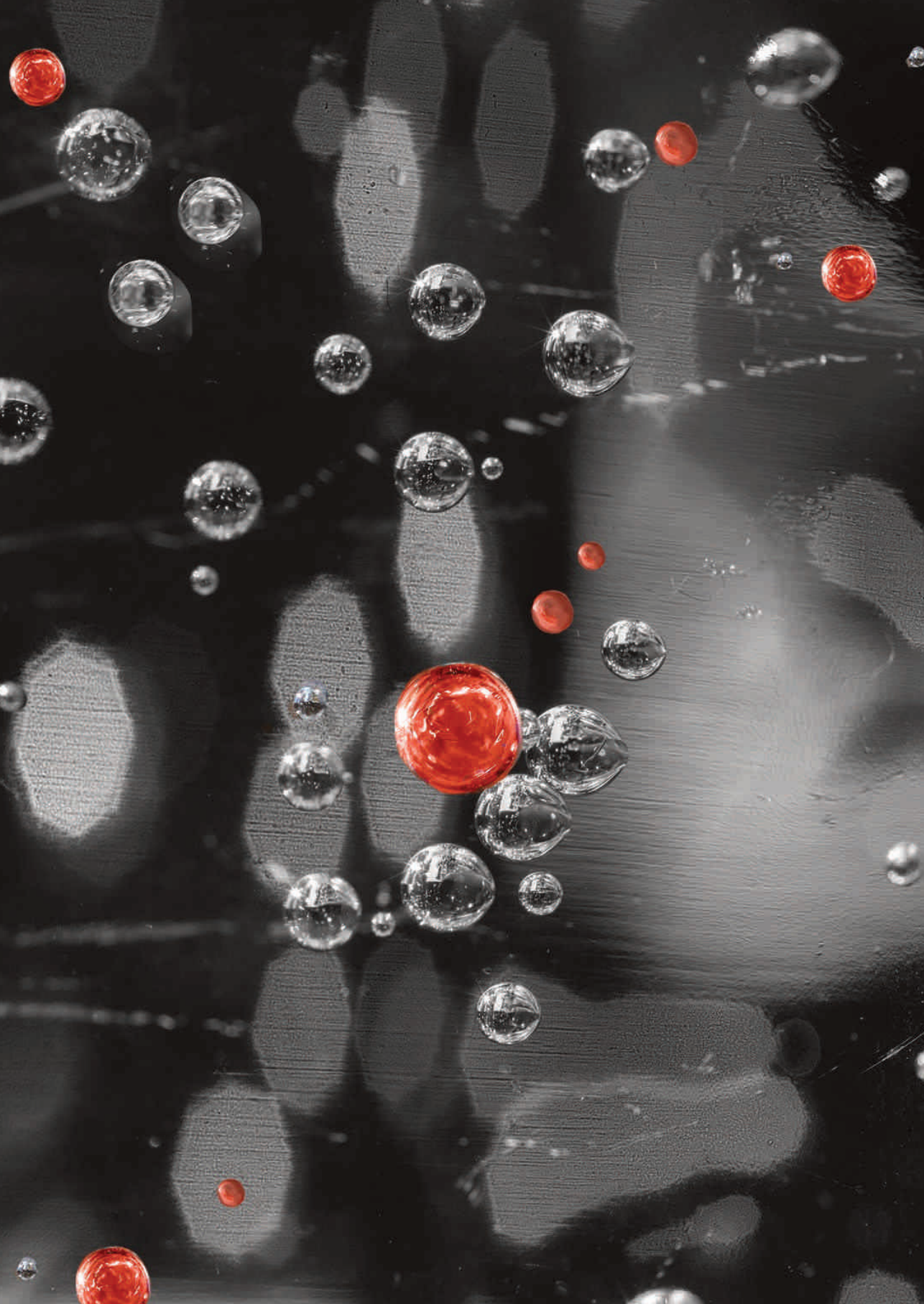

CHAPTER 2

Real-time ultrasound image fusion with FDG PET-CT to perform fused image guided fine needle aspiration in neck nodes: feasibility and diagnostic value

Petra K. de Koekkoek-Doll, Monique Maas, Wouter Vogel, Jonas Castelijns, Laura Smit, MD PhD , Ioannis Zavrakidis, Regina Beets-Tan, Michiel van den Brekel

Published in American Journal of Neuroradiology

Mar 2021; 42:566-72

AJNR http://dx.doi.org/10.3174/ajnr.A6938

Abstract

Background and Purpose: New imaging techniques, such as hybrid imaging of ultrasound and FDG PET-CT, are available but not yet investigated for cervical lymph node staging (N-staging).

The aim of the study is to evaluate the feasibility and added diagnostic value of real-time image fused ultrasound guided fine needle aspiration (Fused-USgFNAC) with FDG PET-CT data for N-staging.

Material and Methods: 96 patients, who were referred for cervical lymph node staging with FDG PET-CT before ultrasound, were prospectively included. After routine USgFNAC all FDG PET-positive nodes were marked on FDG PET-CT and real time image fusing of US and FDG PET-CT was performed using the electromagnetic navigation system Percunav (Philips). Already punctured nodes were confirmed to be PET-positive and additional Fused-USgFNAC was performed in previously missed PET-positive nodes.

Results: Out of 96 patients, 87 (91%) patients had suspicious nodes requiring FNAC. USgFNAC was performed in 175 nodes. Cytology was inconclusive in 9/175 (5%) nodes and 85/166 (51%) nodes were malignant. Target planning was performed in 201 PET-positive nodes. 195/201(97%) of those nodes were fused successfully. 20/175 USgFNAC nodes turned out to be FDG PET-negative and 149/175 (85%) of the Fused-USgFNAC nodes were confirmed to be FDG PET-positive. Out of 201 PET-positive nodes, 46 (23%) were additionally identified and Fused USgFNAC was performed. Cytology was inconclusive in 4/46 nodes (9%) and 13/42 (31%) nodes were malignant.

Conclusion: Real-time US image fusion with FDG PET-positive nodes is feasible in cervical lymph nodes and Fused-USgFNAC increases the number of malignant nodes.

Introduction

TNM stage in head and neck cancer (HNC) is important for prediction of prognosis and stratification of treatment. Besides physical examination, imaging plays a crucial role in defining the TNM stage, assessing tumor volume and nodal involvement.[1,2] Nodal-staging with CT and MRI is limited with a per patient sensitivity ranging from 73-87% for CT and 70-74% for MRI.[3] In clinically node negative neck (cN0) the sensitivity ranges from 14-80 % for CT and from 29-85% for MRI, on average the sensitivity is in the range of 40-60%.[4] Molecular imaging of glucose metabolism with ^{18}F-fluordeoxyglucose positron emission tomography combined with computed tomography (FDG PET-CT) has a higher per-neck-level sensitivity for detection of regional nodal metastases in primary head and neck squamous cell carcinoma (HNSCC) patients, with a sensitivity up to 84% and a specificity up to 96%.[5,6] However for cN0 an overall sensitivity of 21.4% and specificity of 98.4% has been reported.[7] In comparison to sentinel node biopsy (SNB) in cN0 head and neck cancer, MRI and CT are not effective in predicting whether or not prophylactic neck dissection (ND) could be safely avoided and the sensitivity of FDG PET-CT may still not be adequate.[8] In clinical practice ultrasound guided fine needle aspiration (USgFNAC) plays an important role, not only as an upfront imaging technique for the neck but also to determine the diagnosis in equivocal lymph nodes on CT, MRI or FDG PET-CT.[9] Sensitivity of USgFNAC in patients with clinically suspicious nodes (cN+) has been reported to be 88%.[10] but sensitivity drops significantly to 39% in patients with a cN0.[11] Apart from minimizing the chance of sampling errors, selection of the most suspicious nodes that needs aspiration is a major challenge.[12] Selection of nodes by FDG PET-CT SUV might improve selection of the most suspicious nodes for FNAC.

Due to technical improvements it is possible to fuse real time US with cross-sectional imaging techniques such as with PET-CT, CT or MRI.[13] Fusion of US with FDG PET-CT to guide FNAC of nodes can potentially improve the identification and detection of malignant nodes. The aim of our study is firstly to evaluate the feasibility of US real-time fusion with FDG PET-CT data for fused image guidance of fine needle aspiration in suspicious neck nodes and secondly to evaluate if it leads to a more accurate detection of malignant nodes.

Material and Methods

Patient population

We prospectively included 96 patients (Table 1) who were referred for USgFNAC with prior FDG PET-CT and met one of the following criteria: histopathological proven HNC, histologically proven lymph node metastasis with unknown primary or suspicious HN-lesion, not yet proven to be malignant.
After routine ultrasound and USgFNAC, real time fusion of ultrasound and FDG PET-CT took place to confirm PET-positivity of USgFNAC nodes and to perform additional Fused-USgFNAC of missed FDG PET-positive nodes which would change N-stage. This study was approved by the NKI-AVL Institutional Review Board (IRBd20-126). Written informed consent was signed by all patients.
Table 1 shows the diagnosis in number and percentages of all included patients and the number and percentages of HNSCC patients. Table 2 shows an overview of the treatment.

Table 1: Diagnosis of all patients

Diagnose	Number	Percentage
Adeno ca parotid gland	1	1%
Angiosarcoma	1	1%
B-cell lymphoma	1	1%
Lung carcinoma	2	2%
Melanoma	6	6%
Merkel cell carcinoma	2	2%
Rhabdomyosarcoma	1	1%
SCC hypopharyngeal	7	7%
SCC laryngeal	16	17%
SCC nasal cavity sinus	4	4%
SCC nasopharyngeal	1	1%
SCC oral cavity	19	20%
SCC oropharyngeal	25	26%
SCC-skin	1	1%
SCC unknown primary	6	6%
Second branchial cleft	1	1%
Tuberculosis	1	1%
Unknown primary	1	1%
Total	**96**	**100%**

82% of all patients had a SCC.

Table 2: Combination of Treatments of all 96 patients

Treatment		RT	CRT	BRT	PDT	Chemo
Surgery no ND	11	5	1	0	0	0
SND/SNB	20	8	1	0	0	0
No Surgery	63	31	21	6	1	4
No [1] treatment	2	0	0	0	0	0
Total	**96**	44	**23**	**6**	**1**	**4**

RT = radiotherapy, CRT = radio-chemotherapy, BRT = bio-radiotherapy, PDT = photodynamic therapy, Chemo = chemotherapy
ND = neck dissection, SND = selective neck dissection, SNB = sentinel node biopsy

[1] Two patients did not have a tumor treatment because of a benign lesion, Second branchial cleft cyst and Tuberculosis.

FDG PET/CT imaging

For FDG PET/CT images were acquired using a Gemini TF scanner (Philips. Maryland. USA). Patients fasted for 6 hours and were hydrated prior to administration of FDG. Diabetes mellitus needed to be regulated adequately. The plasma glucose level was required to be below 10 mmol/l. A dose of 190-240 MBq was administered depending on body mass index. FDG PET images of the head and neck area were acquired for 3 bed positions of 3 minutes each. They were reconstructed to 2mm isotropic voxels. Low dose CT was acquired for attenuation correction and anatomical orientation with 40 mAs and 2mm slices. In addition, images of the neck-thighs were acquired. All FDG PET/CT images were interpreted by experienced nuclear physicians for clinical staging and this report was available for interpretation of involved nodes in this study.

Ultrasound and FNAC

The FDG PET-CT data were imported into the US device (EpiQ7 G, Philips, Bothell, WA) before the routine procedures. Firstly, routine US evaluation and routine USgFNAC with a 21G needle, without use of FDG PET-CT data, was performed. All USgFNAC were performed by one radiologist (PKD) who has 10 years of USgFNAC experience in HNC. She was aware of the clinical information and available imaging-data including FDG PET-CT before performing the US. FNAC was performed in 1 or 2 neck levels ipsilateral and sometimes contralateral in suspicious nodes in the levels at most risk, corresponding to the site of the primary tumor, as well as in

suspicious nodes at the lowest neck level of each side. Nodes were aspirated a short axis diameter > 1 cm, or <1cm and showed loss of a fatty hilum or showed a thickened or asymmetric cortex or round shape. Also, nodes described in the MRI or FDG PET-CT to be borderline or suspicious were aspirated when identified. Immediately after the routine US and USgFNAC procedures, real-time image fusion of US and FDG PET-CT using the electromagnetic navigation system Percunav (Philips, FDA and CE approved and worldwide available), installed on the same US diagnostic system, took place by the same reader (PKD). US was performed using either a L12-5 or an eL18-4 probe with integrated electromagnetic tracker (both from Philips Medical Systems). During the image fusion steps, a bracket and the respective electromagnetic tracker were added to the L12-5 probe so it could be used with the Percunav system. The Percunav setup was used according to the manufacturer's manual. The patient reference tracker was placed on the forehead of the patient and held in place with tape. The field generator was positioned above the patient neck using a metallic arm. The initial fusion between real-time US and FDG PET-CT was performed by identifying the thyroid on both modalities and using the 'match plane' function on the system (Figure 1).

Figure 1: Match plane fusion

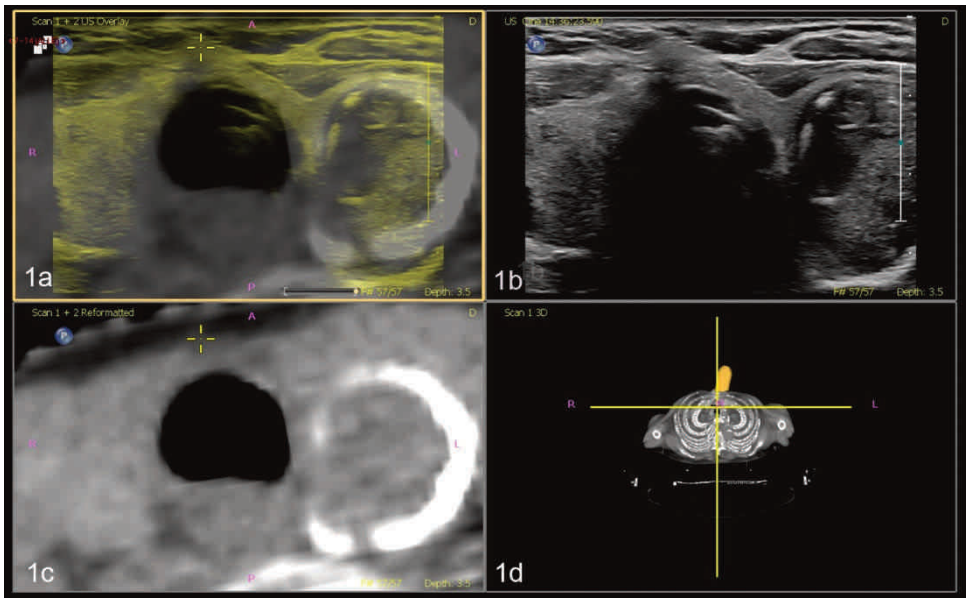

Figure 1 Match plane fusion, manual correction. 1a: overlay US (yellow) and CT (grey); 1b: US image; 1c: reformatted CT image; 1d: volume representation of CT image and probe location.

Additional manual corrections to the fusion were made by identification of known anatomical structures such as the hyoid, submandibular gland, and carotid artery bifurcation. Then a target was created for each FDG PET-CT positive lymph node, using the 'Target Planning' function (including nodes with low risk of malignancy and low SUV values) (Figure 2).

Figure 2: Target planning and real-time fusion of FDG-PET-positive lymph nodes to identify PET-positive nodes.

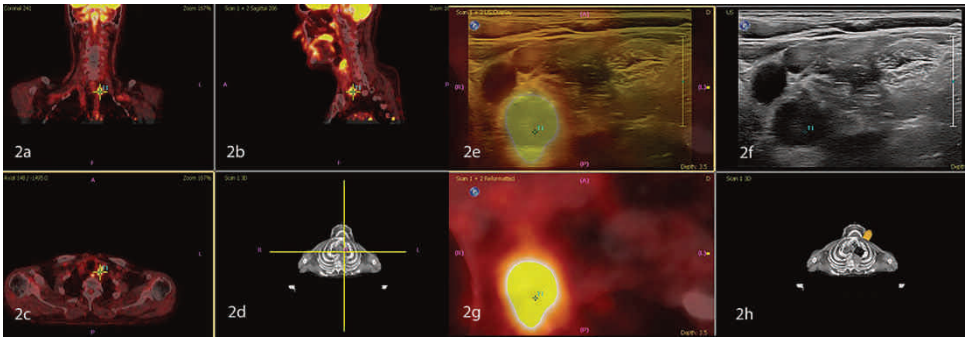

A, Coronal view. B, Sagittal view. C, Axial view. D, Volume representation of FDG-PET/CT image and probe location, PET-positive nodes where targeted, and real-time image fused with ultrasound. E, Overlay US (yellow) and PET/CT (gray). F, US image. G, Reformatted PET/CT image. H, Volume representation of the CT image and probe location. Fusion of PET and CT and target planning took place using the electromagnetic navigation system PercuNav. First, routine ultrasound and routine USgFNAC were performed. Second, ultrasound and FDG-PET-positive nodes were real-time fused. USgFNAC in PET-positive nodes was confirmed, and additional fused-USgFNAC of missed PET-positive nodes was performed

At this time the radiologist identified the on FDG PET-CT targeted nodes and verified if USgFNAC already was performed. (Figure 3). In patients with multiple FDG PET-positive nodes, a selection was made based on level, size and SUV value for fused aspiration. In case the node had not been previously aspirated, Fused-USgFNAC was performed.

Reference standard

Surrogate reference standard was the pathological result of FNAC. As only 19/96 patients underwent ND and 1/96 patients SNB, this series is too small to reliably estimate sensitivity and specificity of USgFNAC, Fused-USgFNAC or FDG PET-CT. If available, histopathology of ND specimen was used as reference standard and pN-stage was compared to pN-stage of USgFNAC and Fused-USgFNAC (Table 3).

Statistical analysis

A two-sample t-test was used to compare the mean size of nodes between USgFNAC and Fused-USgFNAC. Using the mantel-haenszel test the detection rate of malignant nodes in USgFNAC and Fused-USGFNAC was compared. The chi-squared test was used to compare the accuracy of N-stage found with USgFNAC and Fused-USgFNAC in relation to the cytological results.

Results

Nine out of 96 patients (9%), who were selected for the study, did not have any FDG PET-positive nodes nor suspicious nodes on US. In the remaining 87/96 (91%) patients, a total of 221 lymph nodes were aspirated. The median number of aspirated nodes per patient was 2 (1-5).

USgFNAC:
175 out of 221 lymph nodes were aspirated during routine-US, the smallest nodes were 4 mm, the mean minimal axial diameter was 11.7 mm. At USgFNAC 9 out of 175 nodes (5%) were inconclusive at cytology, 85 out of 166 (51%) nodes were malignant.

Fused-USgFNAC:
Target planning was performed in 201 PET-positive nodes. Fusion was technically successful in 195/201 (97%) FDG PET-positive nodes.

149 out of 175 (85%) USgFNAC nodes were confirmed to be FDG PET-positive. Cytology was inconclusive in 9/175 (5%). Out of the remaining 140 confirmed PET-positive nodes, 83 (59%) nodes proved to be malignant. At fusion, 20 of the USgFNAC nodes proved to be FDG PET-negative and only 1 of those nodes was malignant.
Based on fusion, 46/201(23%) FDG PET-positive nodes were additionally identified and Fused-USgFNAC was performed, the smallest nodes were 3 mm, the mean minimal axial diameter was 6.3 mm (range 3-16 mm) which was significantly smaller than in routine USgFNAC (p-value < 0.0001). (Table 3)

Table 3: Size and location of additional Fused-USgFNAC nodes

	total	malignant		benign		insufficient	
level	n	n	*sizes (mm)*	n	*sizes (mm)*	n	*sizes (mm)*
1	2	0	-	1	*3*	1	*8*
1a	1	0	-	1	*4*	0	-
1b	4	1	*9*	3	*4, 3, 6*	0	-
2	12	3	*7, 4, 6*	8	*9, 6, 11, 8, 5, 6, 8, 5*	1	*8*
2b	1	1	*6*	0	-	0	-
3	13	4	*9, 8, 6, 6*	8	*5, 4, 3, 5, 4, 4, 4, 6*	1	*5*
4	7	2	*6, 12*	4		1	*4*
5	3	1	*9*	2	*5, 6*	0	-
parot.gl.	2	0	-	2	*5, 6*	0	-
cheek	1	1	*6*	0	-	0	-
Total	46	13		29		4	

Note:—1 to 5 indicates the neck levels; Parot.gl., parotid gland.

At cytology, 4/46 (9%) were inconclusive and 13 out of 42 (31%) nodes proved to be malignant. Added Fused-USgFNAC increased the number of proven malignant nodes from 85 to 98 (15%). Due to additionally Fused-USgFNAC the percentage of proven PET-positive malignant nodes changed from 83/166 (50%) to 96/182 (53%), statistically not significant p-value < 0.291. (Flow chart Figure 4)

In 74/87 (85%) patients all cytological results were sufficient, and pN-stage was present. pN-stage was compared to the N-stage of routine ultrasound and of fused ultrasound. With USgFNAC pN-stage was equivalent in 31/74 (42%) patients, while with Fused-USgFNAC it was equivalent in 43/74 (55%) patients.

With Fused-USgFNAC pN-stage was upgraded in 8/87 (9%), in 2/8 from N0-stage to N1-stage and in 1/8 from N1-stage to N3-stage. (Figure 5)
N-staging with USgFNAC and Fused-USgFNAC was not significant different (p-value < 0.1).

ND was performed 19/96 (20%) patients and SNB in 1/96 (1%), a total of 610 nodes were removed and in 11 of these 20 patients 52 metastases were present. With USgFNAC, the pathological result was pN0-stage in two of these patients,

while it was pN2b-stage and pN2c-stage in the ND. With Fused-USgFNAC it was pN1 in both of those patients.

Figure 3: Flow chart results of routine USgFNAC and fused-USgFNAC

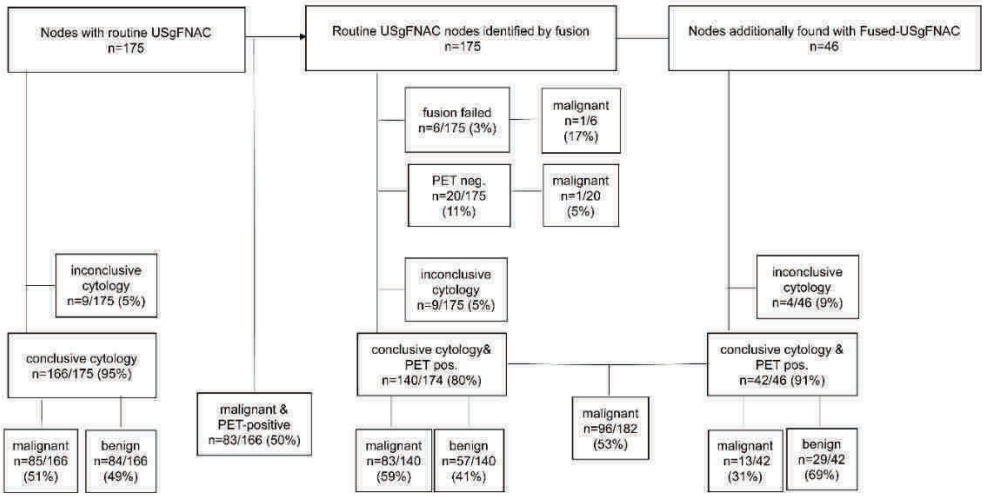

Note: Pos. Indicates positive.

Discussion

Our study shows that real-time US-image fusion with FDG PET-CT is feasible and allows accurate US identification of the FDG PET-positive nodes. In our routine FNAC procedure, clinical information and imaging-data including FDG PET-CT is also available but not fused. In this study we sought to demonstrate the additional effect of using fused USgFNAC, and this was demonstrated by an increase of pathological confirmed malign nodes from 85 without fusion to 98 (15%) with additional fusion. Accurate nodal staging is a major determinant for treatment decision in HNSCC.[14]

Comparing Fused-USgFNAC pN-stage to USgFNAC, 8/87 (9%) patients pN-stage was upgraded though N-staging with USgFNAC and Fused-USgFNAC was not significantly different.

Currently, the neck is staged by clinical palpation, CT, MRI, FDG PET-CT and/or USgFNAC in the case of suspicious nodes. For most imaging modalities, apart from irregularities and shape, the minimal axial diameter is one of the most important criterion for suspicious nodes to be selected for aspiration.[15] For FDG PET-CT, standard uptake value (SUV) is a criterion for metastasis. All these imaging techniques fail to accurately detect very small metastases leading to a sensitivity in the clinically N0 neck in the order of 40-60% [8], due to the higher frequency of small sized nodes. Furthermore FDG PET-CT is limited in resolution and glucose uptake in small nodal metastases.[16] The main reason for this is that 25% of the metastases in clinically N0 necks are under 3 mm and thus will not be easily detected at any individual imaging technique.[11]

Figure 4

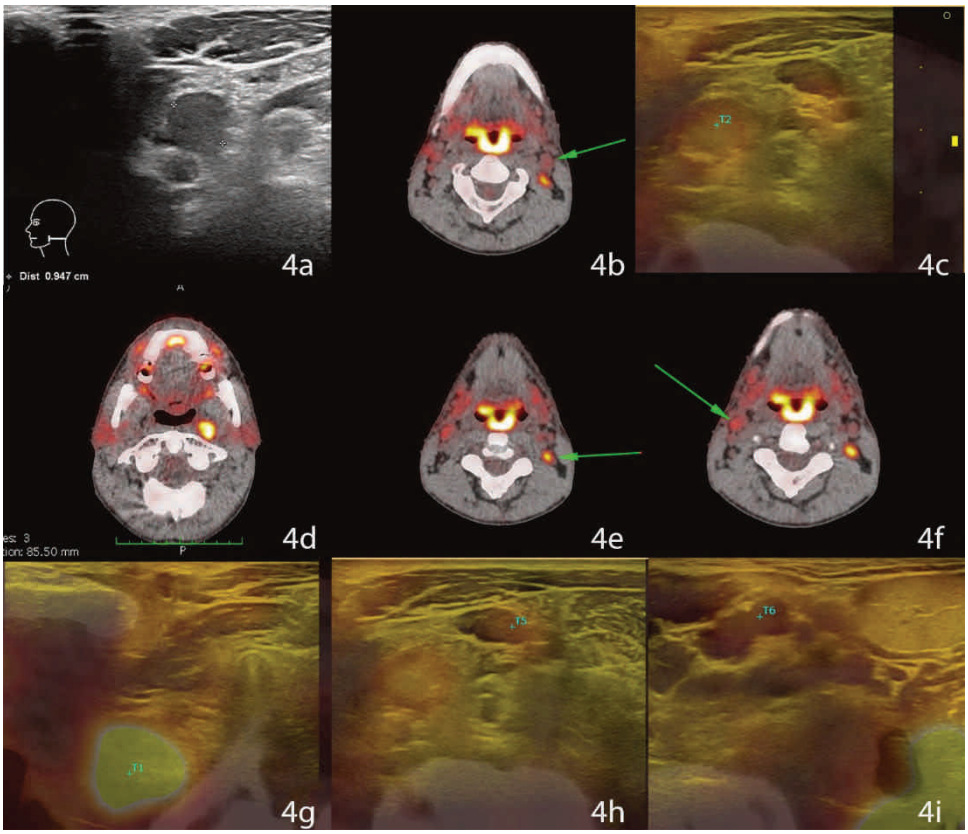

FIG 4. Change of N stage after additional fused-USgFNAC. The patient presented with cT3N0 oropharyngeal squamous cell carcinoma. A, Results of routine USgFNAC N1. B and C, PET/CT of the same node, controlled by image fusion. D–F, Additional nodes on PET/CT; all nodes have been fused, and fused-USgFNAC was performed. G, The deep parapharyngeal node was missed at routine ultrasound and only recognized after fusion. H, A PET-positive node with a normal appearance on routine ultrasound. I, Fused-USgFNAC-proved benign PET-positive contralateral node. Cytologically proved pN stage after fused-USgFNAC was pN2b, while it was N1 with USgFNAC and N2c on PET/CT. The green arrows point to the PET-positive nodes

Treatment decision making in HNC relies on imaging, emphasizing the need for high sensitivity to depict nodal disease.[17,18] Not only the extent of neck dissection, but also the fields and dose of radiotherapy are guided by imaging results. As with FDG PET-CT subtle metabolic active lymph nodes are very difficult to characterize, a subsequent USgFNAC is performed to make the final verdict. USgFNAC of the wrong lymph node or wrong part of the lymph node will lead to false-negative USgFNAC results, with under-treatment as a result.[18] We were

able to show that real-time US image fusion with FDG PET-CT is feasible. Within the 201 FDG PET-positive nodes fusion failed in only six nodes (8%), and this was mainly at the starting period when we were still in the midst of our learning curve. Real-time US image fusion with FDG PET-CT is an excellent method to increase the reliability of the FDG PET-CT results. Especially in borderline, small FDG PET-CT positive lymph nodes, fusion with US can increase the yield of Fused-USgFNAC and diminish sampling errors. Particular for small nodes, real-time US image fusion with FDG PET-CT can improve the sensitivity of ultrasound and the specificity of FDG PET-CT and lead to a higher detection rate of malignant nodes. Although in both, Fused-USgFNAC and USgFNAC, the smallest FDG PET positive malignant lymph nodes were 4 mm, the mean minimal axial diameter of the tumor positive nodes of Fused-USgFNAC (7.8 mm) was significantly smaller than that of USgFNAC (13.4 mm).

Although additional Fused-USgFNAC increased the number of confirmed malignant from 85 to 98, the detection rate of malignant PET-positive nodes increased only from 51% to 53%, which was not significant. This can largely be explained by the smaller size of the additional Fused-USgFNAC nodes, indicating an increase in sensitivity in small nodes. N-stage was upgraded in 8/87 (9%) patients.

Because we do not have definitive pathology of all aspirated lymph nodes, we cannot determine whether the FDG PET-CT was false positive or the aspiration false negative for the cases with negative aspirates. In addition, in 3/21(14%) patients with insufficient FNAC results malignant nodes in elective neck dissection were present, which suggests that every FNAC with insufficient result should be repeated. On FDG PET-CT smaller nodes are more often borderline FDG-positive nodes, which can lead to a diagnostic problem. A visible slightly higher metabolism can be caused by a metastasis as well as by inflammation. Consequently, the specificity of a SUV_{max} value between 2-3 at FDG PET-CT is quite low and can be increased by adding Fused-USgFNAC. On the other hand, the specificity of USgFNAC is almost 100%, so a combination of using FDG PET-CT with a lower threshold and Fused-USgFNAC might improve the sensitivity of the USgFNAC.
The selection of nodes for aspiration in HNC is a difficult issue. Size and location are the most important selection criteria. This study is meant to see if image fusion, with FDG PET-CT, is a helpful tool for nodes selection to provide FNAC.

Especially in small lymph nodes with limited uptake, this technique could be added to USgFNAC. Only one patient with negative FDG PET-CT findings had a suspicious node on ultrasound which proved to be malignant. In all other patients, after fusion all the nodes that underwent routine USgFNAC were to some extent FDG PET-positive. So, the current criteria for aspiration largely overlap with the glucose uptake at FDG PET-CT. One could argue whether aspirating from more and smaller nodes without PET guidance would increase the sensitivity irrespective of adding FDG PET-CT, but selection criteria only guided by size and shape are not very accurate and borderline glucose uptake may well be more reliable.
Although in prostate and liver real time image fused guided biopsies is already used clinically [19,20], the technique has its limitations in head and neck imaging. The mobility of the neck makes fusion much more difficult. Auto-fusion is not successful. Manual fusion and fusion corrections on the different levels of the neck must been done. To get a reliable accurate fusion the radiologist must be well trained. Because fused image guided FNAC is time consuming, with an additional 10-15 minutes examination time, it should be used as a problem-solving tool in small borderline FDG PET-positive nodes, which are difficult to identify on routine USgFNAC. As far as we know this is the first larger study of fused USgFNAC in HNC and therefore reproducibility is not known and because it was only one observer the inter observer variability is also not known. No reliable estimation of sensitivity and specificity could be made due to the small number of patients who underwent neck dissection and sentinel node biopsy.

Conclusion

Real-time US image fusion with FDG PET-CT and Fused-USgFNAC is feasible in head and neck cancer. It can improve the detection and image guided aspiration of suspicious nodes as visualized on FDG PET-CT and might increase sensitivity of USgFNAC by selecting smaller FDG PET-positive borderline nodes for Fused-USgFNAC. Because Fused-USgFNAC is time consuming it should be used as a problem-solving tool in small borderline FDG PET-positive nodes which are difficult to identify on routine USgFNAC.

Acknowledgements

The authors would like to acknowledge Pedro Sanches, PhD and Frans Gleuwink (Philips Benelux, Boschdijk 525, 5621JG Eindhoven) for providing knowledge and training on Percunav image fusion (MR, CT, PET).

References

1. Lodder Frank A Pameijer Coen RN Rasch Michiel W M van den Brekel Alfons JM Balm WL. Prognostic signifi cance of radiologically determined neck node volume: a systematic review. Oncology 2012; 48:.
2. Gődény M. Prognostic factors in advanced pharyngeal and oral cavity cancer; significance of multimodality imaging in terms of 7th edition of TNM. Cancer Imaging 2014; 14:15.
3. Sun J, Li B, Li CJ, Li Y, Su F, Gao QH, Wu FL, Yu T, Wu L, Li LJ. Computed tomography versus magnetic resonance imaging for diagnosing cervical lymph node metastasis of head and neck cancer: A systematic review and meta-analysis. Onco Targets Ther 2015; 8:1291–1313.
4. Castelijns JA, van den Breckel MWM. Imaging of lymphadenopathy in the neck. Eur Radiol 2002; 12:727–738.
5. Sun R, Tang X, Yang Y, Zhang C. (18)FDG-PET/CT for the detection of regional nodal metastasis in patients with head and neck cancer: a meta-analysis. Oral Oncol 2015; 51:314–20.
6. Yongkui L, Jian L, Wanghan, Jingui L. 18FDG-PET/CT for the detection of regional nodal metastasis in patients with primary head and neck cancer before treatment: A meta-analysis. Surg Oncol 2013; 22:e11–e16.
7. Zhang H, Seikaly H, Biron VL, Jeffery CC. Utility of PET-CT in detecting nodal metastasis in cN0 early stage oral cavity squamous cell carcinoma. Oral Oncol 2018; 80:89–92.
8. Liao L-J, Hsu W-L, Wang C-T, Lo W-C, Lai M-S. Analysis of sentinel node biopsy combined with other diagnostic tools in staging cN0 head and neck cancer: A diagnostic meta-analysis. Head Neck 2016; 38:628–634.
9. Akhavan-Moghadam J, Afaaghi M, Maleki AR, Saburi A. Fine needle aspiration: an atraumatic method to diagnose head and neck masses. Trauma Mon 2013; 18:117–21.
10. Ostermann K, Asanau A, Lang FJW. Cervical staging by head and neck surgeon-performed ultrasound and FNAC in N + head and neck cancer. 2018; 7–15.
11. Borgemeester MC, van den Brekel MWM, van Tinteren H, Smeele LE, Pameijer FA, van Velthuysen M-LF, Balm AJM. Ultrasound-guided aspiration cytology for the assessment of the clinically N0 neck: Factors influencing its accuracy. Head Neck 2008; 30:1505–1513.
12. Colnot DR, Nieuwenhuis EJC, Van den Brekel MWM, Pijpers R, Brakenhoff RH, Snow GB, Castelijns JA. Head and neck squamous cell carcinoma: Us-guided fine-needle aspiration of sentinel lymph nodes for improved staging - Initial experience. Radiology 2001; 218:289–293.
13. Wang S-Y. Real-Time Fusion Imaging of Liver Ultrasound Background and principles of ultrasound fusion imaging. J Med Ultrasound 2017; 25:9–11.

14. Edge SB, Compton CC. The American Joint Committee on Cancer: the 7th Edition of the AJCC Cancer Staging Manual and the Future of TNM. no date; .
15. van den Brekel MW, Stel H V, Castelijns JA, Nauta JJ, van der Waal I, Valk J, Meyer CJ, Snow GB. Cervical lymph node metastasis: assessment of radiologic criteria. Radiology 1990; 177:379–84.
16. Nakamura T, Sumi M, Kimura Y, Sumi T. Whole-neck imaging for the screening of metastatic nodes. Jpn Dent Sci Rev 2010; 46:73–77.
17. de Veij Mestdagh PD, Jonker MCJ, Vogel W V., Schreuder WH, Donswijk ML, Klop WMC, Al-Mamgani A. SPECT/CT-guided lymph drainage mapping for the planning of unilateral elective nodal irradiation in head and neck squamous cell carcinoma. Eur Arch Oto-Rhino-Laryngology 2018; 275:2135–2144.
18. van den Brekel MWM, Castelijns JA. What the clinician wants to know: surgical perspective and ultrasound for lymph node imaging of the neck. Cancer Imaging 2005; 5 Spec No:0–16.
19. Shoji S. Magnetic resonance imaging-transrectal ultrasound fusion image-guided prostate biopsy: Current status of the cancer detection and the prospects of tailor-made medicine of the prostate cancer. Investig Clin Urol 2019; 60:4–13.
20. D'Onofrio M, Beleù A, Gaitini D, Corréas JM, Brady A, Clevert D. Abdominal applications of ultrasound fusion imaging technique: liver, kidney, and pancreas. Insights Imaging 2019; 10:.

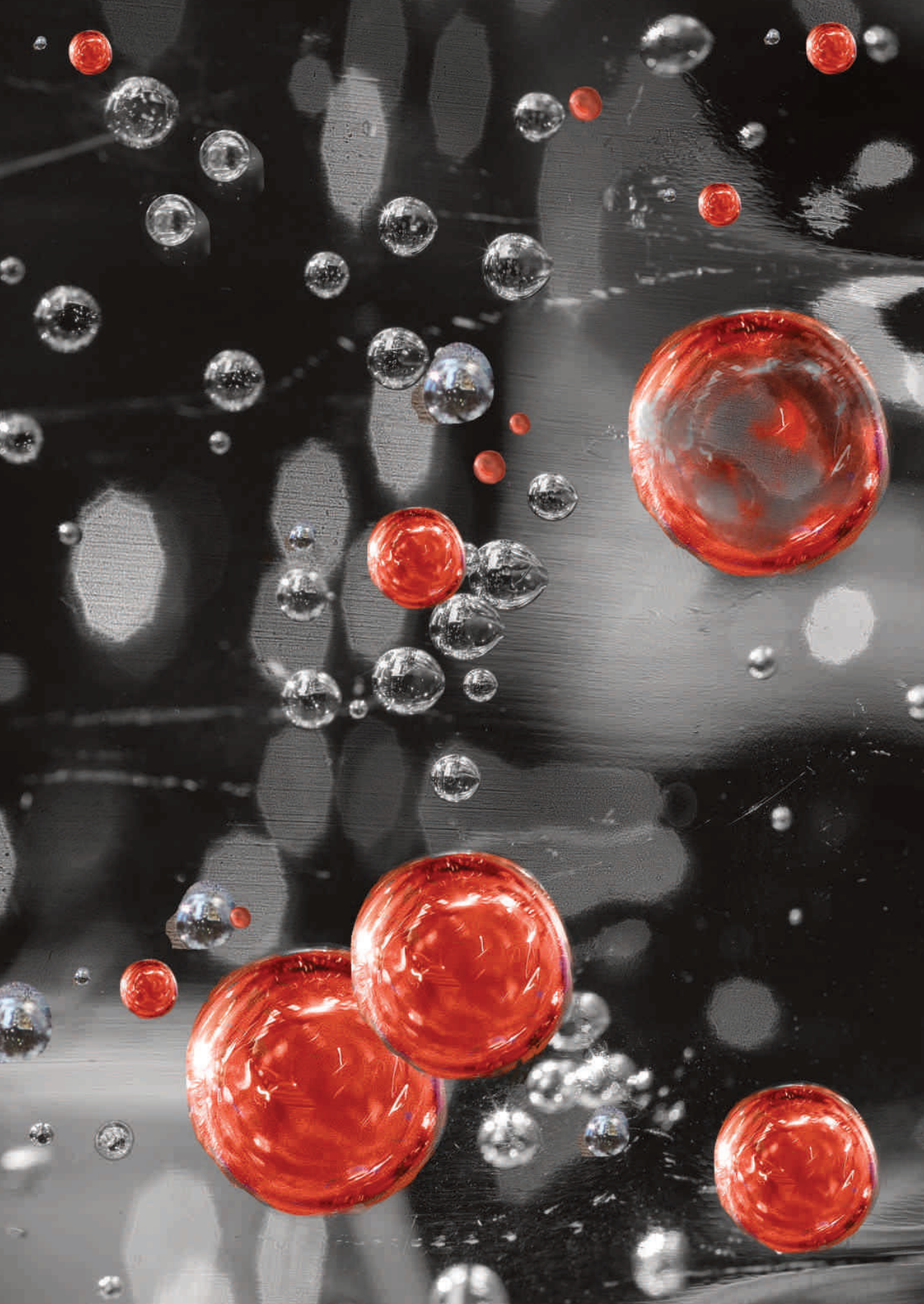

CHAPTER 3

SUV max values at FDG PET-CT to predict malignancy in lymph nodes aspirated by real time image fused USgFNAC in head and neck squamous cell carcinoma

Petra K de Koekkoek-Doll , Wouter Vogel, Monique Maas , Jonas Castelijns , Laura Smit, Joannis Zavrakidis, Regina Beets-Tan, Michiel van den Brekel

Published in American Journal of Nuclear Medicine and Molecular Imaging

Nov 2021; (3):178-187

https://www.ncbi.nlm.nih.gov/pmc/articles/PMC8255217/

Abstract:

Background and Purpose: 18F-fluordeoxyglucose (FDG) positron emission tomography combined with computed tomography (PET-CT) and ultrasound guided fine-needle aspiration cytology (USgFNAC) are commonly used to detect nodal metastases in head and neck squamous cell carcinoma (HNSCC). FDG PET-CT helps to guide selection of borderline suspicious nodes to aspirate using USgFNAC. Real time image fusion of FDG PET-CT with US is a new available technique and can improve this selection. The aim of this study was to determine optimal SUVmax values for USgFNAC node selection to improve USgFNAC sensitivity.

Material and Methods: 118 patients, with histopathological proven HNSCC or proven lymph nodes metastases of SCC of unknown primary, referred for staging of HNSCC with FDG PET-CT and ultrasound, were prospectively included. Additionally to standard USgFNAC of suspicious nodes fusion was performed to confirm that USgFNAC took place in FDG-positive nodes and to add Fused-USgFNAC in missed FDG-positive nodes. Fusion was performed on nodes with reported having metabolic activity. SUVmax values were measured in all Fused-USgFNAC nodes. The reference standard was cytology.
Result: In 118 patients USgFNAC was performed in 281 nodes. At fusion 22/281 (8%) nodes were FDG-negative. Out of 259 FDG-positive nodes 253 (98%) nodes were fused successfully. USgFNAC had conclusive results in 237/253 nodes (94%). In 126/237 nodes (53%) cytology proved to be tumor positive. Below SUVmax of 2.87 no fused FDG-positive nodes proved to be tumor positive at cytology.

Conclusion: To improve sensitivity, only FDG-positive nodes with SUVmax values above 2.87 should be selected for USgFNAC. Image fusion can identify those nodes for USgFNAC selection.

Keywords: Head and neck cancer, lymph node metastasis staging, hybrid imaging, real-time image fusion, ultrasound FDG-PET, SUVmax

Introduction

The prognosis of head and neck squamous cell carcinoma (HNSSC) depends on many factors. Especially in HPV negative tumors the presence or absence of metastatic lymph nodes (N-stage) is one of the most important predictors for loco regional control and risk for distant metastasis and thereby highly influences the patient's management [1]. The number of metastases, their laterality, the involved node levels and the presence of extracapsular spread are important predictive parameters [2]. In a systematic review Lodder et al. reported that increasing volume of involved nodes is correlated with worsening outcome [3].

Management of cervical nodes often includes neck dissection (ND), radiotherapy (RT) or chemo-radiation (CRT). The extent of ND and RT as well as the dose of RT depend on the N-stage. Elective treatment is not always necessary if the risk of occult metastases is very low. To minimize treatment morbidity, accurate staging is thus very important [4-5]. A systematic review and meta-analysis of elective neck dissection vs active surveillance of cT1-T2N0 squamous cell carcinoma (SCC) of the oral cavity showed that elective neck dissection (END) results in fewer regional recurrences than active surveillance [6]. Still, watchful waiting is considered a treatment option in case of a low risk for metastases and a very close follow-up of the neck [7]. For radiotherapy target volume selection and dose it is equally essential to know the N-status [8-9]. Palpation of neck nodes is insufficient with a sensitivity and specificity in the range of 60-70% [10,11]. The detection of malignant nodes by CT and MRI mainly relies on size criteria and has only a moderate sensitivity (74-78%) and specificity (76-80%) [12]. US-guided fine needle aspiration cytology (USgFNAC) has a very high specificity, but to obtain a high level of sensitivity many lymph nodes should be aspirated including nodes with a minimal axial diameter as small as 3-4 mm [13]. The challenge is to sample the right nodes to minimize false-negativity [14].

Precision medicine and molecular imaging technologies play a major rule in cancer diagnostic and therapy [15]. Molecular imaging with ^{18}F-fluordeoxyglucose positron emission tomography combined with computed tomography (FDG PET-CT) is increasingly used as a diagnostic tool to detect metastatic lymph nodes in the neck with a pooled sensitivity and specificity of 84% and 96%, respectively [16]. However, in patients with cT1-T2N0 oral cavity SCC sensitivity of FDG PET-CT drops to 50-58% [12,17]. To increase the sensitivity a lower SUV uptake cut-off could be chosen, but then specificity drops unacceptably. FDG PET-CT frequently

shows lymph nodes with visually borderline metabolic activity. These nodes are difficult to categorize as either malignant or reactive on PET-CT. Image fusion could help to identify and select nodes for Fused-USgFNAC which could help to increase specificity of PET-CT and sensitivity of USgFNAC.

We recently determined that real-time fusion of FDG PET-CT and ultrasound in Head and Neck Cancer (HNC) is technically feasible and allows FNAC-guidance by FDG uptake in lymph nodes (Fused-USgFNAC). In our study we found that 54% of the reported FDG-positive nodes could be proven as malignant at subsequent Fused-USgFNAC [16]. These data also suggested that small FDG-positive nodes can be detected with this technique, which enabled improved detection rate of malignant nodes. Based on these earlier results, the aim of this study is to establish a threshold of the SUVmax value to optimally select nodes to aspirate using USgFNAC.

Materials and Methods

This study was approved by the Institutional Review Board (IRBd20-126). We prospectively included 118 patients with histopathological proven HNSCC or proven lymph nodes metastases of SCC of unknown primary.

All patients were referred for FDG PET-CT and USgFNAC for N-staging. Contrast enhanced CT of the neck or MRI was present. Next to the group analysis including all patients a subgroup analysis of patients with clinically node negative neck (cN0) and of patients with human papillomavirus (HPV) associated HHSCC was performed.

Data were analyzed retrospectively. All retrospective medical data/biospecimen studies at the Netherlands Cancer Institute have been executed pursuant to Dutch legislation and international standards. Prior to 25 May 2019, national legislation on data protection was applied, as well as the International Guideline on Good Clinical Practice. From 25 May 2019 we also adhere to the GDPR. Within this framework, patients are informed and have always had the opportunity to object or actively consent to the (continued) use of their personal data & biospecimens in research. None of the patients included in this study objected to use of their data.

FDG PET/CT imaging

FDG PET/CT images were acquired in the clinical setting using a Gemini TF scanner (Philips, Maryland, USA). Patients fasted for 6 hours and were hydrated prior to administration of FDG. Diabetes mellitus needed to be regulated adequately and the plasma glucose level was required to be <10 mmol/l. A dose of 190-240 MBq was administered depending on BMI. FDG PET images of the head-neck area were acquired for 3 bed positions of 3 minutes each and were reconstructed to 2mm isotropic voxels. Low dose CT was acquired for attenuation correction and anatomical orientation with 40 mAs and 2mm slices. In addition, images of the neck-thighs were acquired. All FDG PET/CT images were assessed by dedicated nuclear medicine radiologists in the clinical setting; reports of these examinations were used for the current study.

Figure1: Flow Chart USgFNAC and image fusion with FDG PET-CT

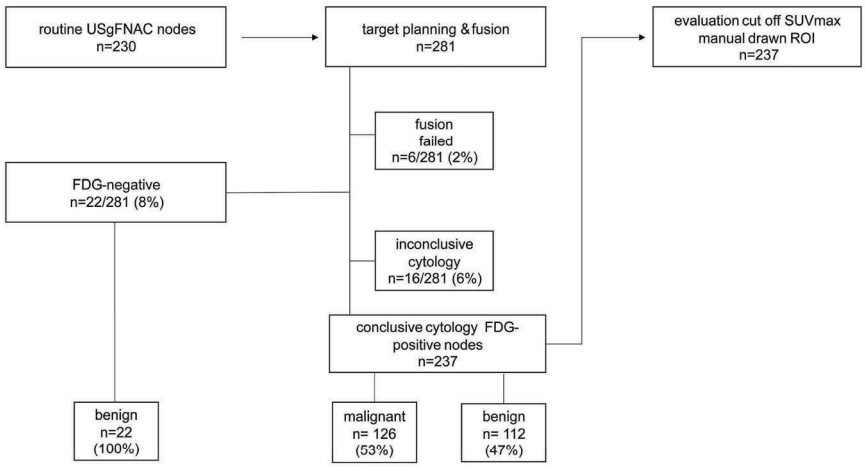

Ultrasound and real time image fusion with FDG PET-CT

All US and FNAC procedures where performed by one radiologist with more than 10 years of US experience in head and neck radiology (PDK). Ultrasound was performed by using an EpiQ7 G US device (Philips Medical Systems, Bothell, WA)

with either an L12-5 or eL18-4 probe. A flow chart of the procedures is shown in Figure 1.

First, routine ultrasound of the ipsilateral and contralateral neck was performed. USgFNAC was performed in suspicious nodes according to Institutional guidelines. Criteria included loss of a fatty hilum, short axial diameter > 6-8 mm (depending on level), thickened or asymmetric cortex, round shape or suspicious nodes according to palpation or as seen on other imaging modalities (including CT, MRI or FDG PET/CT). Subsequently, ultrasound with real time image fusion with FDG PET-CT images was performed by the same radiologist (PKD), using the same US diagnostic system. The Percunav setup (Philips Medical Systems, Best, The Netherlands) was used according to the manufacturer's manual. For the L12-5 probe a bracket and an electromagnetic tracker were added. The eL18-4 probe has an integrated tracker. A patient reference tracker was placed on the forehead of the patient using tape. A field generator was fixed at a metallic arm positioned above the neck of the patient. FDG PET-CT data were imported into the US device and fusion of FDG PET and CT took place in the same device. An initial fusion between live US and FDG PET-CT was performed manually based on the thyroid gland, using the "match plane function". Additional manual corrections of the initial fusion were made, if necessary, by identification of known anatomical structures such as the hyoid bone, submandibular gland or carotid artery bifurcation. After the initial fusion, nodes that showed visible increased FDG uptake (compared to normal surrounding tissues) and that had been reported as suspicious, were selected for real time image fusion by using the "target planning function " (Figure 2).

Nodes that already underwent routine USgFNAC were evaluated again to determine if they corresponded to a FDG-positive node. Thereafter, fused-USgFNAC was performed in visually FDG-positive nodes if missed on routine USgFNAC (Figure 2). USgFNAC of FDG-positive nodes was performed in a maximum of 2 ipsilateral levels, in maximally 2 contralateral levels and in the lowest level of each side. For all nodes that received USgFNAC, the SUV_{max} values were measured by the radiologist who performed the US (PKD) using dyna-CAD by manual drawing of ROIs.

Figure 2: Target planning. fusion. and manual ROI placement of FDG-positive node to measure SUVmax values. A

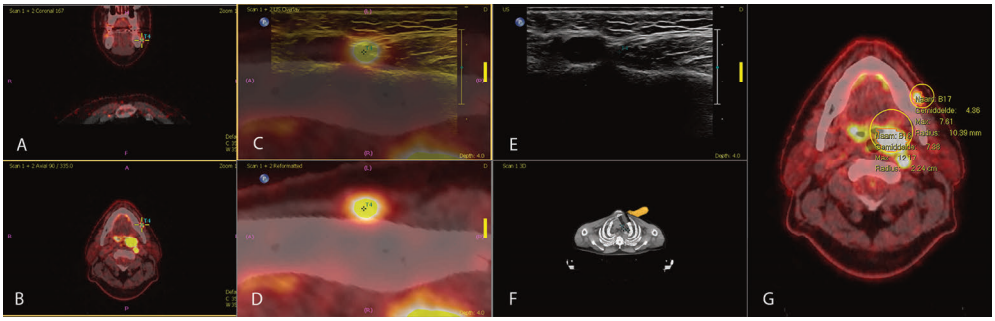

A, B. Target planning PET- positive node 3D view. C. Real time fused PET-posive node, overlay US and PET-CT. D. Reformatted PET-CT image. E. US image. F. Volume representation of CT image and probe location. G. Manual drawing ROI in the Fused-USgFNAC node to measure SUV_{max} values.

Pathology

The reference standard was cytological result from USgFNAC nodes. For aspiration of all nodes an 21G needle was used. Part of the FNAC material was processed in smears, air dried and stained with Giemsa stain. Another part of every aspirate was fixed in 10 ml 4% formalin and embedded in paraffin for further immunohistochemistry if necessary, according to routine diagnostic workup. For clinically staging all samples were evaluated by experienced head and neck pathologists, the cytological results of the clinically setting were used retrospectively for the current study. HPV status was immunohistochemically assessed on formalin-fixed paraffin-embedded tissue samples from tumor biopsies or resections during standard routine diagnostic procedures. Antibodies for p53 (DO-7, 1/7000, DAKO) and p16 (E6H4; ready to use, Ventana Medical systems/Roche) were used in a Benchmark ULTRA autostainer (Ventane Medical systemsReactions were detected using OptiView DAB Detection kit (#760-700; Roche) for visualization p16 and p53 . Finally, the slides were counterstained with Hematoxylin II and Bluing Reagent (Ventana Medical Systems).

Table 1. Diagnosis of all patients

Diagnose	n	%	HPV	HPV+	%	HPV-	%
SCC unkown primary	12	12.2%	12	6	50%	6	50%
SCC oral cavity	25	21.1%					
SCC oropharyngeal	33	28.0%	33	18	54%	15	46%
SCC hypopharyngeal	12	10.2%					
SCC laryngeal	23	19.5%					
SCC nasal cavity paranasal sinuses	6	5.1%	4	2	50%	2	50%
SCC nasopharyngeal	6	5.1%	4	2	50%	2	50%
SCC cutaneus	1	0.8%					
total	118	100 %	53	28	53%	23	47%

Statistical evaluation

Calculation of sensitivity and specificity of the techniques was not possible as not all patients had a neck dissection with a pathology report. We therefore scored the percentage of positive cytology in relation to the SUV values in all nodes that were visually FDG-positive and aspirated at USgFNAC using image fusion. PET-negative nodes, nodes with failed fusion and nodes with inconclusive cytological results were excluded for further evaluation. Baseline characteristics were evaluated by descriptive statistics. A two-sided Independent samples t-test was used to compare the groups and subgroups and the two groups with positive and negative cytology based on their short axis diameter and SUV_{max}. A p-value of </= 0.05 was considered statistically significant.

Results

A total of 118 patients (median age of 63; range 32-89) with HNSCC were included. Diagnoses are shown in Table 1. In these 118 patients USgFNAC was performed in 281 nodes (Figure 1) Out of 281 nodes, 22 (8%) nodes were FDG-negative and all of these 22 nodes proved to be tumor negative at cytology. Image fusion failed in another 6 nodes (2%). Of the remaining 253 FDG-positive nodes, 16 (6%) had inconclusive cytological findings. These nodes were excluded from further evaluation. From the remaining, with image fusion confirmed 237 FDG-positive nodes, 126 (53%) had malignant cytology. The median size (diameter

short axis) of all FDG-positive evaluated nodes was 10.3 mm (range 3-35 mm). The average size of nodes with malignant cytology was significantly larger than nodes with benign cytology, with a median size (diameter short axis) of 13.4 mm (range 4-35 mm) compared to 6.7 mm (range 3-15 mm), p-value<0.0001. The mean SUV_{max} of all evaluated FDG-positive nodes was 7.8 (SD 5.8). The mean SUV_{max} in nodes with malignant cytology was also significant higher with an average 11,0 (SD 6.3) compared to benign nodes with an average 4.3 (SD 1.7), p-value < 0.0001. (Table 2). The lowest SUV_{max} in nodes with malignant cytology was 2.87 and the highest SUV_{max} in nodes with benign cytology was 10,7 (Table 3, Figure 3, Figure 4).

Table 2. Mean SUV_{max} and size (short-axis diameter) in FDG-positive nodes of all HNSCC patients

			size			SUVmax		
nodes	n	%	median	min	max	median	min	max
malignant	125	53%	13.4	4	35	11.0	2.87	40.84
benign	112	47%	6.7	3	15	4.3	1.95	10.7
all	237	100%	10.3	3	35	7.8	1.95	40.84

Table 3. SUV_{max} in ranges and number of malignant and benign nodes

SUV_{max}		nodes			benign		malignant	
>	≤	n	%	mean mm	n	%	n	%
	2	0	0%		0	0%	0	0%
2	2.5	5	2%	5.80	5	5%	0	0%
2.5	3	12	5%	6.42	11	10%	1	1%
3	3.5	29	12%	6.55	28	25%	1	1%
3.5	4	22	9%	6.14	17	15%	5	4%
4	4.5	20	8%	7.95	14	13%	6	5%
4.5	5	10	4%	6.80	8	7%	2	2%
5	5.5	17	7%	7.24	11	10%	6	5%
5.5	6	8	3%	7.00	3	3%	5	4%
6	6.5	6	3%	8.00	4	4%	2	2%
6.5	7	5	2%	8.20	2	2%	3	2%
7	7.5	6	3%	14.33	2	2%	4	3%
7.5	8	7	3%	9.29	1	1%	6	5%
8	8.5	5	2%	14.40	0	0%	5	4%
8.5	9	10	4%	13.90	0	0%	10	8%
9	9.5	7	3%	10.57	0	0%	7	6%
9.5	10	10	4%	13.00	2	2%	8	6%
10	10.5	3	1%	13.00	1	1%	2	2%
10.5	11	8	3%	12.50	2	2%	6	5%
11	11.5	4	2%	15.75	0	0%	4	3%
11.5	12	4	2%	11.75	0	0%	4	3%
12	12.5	3	1%	16.67	0	0%	3	2%
12.5	13	4	2%	16.00	0	0%	4	3%
13	13.5	1	0%	16.00	0	0%	1	1%
13.5	14	2	1%	15.50	0	0%	2	2%
14	14.5	3	1%	14.67	0	0%	3	2%
14.5	15	2	1%	9.50	0	0%	2	2%
15		24	10%	19.63	0	0%	24	19%

Figure 3. Suvmax ranges, n benign and malignant nodes

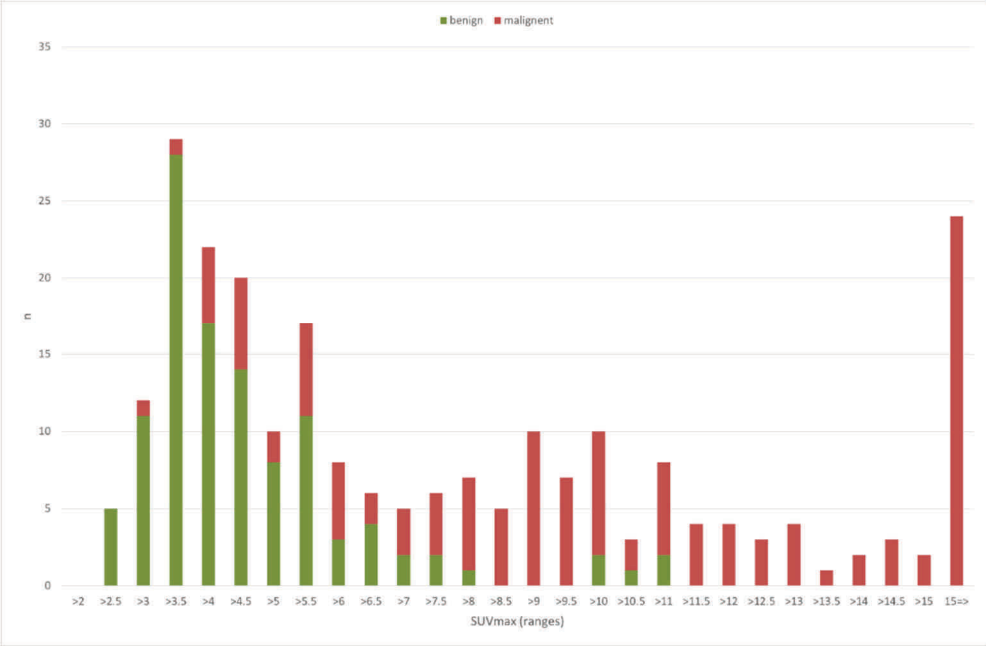

Figure 4. Scatterplot malignant and benign nodes, SUV_{max} and size

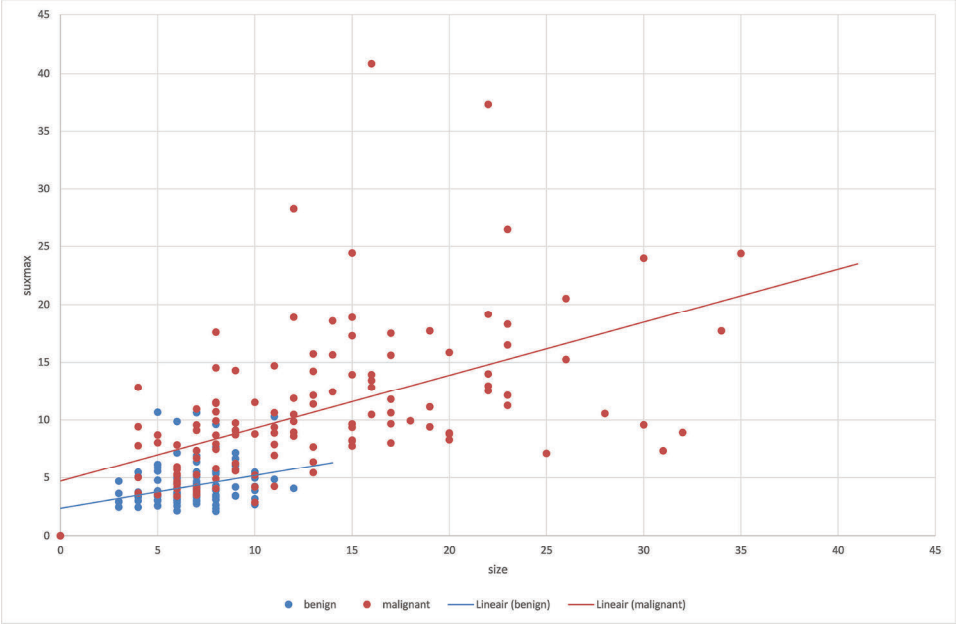

Subgroup analysis of clinically node negative neck (cN0) patients

Clinically 35/118 (30%) patients had a cN0 neck. In these patients, USgFNAC was performed in 71 FDG-positive nodes and 20 out of these (28%) had malignant cytology. The median short axis of nodes in cN0 was significantly smaller, p-value 0.001 (7.8 mm, range 3-23) than in cN+ (10.6 mm, range 3-35). The median short axis of malignant cN0 nodes (10.1 range 4-23) was significant smaller, value 0.039 than in cN+ nodes (13.5, range 4-35). The mean SUV_{max} of cN0 nodes with malignant cytology was significantly higher than in nodes with benign cytology, with an average of 8.3 (SD 5.0) versus 4.45 (SD 1.8), p value < 0.003.

The mean SUV_{max} of malignant nodes in all cN+ necks was 13.5 (SD 7.2) while it was 8.3 (SD 5.0) in cN0 necks, which was significantly lower, p-value 0.002. The lowest SUV_{max} in nodes with malignant cytology was 3.6 and the highest SUV_{max} in nodes with benign cytology was 10.6.

Subgroup cut-off SUV_{max} values in HPV associated SSC of the oropharynx, nasopharynx and unknown primary.

Immunohistochemically results of HPV related tumors were present in 53 patients. In 28/53 patients the tumor was associated with HPV (HPV+) and USgFNAC was performed in 73 nodes. 48/73 nodes were malignant at cytology. Mean short axis was 13.8 mm (SD 7.1) and mean SUV_{max} was 9.6 (SD 4.8). 25/78 nodes were benign at cytology. Mean short axis was 7.2 mm (SD 1.99) and mean SUV_{max} was 4.96 (SD 1.99). The lowest SUV_{max} in nodes with malignant cytology was 3.39 and the highest SUV_{max} in nodes with benign cytology was 10,27.

In 25 /53 patients the tumor was HPV negative (HPV-) and USgFNAC was performed in 45 nodes. 26/45 nodes were malignant at cytology. Mean short axis was 12.2 mm (SD 7.2), mean SUV_{max} was 10.9 (SD 5.1). 19/45 nodes were benign at cytology. Mean short axis was 7.4 mm (SD 2.2), mean SUV_{max} was 4.2 (SD 2.0). The lowest SUV_{max} in nodes with malignant cytology was 2.87 and the highest SUV_{max} in nodes with benign cytology was 10.6. Mean SUV_{max} in HPV - nodes was 10.6 and in HPV+ nodes 9.5, statistically not significant p value = 0.279.

Discussion

The presence of cervical lymph node metastases in HNSCC has a large impact on patients prognosis and treatment [19-20]. To detect occult nodal metastases in clinically node negative neck FDG PET-CT is slightly superior to MRI, CT or ultrasound [16, 21]. On the other hand, however, regarding the detection of cervical lymph node metastases in cN0 HNSCC patients, a recent meta-analysis still showed a low sensitivity and moderate specificity of FDG PET-CT [21]. This can be explained by the nonspecific nature of FDG uptake in small nodes and the difficulty to distinguish between benign, reactive or inflammatory on the one hand and malignant nodes other hand. Although ultrasound enables detection of enlarged nodes and enables evaluation of additional morphological features of nodes, it does not enable detection of micro-metastases in small nodes [22]. In our study only 20/281 nodes which underwent USgFNAC where FDG-negative, none of these nodes proved to be malignant. On ultrasound it might be difficult to identify tiny FDG-positive nodes with regular morphology and the major challenge performing USgFNAC is to select the right tiny FDG-positive node to puncture (based on imaging features on US but also other modalities), whereas the major issue in FDG PET-CT is, how borderline SUV values should be interpreted. Generally, a node with a SUV_{max} value above 4.5 is considered to be metastatic, whereas the nature of nodes with a SUV-value below this value remains uncertain [23].

In our study malignant FDG-positive nodes in cN0 HNSCC patients were significantly smaller than in cN+ HNSCC patients and had a significant lower mean SUV_{max} value.

These small nodes are the nodes that are difficult to accurately select for aspiration with routine US. Due to image fusion we were able to localize small FDG-positive nodes with a normal morphological appearance on ultrasound to perform fused-USgFNAC. Out of the real time image fused guided FDG-positive FNAC nodes 53% proved to be malignant at cytology. Based on Fused USgFNAC none of the FDG-positive nodes with a SUV_{max} of </= 2.87 was malignant. Our data are comparable to a recent study in which comparing PET-CT-data with cytological results, below a SUV_{max} of 2.2 no malignant nodes were found [24]. Therefore, a threshold SUV_{max} >2.87 can be used to guide US-FNAC. Using this value to select nodes for fused-USgFNAC will likely increase the accuracy of detection of malignant nodes in staging of HNSCC.

Based on Fused-USgFNAC at a SUV_{max} of 10.7 or higher all FDG-PET positive nodes were malignant and in fact in these nodes, aspiration might not be needed. A SUV_{max} value between 2.87 and 4.5 poses the major clinical problem, and in these cases, but also up to SUV_{max} 10.7 fused USgFNAC might be helpful to make the diagnosis.

Our results are also comparable with those in a study of Payabvash et al. who reported that at a SUV_{max} ≥2.5 sensitivity for detection of malignant nodes was 100%, with histopathological results as reference standard [25]. Other studies that correlated with histology found higher cut-offs for SUVmax values for malignant nodes. Dequanter et al. compared FDG-PET-CT with histology after neck dissection and proposed a SUV_{max} cut-off-value of 4.05 to detect malignant nodes [26]. Using this cut-off-value in the current study 13 malignant nodes would have been missed. Because accurate N-stage is essential for treatment planning , a lower cut-off SUVmax, like >/=2.87, is preferred to guide Fused-USgFNAC. To minimalize false negative results because of sampling errors, USgFNAC should be repeated in nodes with benign cytological results and a SUV_{max} of >/=2.87, if relevant for treatment decision

SUV_{max} values are reported significantly higher in HPV-negative nodes than in HPV-positive nodes [27]. In a meta-analysis of Fleming et al, a higher SUV_{max} value in HPV- negative tumors was found but PET SUV_{max} scores were unable to reliable differentiate between HPV-positive and HPV- negative tumors [28]. These results are comparable to our results with a statistically not significant higher mean SUV_{max} value in HPV- negative nodes than in HPV+ nodes.

Limitations

Because all Fused-USgFNAC and measurements were performed by one radiologist, the inter observer variability of the procedure is unknown.

In this study histopathological results of neck dissection as a gold standard are not available; therefore sampling error, leading to false negative results of cytology cannot be excluded.

Conclusion

To improve the sensitivity, for FDG- positive nodes with a benign morphological appearance on ultrasound, a SUV_{max} value ≥ 2.87 should be used to select nodes for USgFNAC. Those FDG- positive nodes can be identified by real time image fusion and Fused-USgFNAC can be performed.

References

1. Godény M. Prognostic factors in advanced pharyngeal and oral cavity cancer; Significance of multimodality imaging in terms of 7th edition of TNM. Cancer Imaging 2014; 14:1–13.

2. Woolgar JA. Histopathological prognosticators in oral and oropharyngeal squamous cell carcinoma. Oral Oncol 2006; 42:229–239.

3. Lodder Frank A Pameijer Coen RN Rasch Michiel W M van den Brekel Alfons JM Balm WL. Prognostic signifi cance of radiologically determined neck node volume: a systematic review. Oncology 2012; 48:.

4. Al-Mamgani A, Verheij M, van den Brekel MWM. Elective unilateral nodal irradiation in head and neck squamous cell carcinoma: A paradigm shift. Eur J Cancer 2017; 82:1–5.

5. Nieuwenhuis EJC, Castelijns JA, Pijpers R, van den Brekel MWM, Brakenhoff RH, van der Waal I, Snow GB, Leemans CR. Wait-and-see policy for the N0 neck in early-stage oral and oropharyngeal squamous cell carcinoma using ultrasonography-guided cytology: is there a role for identification of the sentinel node? Head Neck 2002; 24:282–9.

6. Abu-Ghanem S, Yehuda M, Carmel N-N, Leshno M, Abergel A, Gutfeld O, Fliss DM. Elective Neck Dissection vs Observation in Early-Stage Squamous Cell Carcinoma of the Oral Tongue With No Clinically Apparent Lymph Node Metastasis in the Neck. JAMA Otolaryngol Neck Surg 2016; 142:857.

7. Koyama LKS, Matos LL, Kulcsar MAV, de Araújo Filho VJF, Cernea CR. Oral Cancer Treatment: Still an Indication for Elective Neck Dissection? ORL 2018; 80:96–102.

8. van den Bosch S, Vogel W V., Raaijmakers CP, Dijkema T, Terhaard CHJ, Al-Mamgani A, Kaanders JHAM. Implications of improved diagnostic imaging of small nodal metastases in head and neck cancer: Radiotherapy target volume transformation and dose de-escalation. Radiother Oncol 2018; 128:472–478.

9. Navran A, Heemsbergen W, Janssen T, Hamming-Vrieze O, Jonker M, Zuur C, Verheij M, Remeijer P, Sonke J-J, van den Brekel M, Al-Mamgani A. The impact of margin reduction on outcome and toxicity in head and neck cancer patients treated with image-guided volumetric modulated arc therapy (VMAT). Radiother Oncol 2018; .

10. brekel 1990 diagnostic lymfklier meta.pdf. no date; .

11. Nt G, Hallur N, Gayathri Goudar ·, Sikkerimath Bc ·, Santhosh ·, Gudi S. Cervical lymph node metastasis in oral squamous carcinoma preoperative assessment and histopathology after neck dissection. 2009; .

12. Kyzas PA, Evangelou E, Denaxa-Kyza D, Ioannidis JPA. 18F-Fluorodeoxyglucose Positron Emission Tomography to Evaluate Cervical Node Metastases in Patients With Head and Neck Squamous Cell Carcinoma: A Meta-analysis. JNCI J Natl Cancer Inst 2008; 100:712–720.

13. van den Brekel MWM, Castelijns JA. What the clinician wants to know: surgical perspective and ultrasound for lymph node imaging of the neck. Cancer Imaging 2005; 5 Spec No:0–16.

14. Borgemeester MC, van den Brekel MWM, van Tinteren H, Smeele LE, Pameijer FA, van Velthuysen M-LF, Balm AJM. Ultrasound-guided aspiration cytology for the assessment of the clinically N0 neck: Factors influencing its accuracy. Head Neck 2008; 30:1505–1513.

15. Sun R, Tang X, Yang Y, Zhang C. (18)FDG-PET/CT for the detection of regional nodal metastasis in patients with head and neck cancer: a meta-analysis. Oral Oncol 2015; 51:314–20.

16. de Koekkoek-Doll PK, Maas M, Vogel W, Castelijns J, Smit L, Zavrakidis I, Beets-Tan R, van den Brekel M. Real-Time Ultrasound Image Fusion with FDG-PET/CT to Perform Fused Image-Guided Fine-Needle Aspiration in Neck Nodes: Feasibility and Diagnostic Value. Am J Neuroradiol 2021; .

17. Snow GB, Annyas AA, van Slooten EA, Bartelink H, Hart AA. Prognostic factors of neck node metastasis. Clin Otolaryngol Allied Sci 1982; 7:185–92.

18. Leemans CR, Tiwari R, Nauta JJ, van der Waal I, Snow GB. Regional lymph node involvement and its significance in the development of distant metastases in head and neck carcinoma. Cancer 1993; 71:452–6.

19. Sun R, Tang X, Yang Y, Zhang C. 18FDG-PET/CT for the detection of regional nodal metastasis in patients with head and neck cancer: A meta-analysis. Oral Oncol 2015; 51:314–320.

20. Yoon DY, Hwang HS, Chang SK, Rho Y-S, Ahn HY, Kim JH, Lee IJ. CT, MR, US, 18F-FDG PET/CT, and their combined use for the assessment of cervical lymph node metastases in squamous cell carcinoma of the head and neck. Eur Radiol 2009; 19:634–642.

21. Kim S-J, Pak K, Kim K. Diagnostic accuracy of F-18 FDG PET or PET/CT for detection of lymph node metastasis in clinically node negative head and neck cancer patients; A systematic review and meta-analysis. Am J

Otolaryngol 2019; 40:297–305.

22. Richards PS, Peacock TE. The role of ultrasound in the detection of cervical lymph node metastases in clinically NO squamous cell carcinoma of the head and neck. Cancer Imaging 2007; 7:167–178.

23. Lim RSM, Ramdave S, Beech P, Billah B, Karim MN, Smith JA, Safdar A, Sigston E. Utility of SUVmax on 18 F-FDG PET in detecting cervical nodal metastases. Cancer Imaging 2016; 16:1–8.

24. Peltenburg B, de Keizer B, Willem Dankbaar J, de Boer M, Willems SM, P Philippens ME, J Terhaard CH, de Bree R. Acta Oncologica Prediction of ultrasound guided fine needle aspiration cytology results by FDG PET-CT for lymph node metastases in head and neck squamous cell carcinoma patients Prediction of ultrasound guided fine needle aspiration cytology results by FDG PET-CT for lymph node metastases in head and neck squamous cell carcinoma patients. 2018; .

25. Payabvash S, Meric K, Cayci Z. Differentiation of benign from malignant cervical lymph nodes in patients with head and neck cancer using PET/CT imaging. Clin Imaging 2016; 40:101–105.

26. Dequanter D, Shahla M, Aubert C, Deniz Y, Lothaire P. Prognostic value of FDG PET/CT in head and neck squamous cell carcinomas. Onco Targets Ther 2015; 8:2279–2283.

27. Tahari AK, Alluri K, Quon H, Koch W, Wahl RL, Subramaniam RM, Subramaniam R, Morgan RH. FDG PET/CT imaging of Oropharyngeal SCC: Characteristics of HPV positive and negative tumors. Clin Nucl Med 2014; 39:225–231.

28. Fleming JC, Woo J, Moutasim K, Mellone M, Frampton SJ, Mead A, Ahmed W, Wood O, Robinson H, Ward M, Woelk CH, Ottensmeier CH, King E, Kim D, Blaydes JP, Thomas GJ. HPV, tumour metabolism and novel target identification in head and neck squamous cell carcinoma. Br J Cancer 2019; 120.

CHAPTER 4

ADC Values of Cytologically Benign and Cytologically Malignant 18 F-FDG PET-Positive Lymph Nodes of Head and Neck Squamous Cell Carcinoma

Petra K. de Koekkoek-Doll , Sander Roberti , Laura Smit , Wouter V. Vogel , Regina Beets-Tan , Michiel W. van den Brekel, Jonas Castelijns

Published in Cancers

Aug 2022; 14, 4019

https:// doi.org/10.3390/cancers14164019

Simple Summary: In squamous cell carcinoma of the head and neck, 18F-fluordeoxyglucose positron emission tomography (FDG-PET), diffusion-weighted magnetic resonance imaging (DW-MRI) and ultrasound-guided fine needle aspiration are commonly used imaging tools for nodal staging (N-staging). Although FDG-PET has good performance in nodal detection, it is still difficult to distinguish between PET-positive reactive and malignant nodes for the purpose of selecting nodes to be aspirated. DW-MRI can help to detect small lymph node metastases, and an inverse correlation with FDG uptake is expected. We found a mild negative correlation between SUVmax and ADC. Comparing the apparent diffusion coefficient (ADC) values between PET-positive and PET-negative nodes, ADC was significantly higher in PET-negative nodes. Whereas no significantly lower ADC value of cytological malignant nodes could be found overall, in the subgroup of non-HPV-related nodes, the ADC values of cytologically malignant PET-positive nodes were significantly lower than in cytologically benign nodes. This finding might be helpful in selecting nodes for puncture.

Abstract: Nodal staging (N-staging) in head and neck squamous cell carcinoma (HNSCC) is essential for treatment planning and prognosis. 18F-fluordeoxyglucose positron emission tomography (FDG-PET) has high performance for N-staging, although the distinction between cytologically malignant and reactive PET-positive nodes, and consequently, the selection of nodes for ultrasound-guided fine needle aspiration cytology (USgFNAC), is challenging. Diffusion-weighted magnetic resonance imaging (DW-MRI) can help to detect nodal metastases. We aim to investigate the potential of the apparent diffusion coefficient (ADC) as a metric to distinguish between cytologically reactive and malignant PET-positive nodes in order to improve node selection criteria for USgFNAC. PET-CT, real-time image-fused USgFNAC and DW-MRI to calculate ADC were available for 78 patients offered for routine N-staging. For 167 FDG-positive nodes, differences in the ADC between cytologically benign and malignant PET-positive nodes were evaluated, and both were compared to the ADC values of PET-negative reference nodes. Analyses were also performed in subsets of nodes regarding HPV status. A mild negative correlation between SUVmax and ADC was found. No significant differences in ADC values were observed between cytologically malignant and benign PET-positive nodes overall. Within the subset of non-HPV-related nodes, $ADC_{b0\text{-}200\text{-}1000}$ was significantly lower in cytologically malignant PET-positive nodes when compared to benign PET-positive nodes. $ADC_{b0\text{-}1000}$ and $ADCb_{0\text{-}200\text{-}1000}$ were significantly lower (p = 0.018, 0.016, resp.) in PET-negative reference nodes than in PET-positive nodes. ADC was significantly higher in PET-negative reference nodes than in PET-positive nodes. The non-HPV-related subgroup showed significantly (p = 0.03) lower ADC

values in cytologically malignant than in cytologically benign PET-positive nodes, which should help inform the node selection procedure for puncture.

Keywords: DW-MRI; FDG-PET; real-time image fusion; lymph node; head and neck oncology

1. Introduction

Head and neck squamous cell carcinomas (HNSCC) account for around 4% of all malignancies [1]. The presence of cervical lymph node metastases reduces the expected survival rate by approximately 50%, especially in HPV-negative tumors [2]. Therefore, nodal staging (N-staging) in HNSCC is essential for the assessment of prognosis and treatment planning [3]. Clinical examination of the neck detects around 60–70% of metastases [4], which means that about 30–40% of lymph node metastases are missed.

Medical imaging plays a major role in the detection of those clinically occult metastases. Computed tomography (CT), magnetic resonance imaging (MRI), 18F-fluordeoxyglucose (FDG) positron emission tomography combined with computed tomography (PET-CT) and ultrasound-guided fine needle aspiration cytology (USgFNAC) are commonly used for this purpose. In clinically node-negative necks (cN0), the pooled estimates for sensitivity were reported as 52% (95% confidence interval (CI), 39%–65%), 65% (34–87%), 66% (47–80%) and 66% (54–77%) on a per-neck basis for CT, MRI, PET and USgFNAC, respectively [5]. For N-staging with USgFNAC, node selection plays a major role in obtaining high sensitivity, since specificity for FNAC is 100% [6]. In a recent meta-analysis, USgFNAC was found to be the most accurate imaging modality for detecting cervical lymph node metastases [7]. With morphologic imaging, size is one of the most important criteria for node selection, in addition to necrosis, irregular enhancement and signs of extra nodal spread [8]. Although size is important, reactive lymph nodes might also be enlarged and small lymph nodes can contain micro metastases. To differentiate between reactive nodes and metastatic nodes, a minimal axial diameter between 8 and 12 mm has been established as suitable [9,10]. To minimize the risk of overlooking small metastases, small lymph nodes should also be aspirated, i.e., a low cut-off value should be used. However, this will lead to a higher rate of unnecessary lymph node punctures [11].

Functional imaging techniques such as Doppler sonography, PET-CT and diffusion-weighted imaging (DWI)-MRI as an additional modality can provide information concerning the underlying biology/pathology of the imaged lesion. It has been shown that assessing peripheral vascularization with power Doppler sonography is the best sonographic feature to predict malignancy in cervical lymph nodes [12].

18F-FDG PET-CT has good diagnostic performance, although it overlooks 50% of small metastases in cN0 necks [13], and small PET-positive lymph nodes can have normal ultrasound features; real-time fusion would help to recognize those nodes on ultrasound. In a recent study, we showed that real-time image fusion to guide USgFNAC is feasible in head and neck cancer imaging/diagnosis [14]. It remains a notable challenge, however, to distinguish between small PET-positive reactive

nodes and nodes with micro-metastases. Using small cut-off values for the maximal standardized uptake value (SUVmax) in order to select nodes for real-time image-fused-USgFNAC will improve the detection rate of malignant PET-positive nodes, but will lead to a high rate of unnecessary punctures [15].

Diffusion-weighted MRI (DW-MRI) is a method of signal contrast generation based on differences in Brownian motion, and evaluates the molecular function and micro-architecture of the human body. DW-MRI contrast reflects the diffusion of water in tissue, which is reduced in tissue with higher cellularity. By performing DWI using different b values, quantitative analyses by apparent diffusion coefficient (ADC) map are possible. This analysis is usually performed automatically. DW-MRI is widely used in oncological imaging. It has been shown that DW-MRI is a promising non-invasive tool to guide treatment selection in patients with peritoneal metastases of colorectal cancer. It is also a promising imaging tool for the assessment of treatment response and for differentiating between tumor and inflammatory changes [16,17]. It has been shown that for nodal staging, DWI has better performance than turbo spin echo MRI, with higher sensitivity (76% vs. 7%) but slightly lower specificity (94% vs. 99.5%) in detecting sub-centimeter nodal metastases [18]. Previous studies have suggested that a DWI node-negative neck could be considered for a wait and see policy [19]. Due to increased cell density in tumors and metastases, Brownian motion and therefore DWI are more restricted, and ADC might consequently be lower. An inverse correlation between FDG uptake and ADC in malignant lymph nodes has been reported [20].

Infection with high-risk human papillomaviruses (HPV) has been implicated in the pathogenesis of HNSCCs, and HPV-related HNSCCs are known to have a better treatment response and prognosis [21]. A higher FDG uptake in HPV-related malignant lymph nodes of the neck has been reported [22]. It has also been shown that HPV-related primary HNSSC tumors have lower ADC values than non-HPV-related tumors [23].

So far as we know, ADC has not been related to FDG uptake in PET-positive real-time image-fused guided FNAC nodes. Using real-time image fusion, we were able to identify PET-positive nodes for USgFNAC, and we can further compare ADC and FDG uptake in cytologically proven benign and malignant nodes. Locations of nodes on MRI can easily be correlated to the same nodes on PET-CT.

The aim of this study was to evaluate the diagnostic potential performance of DW-MRI in PET-positive nodes. We wanted to investigate if DW-MRI could help to distinguish small reactive lymph nodes with FDG uptake from small metastatic nodes since node selection for FNAC in those nodes is still very challenging. We wanted to investigate the different ADC values in all nodes and in the subgroups of HPV-related and non-HPV-related nodes. We also wanted to compare different

ADC values evaluated on different ADC maps. The main aim was to investigate the potential of ADC to distinguish between PET-positive cytologically malignant and benign nodes in order to improve selection for aspiration and pretreatment lymph node staging.

2. Materials and Methods

2.1. Patients

We retrospectively included 78 patients with either histopathologically proven HNSCC or lymph nodes proven to be SCC metastases of an unknown primary, and with available nodal staging based on real-time PET-CT-image-fused guided FNAC (Table 1).

Table 1. Diagnosis, number and percentage of patients**.**

Diagnosis	*n* Patient	% Patient
scc unknown primary	8	10.3%
scc oral cavity	19	24.4%
scc oropharyngeal	32	41.0%
scc hypopharyngeal	4	5.1%
scc laryngeal	8	10.3%
scc nasal cavity paranasal sinuses	3	3.8%
scc nasopharyngeal	2	2.6%
scc cutaneous	2	2.6%
total	78	100.0%

For all patients, FDG PET-CT and DW-MRI were present. To identify PET-positive nodes, PET-CT was real-time fused with ultrasound (US), and Fused-USgFNAC was performed. To identify the location of the Fused-USgFNAC nodes on MRI, MRI was (visually) correlated with PET-CT and Fused-USgFNAC. Because of the quality of the ADC map on MRI, ADC measurements of these Fused-USgFNAC nodes were only performed in levels I–III.

All retrospective medical data/bio specimen studies at the Netherlands Cancer Institute have been executed pursuant to Dutch legislation and international standards. Prior to 25 May 2019, national legislation on data protection was applied, as well as the International Guideline on Good Clinical Practice. From 25 May 2019, we also adhered to the General Data Protection Regulation (GDPR). Within this framework, patients are informed and have always had the opportunity

to object or actively consent to the (continued) use of their personal data and bio specimens in research. None of the patients included in this study objected to the use of their data. This study was approved by the Institutional Review Board (IRBd20-126).

2.2. FDG PET-CT Imaging

FDG PET-CT images were acquired using a Gemini TF scanner (Philips, Bel Air, MD, USA). Patients were prepared according to European Association of Nuclear Medicine (EANM) guidelines and had to fast for 6 h prior to FDG administration. For patients with diabetes mellitus, the plasma glucose level was required to be <10 mmol/L. A dose between 190 and 240 MBq [18F]-Flourodeoxyglucose (FDG) was administered depending on body mass index (BMI). PET images of head and neck were acquired at 3 min per bed position with a total field of view (FOV) of 576 mm (three bed positions), and reconstructed to 2 mm isotropic voxels using a BLOB-OS algorithm including time-of-flight information. For anatomical orientation and attenuation correction, low-dose CT was acquired with 40 mAs and a slice thickness of 2 mm. All FDG PET/CT images were assessed by dedicated nuclear medicine radiologists in the clinical setting; these reports were used for this study.

2.3. DW-MRI Imaging

Images were acquired on a 3T Achieva dStream scanner, Ingenia 3T or an Achieva Intera 1.5 T (Philips Healthcare, Best, The Netherlands), using a sensitive-encoding head and neck coil. For all patients, conventional MRI of the entire neck was performed.

Axial fat-suppressed T2-weighted turbo spin-echo MRI (TR/TI/TE 8458/180/20 ms), with 3 mm slice thickness, axial T1-weighted spin-echo MRI (TR/TE 799/10) and gadolinium-enhanced T13D (TR/TE 8.8/4.6 ms) with 1 mm slice thickness were performed. DWI was performed before contrast-enhanced T1-weighted MR imaging. Images were obtained in the axial plane with an echo-planar imaging sequence: TR/TE, 4583/76 ms; b-0 (1 averages), b-200 (2 averages) and b-1000 (4 averages) s/mm^2; field of view, 230 mm; matrix size, 112 × 87 pixel; slice thickness, 4 mm; no interslice gap; number of signals, 8; acquisition time, 3:25 min. Parallel imaging techniques (SENSE) with a reduction factor of 2.5 were used. ADC maps were generated automatically on the operating console from concurrent images. For some patients, MRI was performed with DWI b-0 (1 average), b-100 (1 average), b-300 (1 average), b-500 (2 averages) and b-800 (2 averages) s/mm^2; TR/TE,

4333/77 ms; field of view, 250 mm; matrix size, 114 × 101 pixel; slice thickness, 3 mm; no interslice gap; and an acquisition time of 1:06 min.

ADC measurements were performed blinded from pathological results by a single radiologist with more than 10 years' experience in head and neck radiology (PKD) on a PACS workstation (Carestream). To identify PET-positive nodes that underwent Fused-USgFNAC, PET-CT and MRI were visually correlated in an axial and coronal view. Regions of interest (ROIs) were manually drawn and the minimum ADC value was assessed. We placed the ROI in the area of the visually determined lowest signal on the ADC map. In nodes with necrosis, the ROI was placed in the solid part. To avoid partial volume effects from the surrounding tissue, ROIs were placed within the node borders. In the case of small nodes, we placed the ROI in the whole of the node inside the borders. ADC values were obtained not only from $ADC_{b0\text{-}1000}$, but also $ADCb_{0\text{-}200\text{-}1000}$ or $ADC_{b0\text{-}100\text{-}300\text{-}500\text{-}800}$, depending on available DW images. (Figure 1).

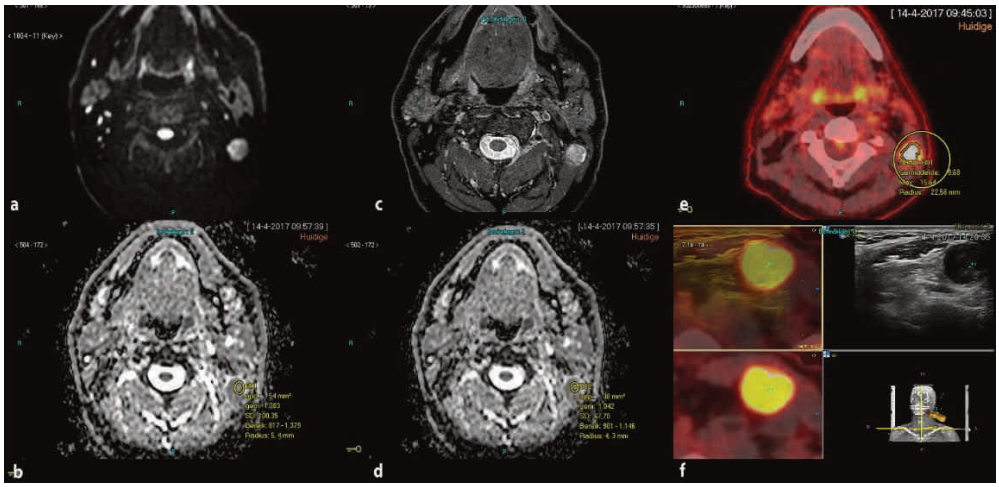

Figure 1. Drawing manual ROI in $ADCb_{0\text{-}1000}$ and $ADC_{b0\text{-}200\text{-}1000}$ in a PET-positive lymph node. (**a**) DWI acquired by b-0-200-1000 s/mm^2; (**b**) ROI in $ADC_{b0\text{-}1000}$; (**c**) axial STIR; (**d**) ROI in $ADC_{b0\text{-}200\text{-}1000}$; (**e**) corresponding PET-positive node; (**f**) corresponding real-time image-fused guided FNAC of the PET-positive node.

To determine a reference value for PET-negative nodes, ADC values were also obtained in PET-negative lymph node, with no visible FDG uptake, for each patient.

2.4. Ultrasound, Real-Time Image Fusion with FDG PET-CT and Real-Time Fused Guided FNAC

Ultrasound, image fusion with FDG PET-CT and Fused-USgFNAC was performed by using an EpiQ7 G US device (Philips Medical Systems, Bothell, WA, USA), with either an L12-5 or eL18-4 probe.

All US (gFNAC) procedures were performed by a radiologist with 10+ years of US experience in head and neck radiology (P.K.d.K.-D.). The Percunav setup (Philips Medical Systems, Best, The Netherlands) was used according to the manufacturer's manual. The eL18-4 probe has an integrated tracker; for the L12-5 probe, a bracket and an electromagnetic tracker were added. A patient reference tracker was placed on the forehead, and a field generator was positioned above the patient's neck. Fusion of the imported FDG PET and CT data took place in the same ultrasound device [14].

After the initial fusion, nodes that were reported as suspicious on FDG PET-CT were marked with the target planning tool and selected for analysis using Fused-USgFNAC. All punctures were performed with a 21G needle. For all nodes that received USgFNAC, the SUVmax values were measured by the radiologist who performed the US (P.K.d.K.-D.), using dyna-CAD and manual drawing of ROIs.

2.5. Pathology

Cytological results in nodes for which Fused-USgFNAC was performed were refereed as reference standard. Part of the FNAC material was processed in smears, air-dried and stained with Giemsa stain. Another portion of every aspirate was fixed in 10 mL 4% formalin and embedded in paraffin for further immunohistochemistry examination if deemed necessary, according to routine diagnostic workup. All samples were evaluated by experienced head and neck pathologists in a clinical setting and the cytological results were used retrospectively. HPV status was assessed immunohistochemically on formalin-fixed paraffin-embedded tissue samples from tumor biopsies or resections during standard routine diagnostic procedures. Antibodies for p53 (DO-7, 1/7000, DAKO) and p16 (E6H4; ready to use, Ventana Medical systems/Roche/Arizona, USA) were used in a Benchmark ULTRA autostainer (Ventana Medical systems). Reactions were detected using the OptiView DAB Detection kit (#760-700; Roche) for visualization of p16 and p53. Finally, the slides were counterstained with Hematoxylin II and Bluing Reagent (Ventana Medical Systems).

2.6. Statistical Analysis

Analyses were performed using nodes with a sufficient cytological result and clear identification on MRI. We determined the mean ADC of the calculated minimum and mean ADC values for cytologically benign and cytologically malignant nodes. To assess the difference in mean ADC value between cytologically benign and cytologically malignant nodes, accounting for inter-patient correlation, we used a linear mixed effects model with ADC as the dependent variable, malignancy as the independent variable, and a random intercept for patients, fitted with restricted maximum likelihood. Significance testing was conducted using a t-test for the malignancy variable. Differences between mean ADC values for cytologically benign or malignant nodes and PET-negative reference nodes were assessed using a linear mixed effects model with the difference as the dependent variable, no independent variables besides an intercept (fixed effect), and a random intercept for patients, fitted with restricted maximum likelihood. Significance testing was then conducted using a t-test for the (fixed effect) intercept. These analyses were also performed in the subgroups of HPV-related and non-HPV-related nodes. Finally, the overall association between ADC and SUVmax, and between ADC and axial node diameter, was assessed by computing Pearson correlations.

All analyses were performed with R statistical software, version 4.1.1. Missing values were excluded separately for each analysis, all statistical tests were two-sided, and *p*-values below 0.05 were considered statistically significant.

3. Results

Real-time image-fused USgFNAC was performed for 140 patients who were referred for N-staging for HNSCC. Patients without PET-positive nodes or without available MRI (*n* = 62) were excluded, leaving 78 patients with a total of 167 PET-positive USgFNAC nodes from levels 1–3 for analysis. The mean age among patients was 62.9 years (range 35–88 years, standard deviation (SD) 10.5). The mean minimal axial diameter for all nodes was 10 mm (range 3–34 mm; SD 6.3). Of the 167 nodes, 91 were cytologically malignant, while the other 76 were cytologically benign. The mean minimal axial diameter was 14 mm (range 3–34 mm; SD 6.9) and 7 mm (range 3–15 mm; SD 2.1) for cytologically malignant and benign nodes, respectively.

Minimum and mean ADC values of DW images were obtained with b-values 0–1000 s/mm^2 for 155 nodes, and for 154 of these nodes additionally with b-values 0-200-

1000 s/mm^2. For the 12 nodes without b-values 0–1000 s/mm^2, the minimum ADC was obtained with b-values 0-100-300-500-800 s/mm^2. The mean value of minimum ADC in cytologically malignant nodes was 0.444 × 10^{-3} mm^2/s (SD 0.186), 0.645 × 10^{-3} mm^2/s (SD 0.188) and 0.625 × 10^{-3} mm^2/s (SD 0.199) for $ADC_{b0\text{-}100\text{-}300\text{-}500\text{-}800}$, $ADC_{b0\text{-}1000}$ and $ADC_{b0\text{-}200\text{-}1000}$, respectively. The mean value of mean ADC in cytologically malignant nodes was 0.721 × 10^{-3} mm^2/s (SD 0.229), 0.834 × 10^{-3} mm^2/s (SD 0.206) and 0.817 × 10^{-3} mm^2/s (SD 0.185) for $ADC_{b0\text{-}100\text{-}300\text{-}500\text{-}800}$, $ADC_{b0\text{-}1000}$ and $ADC_{b0\text{-}200\text{-}1000}$, respectively (Tables 2 and 3).

Table 2. Difference in minimum ADC between cytologically malignant and benign PET-positive nodes.

ADC		Malignant Nodes		Benign Nodes		Significance
Dataset	**Measurement**	***N***	**Mean (sd)**	***N***	**Mean (sd)**	***p*** [1]
Full	ADC 1 [2]	12	0.444 (0.186)	12	0.562 (0.179)	0.138
	ADC 2 [3]	79	0.645 (0.188)	64	0.625 (0.201)	0.620
	ADC 3 [4]	78	0.625 (0.199)	64	0.609 (0.172)	0.666
No HPV	ADC 1 [2]	2	0.381 (0.078)	0		
	ADC 2 [3]	13	0.570 (0.239)	10	0.645 (0.204)	0.086
	ADC 3 [4]	13	0.554 (0.236)	10	0.665 (0.200)	0.031
HPV	ADC 1 [2]	2	0.587 (0.163)	4	0.439 (0.157)	0.132
	ADC 2 [3]	34	0.654 (0.177)	17	0.660 (0.214)	0.996
	ADC 3 [4]	34	0.640 (0.199)	17	0.605 (0.174)	0.434

[1] *p*-value based on *F*-test for the factor variable malignancy in a linear mixed effects model with ADC as the dependent variable, and a random intercept for patients. [2] ADC1 = $ADC_{b0\text{-}b100\text{-}b300\text{-}b500\text{-}b800}$. [3] ADC2 = $ADC_{b0\text{-}b1000}$. [4] ADC3 = $ADC_{b0\text{-}b200\text{-}b1000}$.

Table 3. Difference in mean ADC between cytologically malignant and benign PET-positive nodes.

ADC		Malignant Nodes		Benign Nodes		Significance
Dataset	**Measurement**	**N**	**Mean (sd)**	**N**	**Mean (sd)**	***p*** [1]
Full	ADC 1 [2]	12	0.721 (0.229)	12	0.842 (0.154)	0.400
	ADC 2 [3]	79	0.834 (0.206)	64	0.847 (0.201)	0.605
	ADC 3 [4]	78	0.817 (0.185)	64	0.806 (0.198)	0.747
No HPV	ADC 1 [2]	2	0.602 (0.069)	0		
	ADC 2 [3]	13	0.780 (0.293)	10	0.920 (0.213)	0.018
	ADC 3 [4]	13	0.772 (0.298)	10	0.852 (0.199)	0.132
HPV	ADC 1 [2]	2	0.753 (0.227)	4	0.761 (0.125)	0.256
	ADC 2 [3]	34	0.842 (0.215)	17	0.819 (0.217)	0.683
	ADC 3 [4]	34	0.838 0.169	17	0.770 (0.182)	0.174

[1] *p*-value based on *F*-test for the factor variable malignancy in a linear mixed effects model with ADC as the dependent variable, and a random intercept for patients. [2] ADC1 = $ADC_{b0\text{-}b100\text{-}b300\text{-}b500\text{-}b800}$. [3] ADC2 = $ADC_{b0\text{-}b1000}$. [4] ADC3 = $ADC_{b0\text{-}b200\text{-}b1000}$.

For cytologically benign nodes, the mean minimum ADC values were 0.562×10^{-3} mm^2/s (SD 0.179), 0.625×10^{-3} mm^2/s (SD 0.201) and 0.617×10^{-3} mm^2/s (SD 0.174), for $ADC_{b0\text{-}100\text{-}300\text{-}500\text{-}800}$, $ADC_{b0\text{-}1000}$ and $ADC_{b0\text{-}200\text{-}1000}$, respectively. The mean values of mean ADC were 0.842×10^{-3} mm^2/s (SD 0.154), 0.847×10^{-3} mm^2/s (SD 0.201) and 0.806×10^{-3} mm^2/s (SD 0.198), for $ADC_{b0\text{-}100\text{-}300\text{-}500\text{-}800}$, $ADC_{b0\text{-}1000}$ and $ADC_{b0\text{-}200\text{-}1000}$, respectively. No significant overall difference in ADC between malignant and benign nodes was observed. In the subgroup of non-HPV-related nodes, there was a significant difference for minimum $ADC_{b0\text{-}200\text{-}1000}$, with mean values of 0.554 and 0.665 for cytologically malignant and cytologically benign nodes, respectively (p = 0.03), and for mean $ADC_{b0\text{-}200\text{-}1000}$ there was a significant difference, with mean ADC values of 0.780 and 0.923 for cytologically malignant and cytologically benign nodes, respectively (p = 0.02). Among HPV-related nodes, no significant differences were observed.

With $ADC_{b0\text{-}1000}$, we observed a significantly higher ADC in the PET-negative reference nodes compared to both cytologically malignant PET-positive nodes (minimum ADC difference 0.06, p = 0.05; mean ADC difference 0.2, <0.001) and cytologically benign PET-positive nodes (minimum ADC difference 0.10, p = 0.02; mean ADC difference 0.10, p = 0.004). Only with mean $ADC_{b0\text{-}200\text{-}1000}$, we observed a

significantly higher ADC in the PET-negative reference nodes compared to both cytologically malignant (difference 0.12, p = 0.003;) and cytologically benign (difference 0.10, p = 0.007) PET-positive nodes (Tables 4 and 5).

Table 4. Difference in minimum ADC values between the PET-negative reference node and PET-positive nodes.

ADC		Malignant Nodes			Benign Nodes		
Dataset	**Measurement**	***N***	**Difference[1], Mean (sd)**	***p*** [2]	***N***	**Difference, Mean (sd)**	***p*** [2]
Full	ADC 1 [3]	12	−0.164 (0.291)	0.192	12	−0.089 (0.286)	0.301
	ADC 2 [4]	79	−0.063 (0.279)	0.050	64	−0.095 (0.275)	0.018
	ADC 3 [5]	78	−0.044(0.278)	0.083	64	−0.088 (0.277)	0.016
No HPV	ADC 1 [3]	2	−0.706 (0.078)	0.140	0		
	ADC 2 [4]	13	−0.236 (0.384)	0.155	10	−0.127 (0.198)	0.275
	ADC 3 [5]	13	−0.113 (0.273)	0.301	10	0.035 (0.194)	0.601
HPV	ADC 1 [3]	2	−0.128 (0.152)	0.355	4	−0.169 (0.278)	0.227
	ADC 2 [4]	34	−0.002 (0.233)	0.721	17	−0.161 (0.377)	0.184
	ADC 3 [5]	34	0.002 (0.275)	0.637	17	−0.208 (0.280)	0.030

[1] ADC of node minus ADC of reference node. [2] p-value based on F-test for the factor variable malignancy in a linear mixed effects model with ADC as the dependent variable, and a random intercept for patients. [3] ADC1 = $ADC_{b0\text{-}b100\text{-}b300\text{-}b500\text{-}b800}$. [4] ADC2 = $ADC_{b0\text{-}b1000}$. [5] ADC3 = $ADC_{b0\text{-}b200\text{-}b1000}$.

Table 5. Difference in mean ADC values between the PET-negative reference node and PET-positive nodes.

ADC		Malignant Nodes			Benign Nodes		
Dataset	**Measurement**	***N***	**Difference[1], Mean (sd)**	***p*** [2]	***N***	**Difference [1], Mean (sd)**	***p*** [2]
Full	ADC 1 [3]	12	−0.166 (0.366)	0.201	12	−0.102 (0.196)	0.189
	ADC 2 [4]	79	−0.151 (0.289)	<0.001	64	−0.102 (0.263)	0.004
	ADC 3 [5]	78	−0.117 (0.277)	0.003	64	−0.101 (0.288)	0.007
No HPV	ADC 1 [3]	2	−0.860 (0.069)	0.101	0		
	ADC 2 [4]	13	−0.258 (0.382)	0.125	10	−0.022 (0.217)	0.953
	ADC 3 [5]	13	−0.163 (0.347)	0.247	10	−0.013 (0.191)	0.893
HPV	ADC 1 [3]	2	−0.134 (0.153)	0.341	4	−0.090 (0.067)	0.135
	ADC 2 [4]	34	−0.099 (0.284)	0.087	17	−0.248 (0.326)	0.010
	ADC 3 [5]	34	−0.049 (0.252)	0.257	17	−0.255 (0.316)	0.011

[1] ADC of node minus ADC of reference node. [2] p-value based on F-test for the factor variable malignancy in a linear mixed effects model with ADC as the dependent variable, and a random intercept for patients. [3] ADC1 = $ADC_{b0\text{-}b100\text{-}b300\text{-}b500\text{-}b800}$. [4] ADC2 = $ADC_{b0\text{-}b1000}$. [5] ADC3 = $ADC_{b0\text{-}b200\text{-}b1000}$.

Minimum $ADC_{b0\text{-}200\text{-}1000}$ also differed significantly between the PET-negative reference nodes and benign PET-positive nodes (p = 0.02). In the subgroup of HPV-related nodes, minimum $ADC_{b0\text{-}1000}$ differed significantly between the PET-negative reference nodes and benign PET-positive nodes (p = 0.03), and also mean ADC differed significantly for $ADC_{b0\text{-}1000}$ (p = 0.01) and $ADC_{b0\text{-}200\text{-}1000}$ (p = 0.01). No strong correlations were observed between minimum ADC and SUVmax or minimum ADC and axial node diameter. A moderate negative correlation was found between SUVmax and a minimum $ADC_{b0\text{-}100\text{-}300\text{-}500\text{-}800}$, and mild negative correlation was found for all calculated mean ADC and between all mean ADC and axial node diameter (Figure 2 and Table 6).

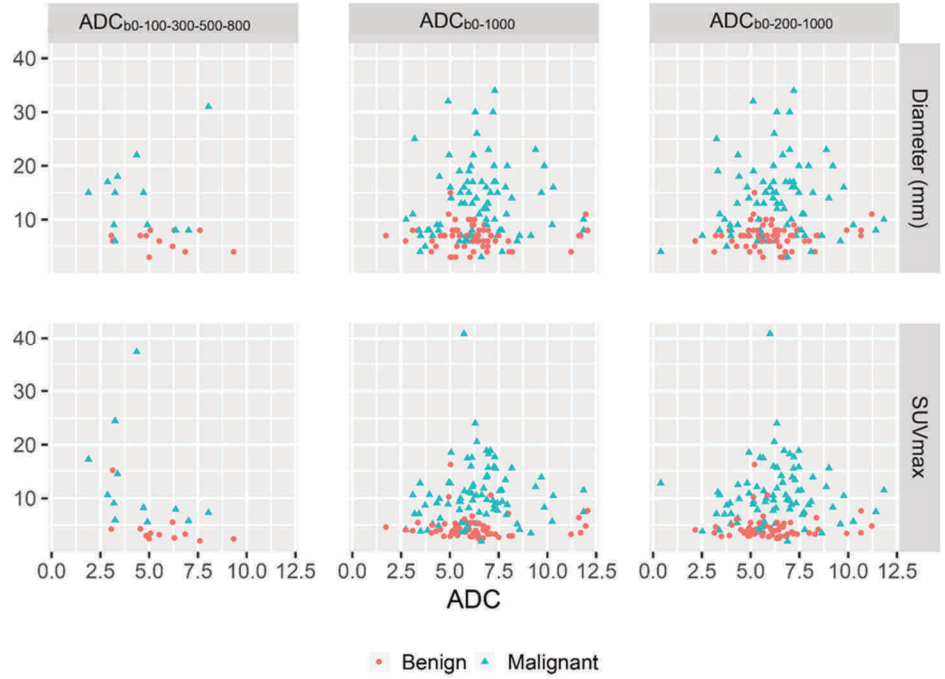

Figure 2. Relationship between ADC and SUVmax, and between ADC and axial node diameter.

Table 6. Correlations between ADC and SUVmax, and between ADC and axial node diameter.

Variable 1	Variable 2	Pearson Correlation Minimum ADC	Pearson Correlation Mean ADC
ADC 1 [1]	SUVmax	−0.45	−0.30
ADC 2 [2]	SUVmax	0.07	−0.06
ADC 3 [3]	SUVmax	0.06	−0.04
ADC 1	Diameter	−0.12	−0.18
ADC 2	Diameter	0.07	−0.04
ADC 3	Diameter	0.09	−0.01

[1] ADC1 = $ADC_{b0\text{-}b100\text{-}b300\text{-}b500\text{-}b800}$. [2] ADC2 = $ADC_{b0\text{-}b1000}$. [3] ADC3 = $ADC_{b0\text{-}b200\text{-}b1000}$.

4. Discussion

Accurate nodal staging is essential for individual treatment planning. With functional imaging, not only anatomical changes, but also metabolic changes in metastases can be detected. As shown in meta-analyses of HNSCC patients, PET-CT has better performance in the detection of metastases than anatomical imaging [24,25]. However, the performance of PET-CT in patients with clinically node-negative neck is poor, with a reported sensitivity of 50–58% [13,26]. Small PET-positive reactive nodes are difficult to distinguish from metastatic nodes, meaning a large number of punctures are requested to improve the sensitivity of imaging.

Due to tumor growth, metastatic nodes often have a higher metabolism and therefore higher FDG uptake. Due to increased cellularity in metastases, DWI is more restricted, which results in a lower ADC.

Significant associations between PET, dynamic contrast-enhanced MRI and DWI parameters have been demonstrated, which indicate a relationship between tumor cellularity, vascular permeability and glucose metabolism in HNSCC [27]. Nakajo et al. demonstrated a significant inverse correlation between FDG uptake and ADC [20]; however, this effect was not observed in other studies [28,29].

In our study, we observed a mild inverse relationship between ADC and SUVmax.

A previous meta-analysis in HNSCC patients showed high diagnostic performance of DW-MRI as a tool to differentiate malignant nodes from benign nodes [30].

Because of real-time image fusion, we were able to compare ADC between truly PET-positive cytologically proven malignant and benign nodes.

Compared to the PET-negative reference nodes, minimum $ADC_{b0\text{-}1000}$ and mean $ADC_{b0\text{-}1000}$ and mean $ADC_{b\text{-}0\text{-}200\text{-}100}$ were significantly lower for both cytologically malignant and cytologically benign PET-positive nodes.

Although we found a significantly lower ADC in malignant PET-positive nodes compared to PET-negative reference nodes, we did not find a significantly lower ADC in cytologically malignant PET-positive nodes than in cytologically benign PET-positive nodes for the whole group. A possible explanation for the observation that we did not find a lower ADC in cytologically malignant PET-positive lymph nodes when compared to cytologically benign PET-positive lymph nodes could be that in reactive lymph nodes, the primary follicles consisting of loose aggregates of small lymphocytes become secondary or reactive lymphoid follicles with low ADC. These consist of a heterogeneous population of highly proliferative lymphoid cells, follicular dendritic cells and histiocytes that form close cellular interactions [31]. Therefore, a lower ADC might be observed not only in cytologically malignant nodes, but also in cytologically benign PET-positive reactive nodes. Our study suggests that when using DW-MRI, we still have the same problem where we were not able to distinguish small metastatic lymph nodes from reactive (PET-positive) lymph nodes. We found a mild inverse relationship between FDG uptake and ADC values. In a previous study, we were able to show that using a low SUVmax cut-off value can help to improve node selection [15]. It would be interesting to investigate whether we are able to define a cut-off value for ADC values and relationship to SUVmax cut values. A study with a larger number of patients would be required in order to address this point. Another possible explanation could be that some of the cytologically benign cases were (in part) false negative cytologies, with very small metastases.

However, we found significantly lower ADC in non-HPV-related cytologically malignant PET-positive nodes as compared to cytologically benign PET-positive nodes. It has to be mentioned that only a limited number (36) of HPV-related patients were included in our study. To investigate the possible differences between ADC values of malignant and benign nodes in subgroups according to HPV status, a study with a larger number of included patients should be performed.

These significant findings indicate that the measurement of ADC might be helpful to differentiate between small malignant HPV-related PET-positive and reactive PET-positive nodes, and this implies that if a node is PET-positive, then DW-MRI will improve node selection for puncture..

Limitations

$ADC_{b0\text{-}200\text{-}1000}$ and $ADC_{b0\text{-}1000}$ measurements to calculate ADC values were performed in the same nodes, and for all nodes, results did not differ between $ADC_{b0\text{-}200\text{-}1000}$ and $ADC_{b0\text{-}1000}$, and the use of these two different maps did not affect the outcome. However in the subgroup of non-HPV-related nodes, we found that only in the case of minimum $ADC_{b0\text{-}200\text{-}1000}$ and mean $ADC_{b0\text{-}200\text{-}1000}$, a significantly lower ADC in cytologically malignant PET-positive nodes compared to cytologically benign PET-positive nodes could be observed. Since $ADC_{b0\text{-}100\text{-}300\text{-}500\text{-}800}$ was only available for 12 patients, we have not been able to show if $ADC_{b0\text{-}100\text{-}300\text{-}500\text{-}800}$ would have a better diagnostic performance, but mainly $ADC_{b0\text{-}100\text{-}300\text{-}500\text{-}800}$ showed a mild inverse relationship between ADC and SUVmax. It would be interesting to investigate this relationship using a larger cohort of patients.

We did not have histopathological results available in order to have a reference standard, but we did have cytological results of real-time fused USgFNAC. FNAC can produce false negative results. To minimize false negative results, USgFNAC should be repeated and distrusted in nodes predicted to be malignant on PET-FT or MRI. However, it should be borne in mind that very small metastases (micro metastases) cannot really be made visible on either PET-CT or MRI-DWI. Moreover, the cytology in these lymph nodes with small metastases is often either non-diagnostic or (false) negative. Because all FNAC was guided by real-time image-fused PET-CT and US, ADC and SUVmax measurements could take place in well-defined cytologically malignant and benign nodes.

5. Conclusions

We found a mild negative correlation between SUVmax and ADC and a significantly higher ADC in PET-negative reference nodes than in PET-positive nodes. In HPV-negative HNSCCs, we found significantly lower ADC values in cytologically malignant PET-positive nodes than in cytologically benign lymph nodes (p = 0.03), although this was only observed for one of the ADC modalities and was based on a small number of patients. In HPV-positive tumors, this difference was not

significant. In non-HPV-related HNSCCs, DW-MRI might therefore help to select which nodes to aspirate from and might increase the accuracy of FDG PET-CT.

Author Contributions: P.K.d.K.-D.: conception or design of the work, data collection, drafting of the article, critical revision of the article, final approval of the version to be published; S.R.: data analysis and interpretation, critical revision of the article; final approval of the version to be published; L.S.: critical revision of the article; W.V.V.: critical revision of the article; R.B.-T.: critical revision of the article; M.W.v.d.B.: critical revision of the article, final approval of the version to be published; J.C.: critical revision of the article, final approval of the version to be published. All authors have read and agreed to the published version of the manuscript.

Funding: This research received no external funding.

Institutional Review Board Statement: The study was conducted in accordance with the Declaration of Helsinki, and approved by NKI-AVL Institutional Review Board (IRBd21-074).

Informed Consent Statement: Data were analyzed retrospectively. All retrospective medical data/biospecimen studies at the Netherlands Cancer Institute have been executed pursuant to Dutch legislation and international standards. Prior to 25 May 2019, national legislation on data protection was applied, as well as the International Guideline on Good Clinical Practice. From 25 May 2019, we also adhered to the GDPR. Within this framework, patients are informed and have always had the opportunity to object or actively consent to the (continued) use of their personal data and biospecimens in research. None of the patients included in this study objected to use of their data.

Data Availability Statement: The data used to support the findings of this study are available from the corresponding author upon request.

Acknowledgments: The authors would like to acknowledge Pedro Sanches and Frans Gleuwink (Philips Benelux, Boschdijk 525, 5621JG Eindhoven) for providing knowledge and use of the eL18-4 transducer, Jacques Meininger for helping with the layout and Jonathan Vosper for correcting English language and style.

Conflicts of Interest: The authors have no conflict of interest to declare that is relevant to the content of this article.

References

1. Singh, P.; Contente, M.; Bennett, B.; Hall, J.; Bailey, H.; Bailey, A.; Zarrelli, L.; Sanchez, C.P. Real-World Treatment Patterns and Outcomes in Patients with Head and Neck Cancer: Point-in-Time Survey of Oncologists in Italy and Spain. *Adv. Ther.* **2021**, *38*, 4722–4735. https://doi.org/10.1007/s12325-021-01851-2.

2. Kelly, H.R.; Curtin, H.D. Chapter 2 Squamous Cell Carcinoma of the Head and Neck—Imaging Evaluation of Regional Lymph Nodes and Implications for Management. *Semin. Ultrasound CT MRI* **2017**, *38*, 466–478. https://doi.org/10.1053/j.sult.2017.05.003.

3. Lodder, W.; Pameijer, F.; Rasch, C.; Brekel, M.V.D.; Balm, A. Prognostic significance of radiologically determined neck node volume in head and neck cancer: A systematic review. *Oral Oncol.* **2012**, *48*, 298–302. https://doi.org/10.1016/j.oraloncology.2011.11.001.

4. van den Brekel, M.W.; Castelijns, J.A. What the clinician wants to know: Surgical perspective and ultrasound for lymph node imaging of the neck. *Cancer Imaging* **2005**, *5*, S41–S49. https://doi.org/10.1102/1470-7330.2005.0028.

5. Liao, L.-J.; Lo, W.-C.; Hsu, W.-L.; Wang, C.-T.; Lai, M.-S. Detection of cervical lymph node metastasis in head and neck cancer patients with clinically N0 neck—a meta-analysis comparing different imaging modalities. *BMC Cancer* **2012**, *12*, 236–236. https://doi.org/10.1186/1471-2407-12-236.

6. Chaturvedi, P.; Datta, S.; Arya, S.; Rangarajan, V.; Kane, S.V.; Nair, D.; Nair, S.V.; Chaukar, D.A.; Pai, P.S.; Pantvaidya, G.; et al. Prospective study of ultrasound-guided fine-needle aspiration cytology and sentinel node biopsy in the staging of clinically negative T1 and T2 oral cancer. *Head Neck* **2014**, *37*, 1504–1508. https://doi.org/10.1002/hed.23787.

7. De Bondt, R.; Nelemans, P.; Hofman, P.; Casselman, J.; Kremer, B.; van Engelshoven, J.; Beets-Tan, R. Detection of lymph node metastases in head and neck cancer: A meta-analysis comparing US, USgFNAC, CT and MR imaging. *Eur. J. Radiol.* **2007**, *64*, 266–272. https://doi.org/10.1016/j.ejrad.2007.02.037.

8. Van den Brekel, M.W. Lymph node metastases: CT and MRI. *Eur. J. Radiol*. **2000**, *33*, 230–238.

9. Brekel, M.W.V.D.; Stel, H.V.; Castelijns, J.A.; Nauta, J.J.; Van Der Waal, I.; Valk, J.; Meyer, C.J.; Snow, G.B. Cervical lymph node metastasis: Assessment of radiologic criteria. *Radiology* **1990**, *177*, 379–384. https://doi.org/10.1148/radiology.177.2.2217772.

10. Ying, M.; Ahuja, A.T.; Metreweli, C. Diagnostic accuracy of sonographic criteria for evaluation of cervical lymphadenopathy. *J. Ultrasound Med.* **1998**, *17*, 437–445. https://doi.org/10.7863/jum.1998.17.7.437.

11. Van den Brekel, M.W.; Castelijns, J.A.; Snow, G.B. The size of lymph nodes in the neck on sonograms as a radiologic criterion for metastasis: How reliable is it? *Am. J. Neuroradiol.* **1998**, *19*, 695–700.

12. Chammas, M.C.; Macedo, T.A.A.; Lo, V.W.; Gomes, A.C.; Juliano, A.; Cerri, G.G. Predicting malignant neck lymphadenopathy using color duplex sonography based on multivariate analysis. *J. Clin. Ultrasound* **2016**, *44*, 587–594. https://doi.org/10.1002/jcu.22380.

13. Kyzas, P.A.; Evangelou, E.; Denaxa-Kyza, D.; Ioannidis, J.P.A. 18F-Fluorodeoxyglucose Positron Emission Tomography to Evaluate Cervical Node Metastases in Patients with Head and Neck Squamous Cell Carcinoma: A Meta-analysis. *JNCI: J. Natl. Cancer Inst.* **2008**, *100*, 712–720. https://doi.org/10.1093/jnci/djn125.

14. De Koekkoek-Doll, P.; Maas, M.; Vogel, W.; Castelijns, J.; Smit, L.; Zavrakidis, I.; Beets-Tan, R.; Brekel, M.V.D. Real-Time Ultrasound Image Fusion with FDG-PET/CT to Perform Fused Image-Guided Fine-Needle Aspiration in Neck Nodes: Feasibility and Diagnostic Value. *Am. J. Neuroradiol.* **2021**, *42*, 566–572. https://doi.org/10.3174/ajnr.a6938.

15. De Koekkoek-Doll, P.K.; Vogel, W.; Maas, M.; Castelijns, J.; Smit, L.; Zavrakidis, J.; Beets-Tan, R.; van den Brekel, M. SUVmax values at FDG PET-CT to predict malignancy in lymph nodes aspirated by real time image fused USgFNAC in head and neck squamous cell carcinoma. *Am. J. Nucl. Med. Mol. Imaging* **2021**, *11*, 178.

16. Sant, I.V.; Van Eden, W.J.; Engbersen, M.; Kok, N.F.M.; Woensdregt, K.; Lambregts, D.M.J.; Shanmuganathan, S.; Beets-Tan, R.G.H.; Aalbers, A.G.J.; Lahaye, M.J. Diffusion-weighted MRI assessment of the peritoneal cancer index before cytoreductive surgery. *Br. J. Surg.* **2018**, *106*, 491–498. https://doi.org/10.1002/bjs.10989.

17. Beets-Tan, R.G.H.; Beets, G. MRI for assessing and predicting response to neoadjuvant treatment in rectal cancer. *Nat. Rev. Gastroenterol. Hepatol.* **2014**, *11*, 480–488. https://doi.org/10.1038/nrgastro.2014.41.

18. Vandecaveye, V.; De Keyzer, F.; Poorten, V.V.; Dirix, P.; Verbeken, E.; Nuyts, S.; Hermans, R. Head and Neck Squamous Cell Carcinoma: Value of Diffusion-weighted MR Imaging for Nodal Staging. *Radiology* **2009**, *251*, 134–146. https://doi.org/10.1148/radiol.2511080128.

19. Barchetti, F.; Pranno, N.; Giraldi, G.; Sartori, A.; Gigli, S.; Barchetti, G.; Mele, L.L.; Marsella, L.T. The Role of 3 Tesla Diffusion-Weighted Imaging in the Differential Diagnosis of Benign versus Malignant Cervical Lymph Nodes in Patients with Head and Neck Squamous Cell Carcinoma. *BioMed Res. Int.* **2014**, *2014*, 532095. https://doi.org/10.1155/2014/532095.

20. Nakajo, M.; Nakajo, M.; Kajiya, Y.; Tani, A.; Kamiyama, T.; Yonekura, R.; Fukukura, Y.; Matsuzaki, T.; Nishimoto, K.; Nomoto, M.; et al. FDG PET/CT and diffusion-weighted imaging of head and neck squamous cell carcinoma: Comparison of prognostic significance between primary tumor standardized uptake value and apparent diffusion coefficient. *Clin. Nucl. Med.* **2012**, *37*, 475–480. https://doi.org/10.1097/rlu.0b013e318248524a.

21. Kobayashi, K.; Hisamatsu, K.; Suzui, N.; Hara, A.; Tomita, H.; Miyazaki, T. A Review of HPV-Related Head and Neck Cancer. *J. Clin. Med.* **2018**, *7*, 241. https://doi.org/10.3390/jcm7090241.

22. Kendi, A.T.K.; Magliocca, K.; Corey, A.; Nickleach, D.C.; Galt, J.; Higgins, K.; Beitler, J.J.; El-Deiry, M.W.; Wadsworth, J.T.; Hudgins, P.A.; et al. Do 18F-FDG PET/CT Parameters in Oropharyngeal and Oral Cavity Squamous Cell Carcinomas Indicate HPV Status? *Clin. Nucl. Med.* **2015**, *40*, e196–e200. https://doi.org/10.1097/rlu.0000000000000691.

23. Payabvash, S.; Chan, A.; Maralani, P.J.; Malhotra, A. Quantitative diffusion magnetic resonance imaging for prediction of human papillomavirus status in

head and neck squamous-cell carcinoma: A systematic review and meta-analysis. *Neuroradiol. J.* **2019**, *32*, 232–240. https://doi.org/10.1177/1971400919849808.

24. Sun, R.; Tang, X.; Yang, Y.; Zhang, C. 18FDG-PET/CT for the detection of regional nodal metastasis in patients with head and neck cancer: A meta-analysis. *Oral Oncol.* **2015**, *51*, 314–320. https://doi.org/10.1016/j.oraloncology.2015.01.004.

25. Yongkui, L.; Jian, L.; Wanghan; Jingui, L. 18FDG-PET/CT for the detection of regional nodal metastasis in patients with primary head and neck cancer before treatment: A meta-analysis. *Surg. Oncol.* **2013**, *22*, e11–e16. https://doi.org/10.1016/j.suronc.2013.02.002.

26. Kim, S.J.; Pak, K.; Kim, K. Diagnostic accuracy of F-18 FDG PET or PET/CT for detection of lymph node metastasis in clinically node negative head and neck cancer patients. A systematic review and meta-analysis. *Am. J. Otolaryngol. Head Neck Med. Surg.* **2019**, *40*, 297–305.

27. Bülbül, H.M.; Bülbül, O.; Sarıoğlu, S.; Özdoğan, Ö.; Doğan, E.; Karabay, N. Relationships Between DCE-MRI, DWI, and ^{18}F-FDG PET/CT Parameters with Tumor Grade and Stage in Patients with Head and Neck Squamous Cell Carcinoma. *Mol. Imaging Radionucl. Ther.* **2021**, *30*, 177–186. https://doi.org/10.4274/mirt.galenos.2021.25633.

28. Zhang, L.; Song, T.; Meng, Z.; Huang, C.; Chen, X.; Lu, J.; Xian, J. Correlation between apparent diffusion coefficients and metabolic parameters in hypopharyngeal squamous cell carcinoma: A prospective study with integrated PET/MRI. *Eur. J. Radiol.* **2020**, *129*, 109070. https://doi.org/10.1016/j.ejrad.2020.109070.

29. Fruehwald-Pallamar, J.; Czerny, C.; Mayerhoefer, M.E.; Halpern, B.S.; Eder-Czembirek, C.; Brunner, M.; Schuetz, M.; Weber, M.; Fruehwald, L.; Herneth, A.M. Functional imaging in head and neck squamous cell carcinoma: Correlation of PET/CT and diffusion-weighted imaging at 3 Tesla. *Eur. J. Pediatr.* **2011**, *38*, 1009–1019. https://doi.org/10.1007/s00259-010-1718-4.

30. Suh, C.; Choi, Y.; Baek, J.H.; Lee, J. The Diagnostic Value of Diffusion-Weighted Imaging in Differentiating Metastatic Lymph Nodes of Head and Neck

Squamous Cell Carcinoma: A Systematic Review and Meta-Analysis. *Am. J. Neuroradiol.* **2018**, *39*, 1889–1895. https://doi.org/10.3174/ajnr.a5813.

31. Medeiros, L.D. Ioachim, H.L. *Ioachim's Lymph Node Pathology*, 5th ed.; Lippincott Williams & Wilkins: Philadelphia, PA, USA, 2022; ISBN: 978-1-45-119357-2.

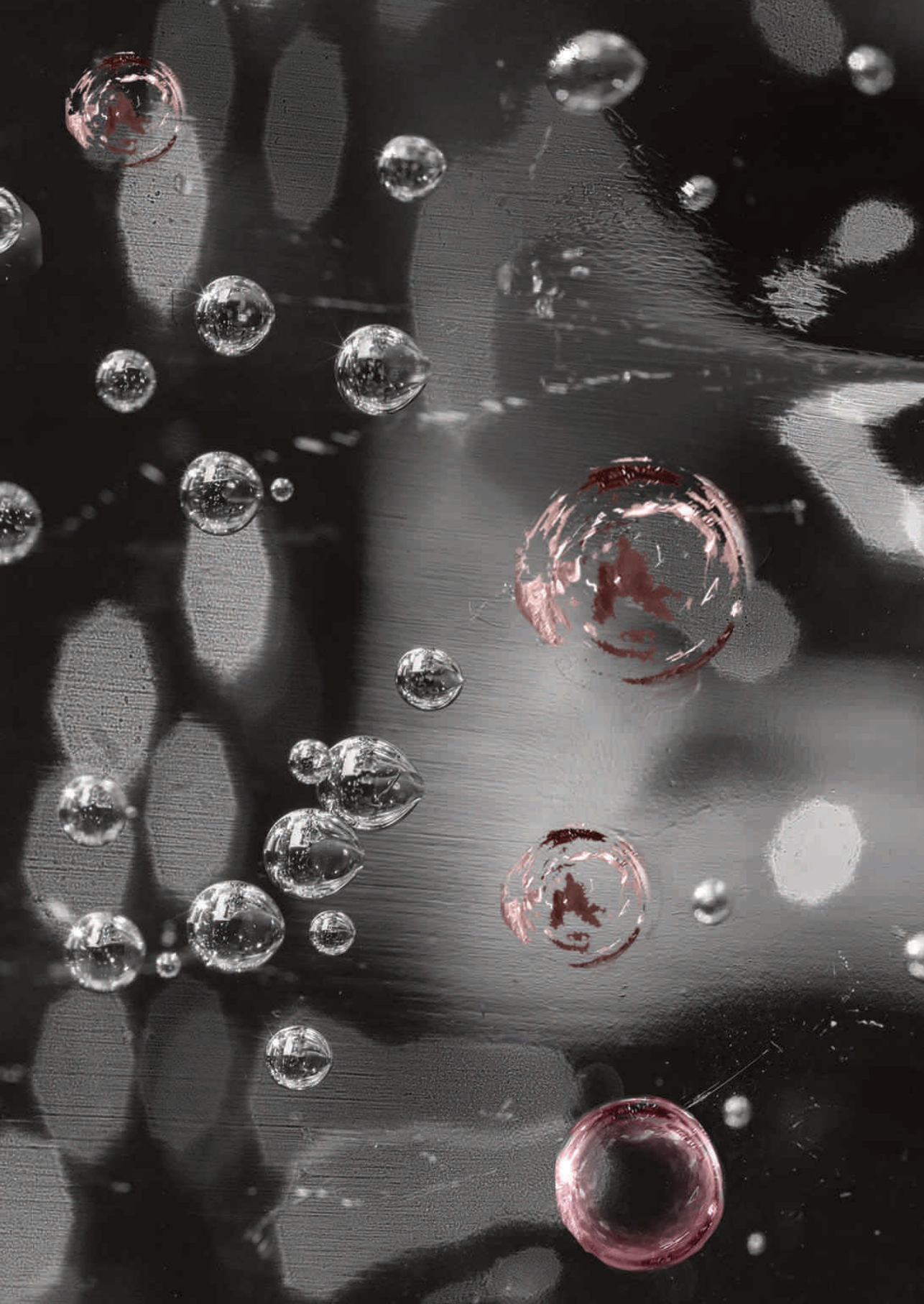

CHAPTER 5

Value of Assessing Peripheral Vascularization With Micro-flow Imaging, Resistive Index and Absent Hilum Sign as Predictor for Malignancy in Lymph Nodes in Head and Neck Squamous Cell Carcinoma

Petra K. de Koekkoek-Doll , Sander Roberti , Michiel W. van den Brekel , Monique Maas, Laura Smit, Regina Beets-Tan, Jonas Castelijns

Published in Cancers

Oct. 2021; 13, 5071

Cancers 2021.13,571. https://doi.org/10.3390/cancers13205071

Simple Summary:

Ultrasound-guided fine needle aspiration cytology (USgFNAC) is commonly used for N-staging in head and neck squamous cell carcinoma (HNSCC). The specificity of USgFNAC is always in the order of 100% as false positive cytology is rare. The difference in sensitivity is mainly attributable to selection of the lymph nodes to aspirate and aspiration technique. The aim of this study was to improve the selection criteria of lymph nodes to aspirate. Ultrasound features of nodes such as a short axis diameter, S/L ratio, loss of a fatty hilum sign, resistive index, and peripheral or mixed hilar and peripheral vascularization, obtained by Micro-flow imaging (MFI), which is a new technique to obtain micro-vascularization, were evaluated. To calculate the sensitivity and PPV of each feature, data of sonographic findings and cytological results of all aspirated nodes were statistically analyzed. We found that next to size, peripheral vascularization obtained by MFI and absent hilum sign have a high predictive value for malignancy and should be added as selection criteria for fine needle aspiration in lymph nodes

Abstract:

Background and Purpose: Ultrasound-guided fine needle aspiration cytology (USgFNAC) is commonly used for nodal staging in head and neck squamous cell cancer (HNSCC). Peripheral vascularity is a described feature for node metastasis. Micro-flow imaging (MFI) is a new sensitive technique to evaluate micro-vascularization. Our goal is to assess the additional value of MFI to detect malignancy in lymph nodes.

Material and Method: A total of 102 patients with HNSCC were included prospectively. USgFNAC was performed with the Philips eL18–4 transducer. Cytological results served as a reference standard to evaluate the prediction of cytological malignancy depending on ultrasound features such as resistive index (RI), absence of fatty hilum sign, and peripheral vascularization. Results were obtained for all US examinations and for the subgroup of clinically node-negative neck (cN0).

Result: USgFNAC was performed in 211 nodes. Peripheral vascularization had a positive predictive value (PPV) of 83% (cN0: 50%) and the absence of a fatty hilum had a PPV of 82% (cN0 50%) The combination of peripheral vascularization and absent fatty hilum had a PPV of 94% (cN0: 72%). RI (threshold: 0.705) had a PPV of

61% (cN0: RI-threshold 0.615, PPV 20%), whereas the PPV of short axis diameter (threshold of 6.5mm) was 59% for all patients and 19% in cN0 necks (threshold of 4 mm).

Conclusion: Peripheral vascularization assessed by MFI and absent hilum has a high predictive value for cytological malignancy in neck metastases. Next to size, both features should be used as additional selection criteria for USgFNAC.

Keywords: SCC; Head and Neck; Lymph nodes; Ultrasound; Micro-flow imaging; Hilum sign; Resistive Index

1. Introduction

One of the most important predictors for the survival of patients with head and neck squamous cell carcinoma (HNSCC) is the nodal status [1]. Metastatic disease that spreads from the primary lymph node to distant organs causes 90% of all HNSCC deaths. Accurate staging is therefore essential for prognostication and optimal treatment planning with the goal to obtain the best cure and avoid treatment morbidity [2,3].

Neck palpation for lymph nodes in patients with HNSSC has a sensitivity and specificity to detect metastatic disease of 60–70% [4]. That means that around 30 to 40% of the nodal metastases are clinically occult (cN0).

Commonly used imaging tools to detect these occult metastases are ultrasound (US), magnetic resonance imaging (MRI), contrast enhanced computer tomography (CT), FDG PET-CT, and ultrasound-guided fine needle aspiration-cytology (USgFNAC). MRI and CT are frequently used to stage the primary tumor and neck, but use morphological criteria for metastases with a relatively low accuracy (74–78%) [5]. 18FDG PET-CT enables, next to the morphological criteria, use of metabolic criteria, and is reported to be superior to MRI and CT with a sensitivity and specificity of 84% and 96%, respectively [6]. However, for cN0 neck, with only small metastases, the sensitivity is in the range of 40–60% and thus not very high [7].

USgFNAC can reduce the risk from an initial risk of occult metastases of 40% to a risk of 10–20%, which can be considered acceptable to refrain from elective treatment, although this remains a controversial topic [8].

High-resolution US to guide FNAC is an important diagnostic tool and well established. Gray scale ultrasound enables assessment of morphological criteria such as nodal size, nodal boundary, cystic transformation, or other internal reflective patterns, fatty hilum sign, surrounding edema, or infiltration of the surrounding tissue [9–11].

Power Doppler sonography has been shown to be a reliable method for the assessment of the vascularity of cervical lymph nodes. [12] It allows to evaluate the pattern of the intra-nodular macro vascularization and to measure the resistive index (RI). It has been shown that normal lymph nodes have a hilar vascularity while metastatic nodes may have a peripheral or mixed hilar and

peripheral vascularity [13,14]. The RI is reported to be higher in metastatic nodes than in reactive lymph nodes. In a recent review, Ying at al described an optimal cut-off for RI at 0.7 for differentiating between metastatic and reactive lymph nodes, with a sensitivity of 47–81% and a specificity of 81–100% [15]. Because Doppler ultrasound techniques display the changes of macro vascularization, vascularity is often not detected in small lymph nodes [16].

Micro-flow imaging (MFI) is a relatively new mode designed to detect small vessel flow with high resolution and minimal artefacts. Recent studies have shown that MFI has a higher sensitivity to detect tumoral vascularity compared with color Doppler imaging (CDI) and power Doppler imaging (PDI) [17–19]. MFI can also improve the visualization of peripheral vascularization in neck lymph nodes as a feature of metastasis. To our knowledge the value of MFI has not been examined in cervical lymph nodes.

The aim of this study was to evaluate the additional value of peripheral vascularization in lymph nodes as assessed by MFI as a criterion to diagnose metastasis or select lymph nodes to be punctured by USgFNAC next to other criteria such as nodal size, fatty hilum sign, and RI obtained in the same nodes.

2. Materials and Methods

2.1. Patients

A total of 102 patients with histopathologically proven HNSCC were included prospectively; data were analyzed retrospectively. All patients were referred for nodal staging (N-staging) by USgFNAC. USgFNAC was performed in all suspicious nodes as in a usual clinically setting. The median age was 65 years (range: 34–87yrs); 27/102 (26%) patients were female, and 73/102 (72%) patients were male. (Table 1)

Table 1. Patient data.

	All cN Stages			cN0-Stage		
	Total	**Female**	**Male**	**Total**	**Female**	**Male**
N patients	102	27 (26%)	73 (72%)	56	16 (29%)	38 (68%)
Mean age (range)	65 (34–87)	63 (45–87)	65 (34–84)	65 (34–87)	63 (51–87)	66 (34–84)
N aspirated nodes	211			99		
Mean nodes/patient (range)	2.07 (1–5)			1.77 (1–5)		

2.2. Ultrasound and USgFNAC

Ultrasound was performed with an EpiQ7 ultrasound system (Philips, Bothell, WA, USA), using a dedicated protocol for N-staging of HNSCC. The eL18–4 transducer (Philips) was used for conventional ultrasound (B mode), color Doppler sonography (CDI) for measurement of the resistive index (RI), and micro-flow imaging (MFI) for assessing peripheral vascularization. Before aspiration, the short axis diameter and morphological features of the node were assessed. MFI with monochrome subtraction mode imaging was used to detect the presence or absence of peripheral vascularity. The sampling window was placed such that it covered the whole lymph node and surrounding tissue. Images of the nodes with present or absent hilum sign and peripheral vascularization were obtained and categorized. The RI is calculated from the index of the peak systolic blood velocity (Vmax) relative to the minimal diastolic flow velocity (Vmin) reflecting the resistance of the microvascular flow distal of the measurement. All RI measurements were obtained in the hilum if present, and within the node otherwise. To avoid pulsation noise from the carotid artery while maximizing blood vessel visualization, MFI and color gain were adjusted dynamically.

USgFNAC was performed in all nodes with a short axis diameter ≥ 7 mm, or in nodes <7 mm with loss of a fatty hilum sign, peripheral or mixed hilar and peripheral vascularity, a round shape, or an asymmetric thickened cortex. (Figures 1–3)

Figure 1. MFI of peripheral vascularity in a patient with oropharyngeal SCC.

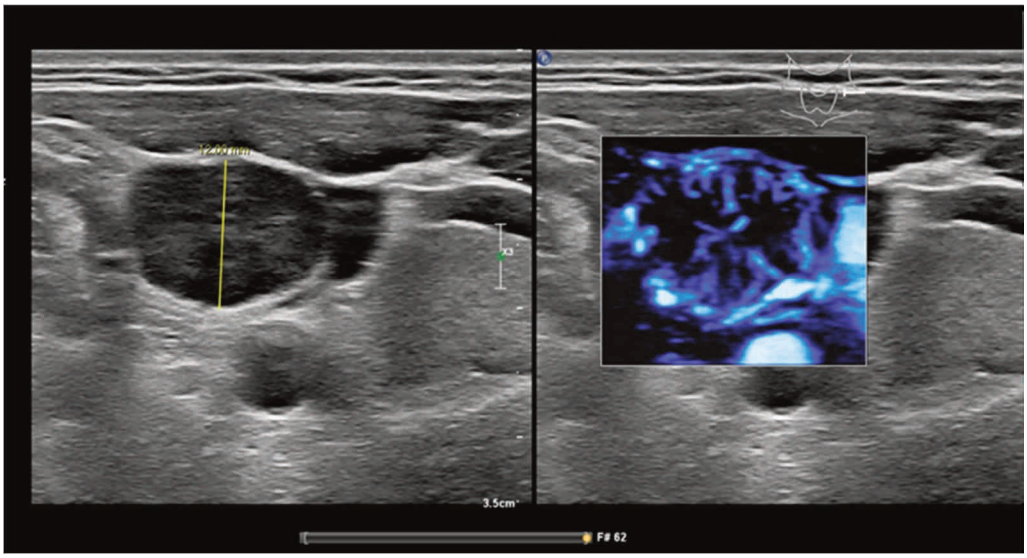

At cytology metastasis SCC, MFI shows a strong peripheral vascularity which indicates malignancy; fatty hilum sign is absent.

Figure 2. Measurement of the RI

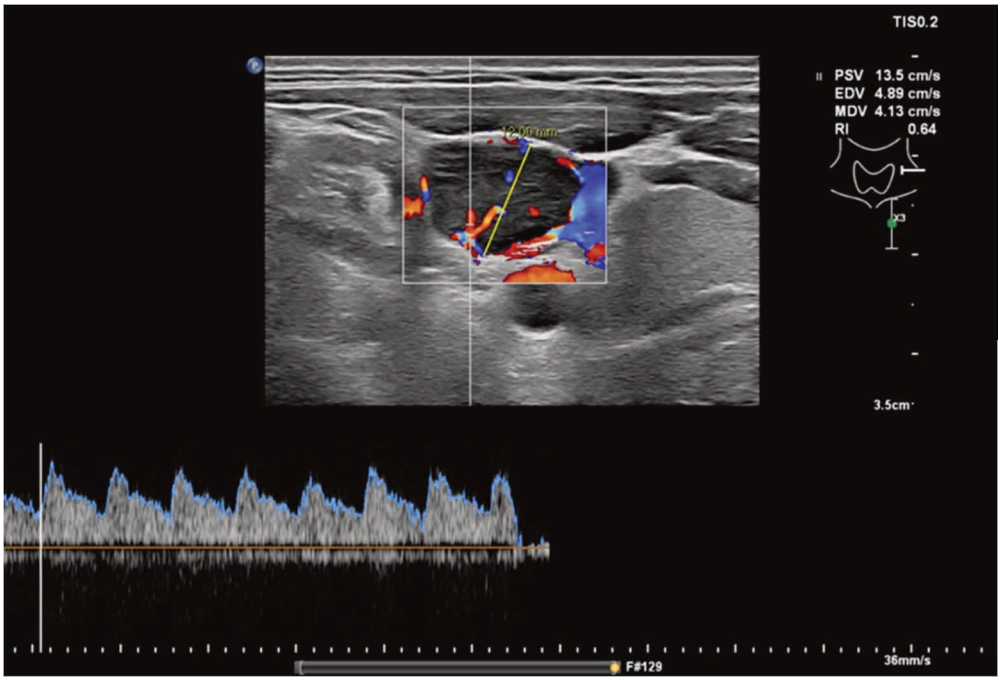

in the same node as in Figure 1 with a value of 0.64, which would indicate a benign node.

Figure 3. Ultrasound features of a benign node.

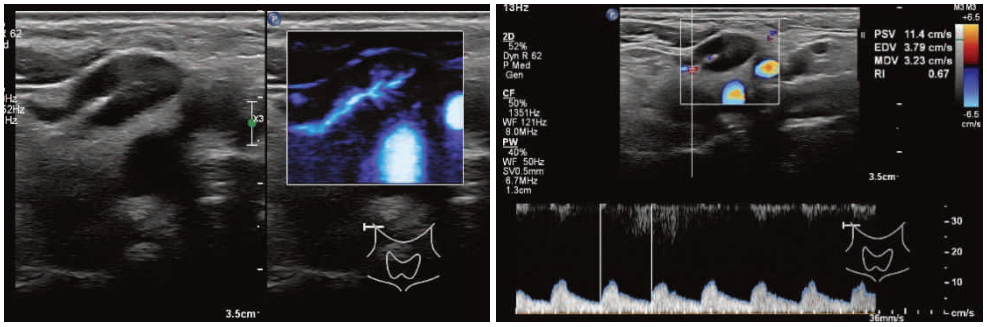

(a) (b)

(**a**) Hilum sign in a benign node, no peripheral vascularity. (**b**) Measurement RI 0.67.

In all nodes, USgFNAC was performed with a 21G needle and cytological results served as the reference standard in assessing the predictive value of the US features. All measurements and FNAs took place by the same experienced

neuroradiologist with over 10 years' experience in head and neck USgFNAC (P.K.d.K.-D).

2.3. Cytology

FNAC material was processed in smears, air dried, and stained with Giemsa stain. Part of the material was fixed in 10 mL 4% formalin and embedded in paraffin for further immunohistochemistry, if necessary, according to routine diagnostic workup. All samples were evaluated by experienced cytopathologists.

2.4. Statistical Analysis

Data of sonographic findings and cytological results of USgFNAC were statistically analyzed for all aspirated nodes and separately for two subsets of aspirated nodes: nodes from clinically node-negative necks (cN0) and nodes with a short axis diameter of 6 mm or less.

In contrast to most reports in the literature, we calculated sensitivity and other parameters per aspirated lymph node, not per neck side or patient, as we were interested in the optimal criteria and not the reliability in clinical practice. We assessed the performance of nodal size (short axis diameter and short/long axis(S/L) ratio, dichotomized using S/L > 0.5, absent fatty hilum sign, presence of peripheral vascularization and RI in predicting cytological malignancy of an aspirated lymph node, using sensitivity, specificity, positive predictive value (PPV) and negative predictive value (NPV). For binary (including dichotomized) variables, these metrics were determined using the 2x2 confusion matrix. For the continuous variables (short axis diameter and RI), a threshold was first determined using ROC curve analysis such that the sensitivity was at least as large as for the classification using peripheral vascularization obtained by MFI. For short axis diameter, an additional threshold based on the literature was used (6 mm for all nodes, and 4 mm for cN0 subgroups) [20]. Additionally, the smallest cutoff with a corresponding PPV of 100% in all nodes was determined for the short axis diameter.

All analyses with RI were done on the subset of lymph nodes with an available RI measurement. Measurement of the RI failed in 8% of the nodes, mainly in tiny or necrotic nodes. The performance of peripheral vascularization obtained by MFI was also assessed in two additional subsets of nodes: nodes with absent fatty hilum sign, and nodes from clinically node-negative neck with absent fatty hilum

sign. Note that any PPV estimate obtained in these subset analyses is by definition the same as would be obtained from combining the features, e.g., the PPV for peripheral vascularization in nodes with absent fatty hilum is the same as the PPV that would be obtained in the set of all nodes by predicting malignancy for nodes with both absent fatty hilum sign and peripheral vascularization.

We assessed whether short axis diameter or S/L ratio differed significantly between cytologically malignant and cytologically benign nodes as shown by USgFNAC, within all nodes and in the subset cN0. Further, we assessed whether short axis diameter or short/long ratio of malignant nodes differed significantly between patients with cN+ and cN0 stage. For this, we used linear mixed effects models with short axis diameter or ratio as the dependent variable, the categorical variable of interest (cytological malignancy or cN stage) as a fixed effect, and patient number as a random intercept. The significance of the categorical variable was then determined using a likelihood ratio test with a 5% significance level.

To determine 95% confidence intervals for the obtained predictive performance measures, accounting for the dependence between nodes from the same patient, we used a bootstrap procedure with 10,000 iterations. During each iteration, a bootstrap sample was generated by resampling patients with a replacement from the original dataset. Then, the sensitivity, specificity, PPV, and NPV were obtained for all variables as described above. From the full set of these results, the 95% bias-corrected accelerated confidence interval [21] was determined. This was not possible for all metrics, as some metrics had the same value in all bootstrap samples. Further, some bootstrap samples did not have at least one malignant and benign node in each category for certain variables, resulting in a missing value for that metric. When for a certain metric the computation of the BCa interval was not possible, when at least 5.5% of bootstrap estimates were missing, or when the BCa interval used order statistics among the first or last 10, the 95% binomial proportion confidence interval was computed for that metric instead.

All analyses were performed with R statistical software, version 3.6.1 (R Core Team (2021) . R: A language and environment for statistical computing. The R Foundation for Statistical Computing, Vienna, Austria).

3. Results

3.1. Analysis in Entire Set of Nodes

USgFNAC was performed in 211 nodes from 102 patients. (Table 1) The mean number of USgFNAC punctures per patient was 2.07 (range 1–5). Out of 211 nodes, 8 (4%) were inconclusive at cytology, 95 (45%) proved to be malignant, and 108 (51%) did not show malignant cells. Nodes that were inconclusive at cytology were excluded from further analyses.

3.1.1. Short Axis Diameter

Malignant nodes at cytology had a significantly larger short axis diameter than benign nodes (*p*-value <.0001). The mean short axis diameter of all nodes was 9.8 mm (SD 6.4), while it was 6.7 mm (SD 2.1) for cytologically benign nodes and 13.3 mm (SD 7.7) for cytologically malignant nodes.

Predicting cytological malignancy for short axis diameters ≥ 6.5 mm had a sensitivity of 0.88 (95% CI 0.80–0.95), a specificity of 0.45 (95% CI 0.19–0.81), a PPV of 0.59 (95% CI 0.45–0.82), and an NPV of 0.82 (0.59–0.89; Table 2). With a threshold of 6.0 mm (based on the literature), the sensitivity was 0.95 (95% CI 0.89–0.98), the specificity was 0.25 (95% CI 0.17–0.35), the PPV was 0.53 (95% CI 0.43–0.62), and the NPV was 0.84 (95% CI 0.68–0.94; Table 2, 3).

Table 2. Predictive performance of features in different subsets of nodes.

Data	Specificity	Sensitivity	NPV	PPV	Threshold
all nodes					
p. vascularization	0.84 (0.77–0.90)	0.87 (0.80–0.93)	0.88 (0.80–0.94)	0.83 (0.74–0.90)	
absent fatty hilum	0.84 (0.77–0.90)	0.84 (0.77–0.90)	0.86 (0.76–0.92)	0.82 (0.72–0.90)	
short axis diameter	0.45 (0.19–0.81)	0.88 (0.80–0.95)	0.82 (0.59–0.89)	0.59 (0.45–0.82)	6.5 [1]
short axis diameter	0.25 (0.17–0.35)	0.95 (0.89–0.98)	0.84 (0.68–0.94)	0.53 (0.43–0.62)	6.0 [2]
resistive index	0.54 (0.34–0.70)	0.88 (0.78–0.93)	0.85 (0.72–0.92)	0.61 (0.50–0.74)	0.705 [1]
S/L ratio [3]	0.45 (0.37–0.53)	0.88 (0.82–0.93)	0.82 (0.69–0.90)	0.59 (0.49–0.67)	0.5
cN0 patients					
p. vascularization	0.79 (0.70–0.88)	0.94 (0.56–1.00)	0.98 (0.92–1.00)	0.50 (0.27–0.71)	
absent fatty hilum	0.82 (0.73–0.89)	0.82 (0.60–1.00)	0.96 (0.89–0.99)	0.50 (0.24–0.72)	
short axis diameter	0.26 (0.15–0.55)	0.94 (0.57–1.00)	0.95 (0.59–1.00)	0.22 (0.11–0.38)	5.5 [1]
short axis diameter	0.05 (0.01–0.11)	1.00 (0.80–1.00)*	1.00 (0.40–1.00)*	0.19 (0.09–0.32)	4.0 [2]
resistive index	0.25 (0.15–0.36)*	1.00 (0.77–1.00)*	1.00 (0.81–1.00)*	0.20 (0.06–0.31)	0.615 [1]
S/L ratio [3]	0.46 (0.36–0.56)	0.88 (0.71–1.00)	0.95 (0.82–1.00)	0.26 (0.14–0.42)	0.5
absent fatty hilum					
p. vascularization	0.71 (0.45–0.89)	0.92 (0.85–0.97)	0.67 (0.38–0.85)	0.94 (0.86–0.98)	
cN0 and absent fatty hilum absent					
p. vascularization	0.64 (0.36–0.88)	0.93 (0.50–1.00)	0.90 (0.55–1.00)*	0.72 (0.40–0.92)	
short axis diameter					
mm ≤ 6					
p. vascularization	0.90 (0.79–0.96)	0.73 (0.33–0.93)	0.94 (0.82–0.98)	0.62 (0.30–0.86)	
absent fatty hilum	0.80 (0.67–0.89)	0.91 (0.00–1.00)	0.98 (0.86–1.00)	0.50 (0.23–0.72)	
resistive index	0.26 (0.00–0.58)	0.80 (0.38–1.00)	0.86 (0.57–0.98) *	0.19 (0.07–0.30)	0.615 [1]
S/L ratio [3]	0.61 (0.49–0.73)	0.82 (0.40–1.00)	0.94 (0.79–1.00)	0.32 (0.16–0.52)	0.5

The given confidence intervals are 95% bias-corrected accelerated bootstrap confidence intervals when possible. * 95% binomial proportion confidence interval. [1] threshold determined such that sensitivity ≥ sensitivity for peripheral vascularization. [2] threshold based on the literature. [3] ratio short axis diameter / long axis diameter.

Table 3. Numbers of cytologically proven malignant and benign nodes by categories of sonographic features.

	Nodes at all cN Stages					Nodes at cN0 Stages					Nodes with Short Axis mm ≤ 6 mm				
Features	**N**	**Mal [3]**	***%.***	**Ben [4]**	***%.***	**N**	**Mal [3]**	***%.***	**Ben [4]**	***%***	**N**	**Mal [3]**	***%***	**Ben [4]**	***%***
hilus + [1]	106	15	14%	91	86%	67	3	4%	64	96%	40	1	3%	39	98%
hilus – [1]	97	80	82%	17	18%	28	14	50%	14	50%	20	10	50%	10	50%
p. vasc + [2]	100	83	83%	17	17%	32	16	50%	16	50%	13	8	62%	5	38%
p. vasc – [2]	103	12	12%	91	88%	63	1	2%	62	98%	47	3	6%	44	94%
hilus–/ *p*. vasc +	79	74	94%	5	6%	18	13	72%	5	28%	9	7	78%	2	22%
hilus–/ *p*. vasc -	18	6	33%	12	67%	10	1	10%	9	90%	11	3	27%	8	73%

[1] Hilus +/-: present and absent fatty hilum sign. [2] *p*. vasc +/-: present and absent peripheral vascularization. [3] mal = cytologically proven malignant nodes. [4] ben= cytologically proven benign nodes.

The lowest cut-off for the short axis diameter with a PPV of 100% was 14 mm.

3.1.2. S/L Ratio

The mean S/L ratio was 0.62 (SD 0.17) for all nodes, 0.55 (SD 0.16) for cytologically benign nodes, and 0.71 (SD 0.15) for cytologically malignant nodes. Malignant nodes had a significantly larger S/L ratio than benign nodes (*p*-value <.0001). Using S/L ratio to predict cytological malignancy for nodes with a ratio > 0.5 had a sensitivity of 0.88 (95% CI 0.82–0.93), a specificity of 0.45 (95% CI 0.37–0.53), a PPV of 0.59 (95% CI 0.49–0.67), and an NPV of 0.82 (95% 0.69–0.90; Table 2).

3.1.3. Resistive Index

RI was successfully obtained for 187/203 (92%) nodes. Predicting cytological malignancy for nodes with RI ≥ 0.705 had a sensitivity of 0.88 (95% CI 0.78–0.93), a specificity of 0.54 (95% CI 0. 0.34–0.70), a PPV of 0.61 (95% CI 0.50–0.74), and an NPV of 0.85 (0.72–0.92; Table 2).

3.1.4. Peripheral Vascularization

Peripheral vascularization as shown by MFI was present in 100/203 (49.3%) nodes. Predicting cytological malignancy had a sensitivity of 0.87 (95% CI 0.80–0.93), a

specificity of 0.84 (95% CI 0.77–0.90), a PPV of 0.83 (95% CI 0.74–0.90), and an NPV of 0.88 (0.80–0.94. (Table 2, 3).

3.1.5. Absent Hilum Sign

Hilum sign was absent in 97/203 (47.8%) nodes and had a sensitivity of 0.84 (95% CI 0.77–0.90), a specificity of 0.84 (95% CI 0.77–0.90), a PPV of 0.82 (95% CI 0.72–0.90), and an NPV of 0.86 (0.76–0.92) in predicting cytological malignancy.

Among nodes with absent fatty hilum sign, peripheral vascularization obtained by MFI predicted cytological malignancy with a sensitivity of 0.92 (95% CI 0.85–0.97), a specificity of 0.71 (95% CI 0.45–0.89), a PPV of 0.94 (95% CI 0.86–0.98), and an NPV of 0.67 (0.38–0.85; Table 2, 3).

3.2. Subgroup Analysis of Clinically N0-Stage

Of the 102 patients, in 56 (55%), no suspicious lymph nodes were palpable, and these were categorized as cN0. In these patients, USgFNAC was performed in 99 lymph nodes (Table 1). Cytological results were insufficient for 4 out of 99 (4%) nodes; these nodes were excluded. Of the remaining 95 nodes, 17 (18%) were cytologically malignant.

3.2.1. Short Axis Diameter

The mean short axis diameter was 7.4 mm (SD 3.1) for all aspirated nodes, and 6.6 mm (SD 2.1) and 10.8 mm (SD 4.7) for cytologically confirmed benign and malignant nodes, respectively.

Cytologically confirmed malignant nodes had a significantly larger short axis diameter than cytologically confirmed benign nodes (*p*-value <.0001).

The short axis diameter of cytologically confirmed malignant nodes was not significantly different between patients with cN0 and cN+ stage (*p*-value = 0.129).

Predicting cytological malignancy for nodes with short axis diameter ≥ 5.5 mm had a sensitivity of 0.94 (95% CI 0.57–1.00), a specificity of 0.26 (95% CI 0.15–0.55), a PPV of 0.22 (95% CI 0.11–0.38), and an NPV of 0.95 (0.59–1.00; Table 2). With a threshold of 4.0 mm (based on the literature) the sensitivity was 1.00 (95% CI 0.80–1.00), the specificity was 0.05 (95% CI 0.01–0.11), the PPV was 0.19 (95% CI 0.09–0.32), and the NPV was 1.00 (95% CI 0.40–1.00; Table 2, 3).

3.2.2. Resistive Index

RI was successfully obtained for 88/95 (92%) of aspirated lymph nodes. Predicting cytological malignancy for nodes with RI ≥ 0.615 had a sensitivity of 1.00 (95% CI 0.77–1.00.), a specificity of 0.25 (95% CI 0.15–0.36), a PPV of 0.20 (95% CI 0.06–0.31), and an NPV of 1.00 (0.81–1.00; Table2).

3.2.3. S/L Ratio

The mean S/L ratio was 0.6 (SD 0.17) for all nodes, and was 0.5 (SD 0.16) and 0.7 (SD 0.16) for cytologically confirmed benign and malignant nodes, respectively. Malignant nodes had a significantly larger S/L ratio than benign nodes (*p*-value <.001). Using S/L ratio to predict cytological malignancy for nodes with a ratio > 0.5 had a sensitivity of 0.88 (95% CI 0.71–1.00), a specificity of 0.46 (95% CI 0.36–0.56), a PPV of 0.26 (95% CI 0.14–0.42), and an NPV of 0.95 (95% 0.82–1.00; Table 2).

3.2.4. Peripheral Vascularization by MFI

Peripheral vascularization obtained by MFI was present in 32/95 (33.7%) nodes. Predicting cytological malignancy had a sensitivity of 0.94 (95% CI 0.56–1.00), a specificity of 0.79 (95% CI 0.70–0.88), a PPV of 0.50 (95% CI 0.27–0.71); and an NPV of 0.98 (0.92–1.00; Table 2, 3).

3.2.5. Absent Hilum Sign

Fatty hilum sign was absent in 28/95 (29.5%) nodes. Predicting cytological malignancy had a sensitivity of 0.82 (95% CI 0.60–1.00), a specificity of 0.82 (95% CI 0.73–0.89), a PPV of 0.50 (95% CI 0.24–0.72), and an NPV of 0.96 (0.89 -0.99; Table 2, 3).

Among nodes with absent hilum sign, peripheral vascularization obtained by MFI had a sensitivity of 0.93 (95% CI 0.50–1.00), a specificity of 0.64 (95% CI 0.36–0.88), a PPV of 0.72 (95% CI 0.40–0.92), and an NPV of 0.90 (0.55–1.00) for the prediction of cytological malignancy (Table 2, 3).

3.3. Subgroup Nodes with Short Axis Diameter ≤ 6 mm

Short axis diameter was ≤ 6 mm for 60/203 (29.6%) nodes.

3.3.1. Resistive Index

RI was successfully obtained for 56/60 (93%) nodes. Predicting cytological malignancy for nodes with RI ≥ 0.615 had a sensitivity of 0.80 (95% CI 0.38–1.00.),

a specificity of 0.26 (95% CI 0.00–0.58), a PPV of 0.32 (95% CI 0.07–0.30), and an NPV of 86 (0.57–0.98).

3.3.2. S/L Ratio

Using the S/L ratio to predict cytological malignancy for nodes with a ratio > 0.5 had a sensitivity of 0.82 (95% CI 0.40–1.00), a specificity of 0.61 (95% CI 0.49–0.73), a PPV of 0.32 (95% CI 0.16–0.52), and an NPV of 0.94 (95% 0.79–1.00; Table 2).

3.3.3. Peripheral Vascularization by MFI

Peripheral vascularization obtained by MFI was present in 13/60 (21.7%) nodes. Predicting cytological malignancy had a sensitivity of 0.73 (95% CI 0.33–0.93), a specificity of 0.90 (95% CI 0.79–0.96), a PPV of 0.62 (95% CI 0.30–0.86), and an NPV of 0.94 (0.82–0.98; Table 2, 3).

3.3.4. Absent Hilum Sign

Fatty hilum sign was absent in 20/60 (33.3%) nodes. Predicting cytological malignancy had a sensitivity of 0.91 (95% CI 0.00–1.00), a specificity of 0.80 (95% CI 0.67–0.89), a PPV of 0.50 (95% CI 0.23–0.72), and an NPV of 0.98 (0.86–1.00; Table 2, 3)

4. Discussion

Ultrasound enables better assessment of the morphology of small nodes than other modalities [22]. USgFNAC is commonly used to detect metastatic spread and is reported to have a sensitivity of 81% [23]. In a systematic review, USgFNAC has been shown to be much less sensitive for patients with cN0 neck with a pooled sensitivity of 66% (95% CI 54–77%) [24].

Nodal size is an important feature used for selecting nodes for USgFNAC. Van den Brekel et al. showed that different radiologists obtain varying sensitivities, mainly based on selection of lymph nodes being aspirated. The more rigorous the aspiration policy, the higher the sensitivity [20]. In general, it has been concluded by Borgemeester et al. that, apart from features such as round shape, cortical widening, and absence of a hilum, in cN0 necks, nodes should be aspirated when they have a short axis diameter of at least 5–6 mm for level II and 4–5 mm for the rest of the neck levels [25].

Using these small cut-off values, we will have to deal with more reactive lymph nodes as well as more non-diagnostic aspirates. On the other hand, using a larger cut-off diameter for selection will lead to more false negatives. We should also realize that micro metastases and metastases smaller than 4mm will rarely be detected by USgFNAC and these metastases might well be the only metastases present in up to 25% of cN0 necks with clinically occult metastases [26].

Although selection of the nodes to aspirate is important for increasing sensitivity, on the other hand, aspiration can be obviated in lymph nodes that have morphological criteria for malignancy that cannot be ignored in treatment selection. In fact, this means that in lymph nodes that are truly enlarged, necrotic, or otherwise almost certainly malignant, cytological confirmation is not necessary in case of a known primary cancer.

We found that a large, short axis diameter was very reliable in predicting cytological malignancy. In fact, all of the aspirates of lymph nodes with a short axis length of at least 14 mm were tumor positive. Of those with a shorter short axis, 63% were benign.

However, to achieve a high sensitivity, smaller lymph nodes should also be aspirated. Comparing diameter as a criterion with MFI, we found that the short axis criterion with the same sensitivity as peripheral vascularization obtained by MFI yielded a substantially lower specificity (45% vs. 84% in all nodes and 26% vs. 79% in nodes from patients with cN0 neck).

Another important predictor for cytologically confirmed malignancy is the nodal shape, as malignant nodes tend to be more round with a S/L ratio above 0.5. [27] [10]. In our study we also found a significantly larger S/L ratio in cytologically malignant nodes than in benign nodes. A ratio >0.5 predicted cytological malignancy correctly in 59% of all nodes, with a sensitivity of 88% and a specificity of 45%. This performance is very similar to that of the short axis diameter with our determined threshold of 6.5 mm. Similar results were obtained in the subset of patients with cN0 neck.

Size and S/L ratio are important features to select nodes for FNAC, but this study shows that selection criteria can be improved when combining them with morphological criteria.

In our study, we evaluated the absence of a fatty hilum sign as the presence of an echogenic hilum in a lymph node can be a sign of a benign lymph node [13]. Including the entire cN0 and cN+ patient group, 82% of the nodes with an absent fatty hilum sign were malignant at cytology, while this was 50 % in N0 necks. The sensitivity of this criterion for all lymph nodes and for the lymph nodes in the cN0 necks was 91% and 82%, whereas specificity was 80% and 82%, respectively.

Ghafoori et al. showed that vascular patterns had better performance than size and RI when predicting cytological malignancy of a node in a study of large palpable cervical lymph nodes (accuracy 89%, sensitivity 85%, specificity 93%). [28]. However, in this study only the largest palpable lymph nodes with a mean short axis diameter of 22.6 mm for malignant nodes and 16.6 mm for benign nodes were evaluated, which are large compared with our study. Visualization of morphological changes and vascular patterns is much more difficult in small lymph nodes. MFI is designed to improve the visualization of blood flow, especially in micro vessels [29]. Using MFI, we were able to detect peripheral micro vascularization in small nodes. Peripheral vascularization had a PPV of 50% in nodes from cN0 patients (NPV 98%, sensitivity 94%, specificity 79%), while the PPV was 83% in nodes from all cN stages (NPV 88%, sensitivity 87%, specificity 84%).

In nodes with absent hilum sign and present peripheral vascularization from patients with all cN stages, 94% of the nodes were malignant at USgFNAC, while 72% were malignant for patients with cN0 neck. The sensitivity in both groups is comparable (92% for all patients, 93% for patients with cN0 neck) and specificity is reasonably high (79% and 64%).

The sensitivity of USgFNAC in patients with cN0 is reported to be in the range of 42–73% [30]. The specificity of USgFNAC is always in the order of 100% as false positive cytology is rare. The difference in sensitivity is mainly attributable to selection of the lymph nodes to aspirate and for aspiration technique. Selection of the most suspicious lymph nodes is on the one hand guided by location of the primary tumor, with known patterns of metastases, and on the other hand by size, shape and morphological criteria. In our study we found clear evidence that selection of the lymph nodes for aspiration can be improved by using not only size and shape, but also peripheral vascularization as detected by MFI. In nodes with a short axis diameter of 6 mm and smaller, 62% of the nodes with present peripheral vascularization and 50% with absent fatty hilum sign were malignant. In those small nodes, absence of fatty hilum sign had a higher sensitivity (91%) than peripheral

vascularization (73%), but a lower specificity (80% vs. 90%). The positive predictive value was highest when combining absent fatty hilum sign and peripheral vascularization, although only a few nodes showed this combination. Assessment of peripheral vascularization with MFI can be done while adding hardly any examination time.

However, not all metastatic lymph nodes have peripheral vascularization or an absent hilum, so absence of these features should not be used as the sole reason not to aspirate from these lymph nodes. The size and location in the neck, relative to the primary tumor, are important selection criteria as well.

Adding RI measurements is time consuming, especially in tiny nodes. In large necrotic nodes, the RI is sometimes not measurable. In accordance with the findings of Ahuja et al, our results show that the intravascular pattern appears more useful in distinguishing malignant from benign nodes than the RI [31].

Because we tested these criteria in patients treated with organ preservation, we only have cytological results and no histopathology of the neck dissection. In general, USgFNAC overlooks 20–40% of the neck sides with occult metastases, mostly very small nodes [4]. Some of these micro metastases likely will not have features related to size, shape, hilum, or vascularization. As a consequence, US criteria for these small metastases are likely never to be found and a certain limit of the accuracy has to be accepted. However, our study reflects the clinical workflow in most hospitals, where USgFNAC is used together with PET-CT (or other modalities) for the purpose of nodal staging and treatment selection. The results of our study can therefore be used to better identify nodes for which USgFNAC should be performed.

Another issue is that in some patients with a known head and neck cancer and already clinically apparent lymph node metastases, nodes with US features (large diameter, peripheral vascularization, no hilum) that are almost pathognomonic for metastases are found on ultrasound. For these patients, cytological proof has no clinical significance, as these nodes need treatment, and a negative cytology is not trustworthy. From our study, we can conclude that lymph nodes with a minimal axial diameter larger than 14 mm, but also lymph nodes without a hilum and with peripheral vascularization, have such a high incidence of positive cytology that one could consider refraining from aspiration in these nodes and categorize them as malignant, based on morphological criteria.

5. Conclusions

Detection of peripheral vascularization in lymph nodes using MFI has, similar to the loss of fatty hilum, a high predictive value in predicting metastases by USgFNAC. Peripheral vascularization has a high sensitivity and can also be (quickly) assessed in small nodes, such as nodes from cN0 necks. Although in all necks peripheral vascularization has a similar PPV as absent fatty hilum, in nodes with clinical N0-stage the sensitivity is remarkably higher (94%) than for the absent fatty hilum sign (82%). Peripheral vascularization should be used in combination with an absent fatty hilum sign, nodal size and shape to select lymph nodes for USgFNAC. As USgFNAC can also have false negative cytological results, a negative cytology in nodes which show these US criteria should be distrusted and USgFNAC should be repeated.

Authors' contributions: Conceptualization, P.K.d.K.-D.; methodology, P.K.d.K.-D. and M.W.v.d.B.; validation, L.S.; formal analysis, S.R.; investigation, P.K.d.K.-D.; data curation, P.K.d.K.-D. and S.R.; writing—original draft preparation, P.K.d.K.-D.; writing—review and editing, P.K.d.K.-D., S.R., M.W.v.d.B., M.M., L.S., R.B.-T. and J.C.; visualization, P.K.d.K.-D.; supervision, M.W.v.d.B. and J.C.; project administration, P.K.d.K.-D. All authors have read and agreed to the published version of the manuscript.

Funding: This research received no external funding.

Institutional Review Board Statement: This study was approved by The Netherlands Cancer Institute- Antoni van Leeuwenhoek Hospital NKI-AVL Institutional Review Board (IRBd21-074).

Informed Consent Statement: Data were analyzed retrospectively. All retrospective medical data/bio specimen studies at the Netherlands Cancer Institute have been executed pursuant to Dutch legislation and international standards. Prior to 25 May 2019, national legislation on data protection was applied, as well as the International Guideline on Good Clinical Practice. From 25 May 2019 we also adhere to the GDPR. Within this framework, patients are informed and have always had the opportunity to object or actively consent to the (continued) use of their personal data and biospecimens in research. None of the patients included in this study objected to use of their data.

Data Availability Statement: The data used to support the findings of this study are available from the corresponding author upon request.

Acknowledgments: The authors would like to acknowledge Pedro Sanches, and Frans Gleuwink (Philips Benelux, Boschdijk 525, 5621JG Eindhoven) for providing knowledge and use of the eL18–4 transducer.

Conflicts of interest: The authors have no conflict of interest to declare that are relevant to the content of this article.

References

1. Hanahan, D.; Weinberg, R.A. The hallmarks of cancer. *Cell* **2000**, *100*, 57–70. Available online: https://pubmed.ncbi.nlm.nih.gov/10647931/ (accessed on 19 August 2021)

2. Lodder, W.; Pameijer, F.A.; Coen, R.N.; Rasch, C.R.N.; van den Brekel, M.W.M.; Balm, A.J.M. Prognostic significance of radiologically determined neck node volume: a systematic review. *Oral Oncol.* **2012**, *48*, 298–302. Available online:

3. https://pure.uva.nl/ws/files/2311657/127130_09.pdf (accessed on 11 October 2018)

4. Godény, M. Prognostic factors in advanced pharyngeal and oral cavity cancer; Significance of multimodality imaging in terms of 7th edition of TNM. *Cancer Imaging* **2014**, *14*, 1–13.

5. van den Brekel, M.W.M.; Castelijns, J.A. What the clinician wants to know: surgical perspective and ultrasound for lymph node imaging of the neck. *Cancer Imaging* **2005**, *5*, S41–S49. Available online: http://www.ncbi.nlm.nih.gov/pubmed/16361135 (accessed on 11 October 2018)

6. Kyzas, P.A.; Evangelou, E.; Denaxa-Kyza, D.; Ioannidis, J.P.A. 18F-Fluorodeoxyglucose Positron Emission Tomography to Evaluate Cervical Node Metastases in Patients with Head and Neck Squamous Cell Carcinoma: A Meta-analysis. *JNCI J. Natl. Cancer Inst.* **2008**, *100*, 712–720. Available online: https://academic.oup.com/jnci/article-lookup/doi/10.1093/jnci/djn125 (accessed on 11 October 2018)

7. Sun, R.; Tang, X.; Yang, Y.; Zhang, C. (18)FDG-PET/CT for the detection of regional nodal metastasis in patients with head and neck cancer: a meta-analysis. *Oral Oncol.* **2015**, *51*, 314–320. Available online: http://www.ncbi.nlm.nih.gov/pubmed/25619735 (accessed on 11 October 2018)

8. Castelijns, J.A.; van den Breckel, M.W.M. Imaging of lymphadenopathy in the neck. *Eur. Radiol.* **2002**, *12*, 727–738.

9. Van den Brekel, M.W.; Leemans, C.R.; Snow, G.B. Assessment and management of lymph node metastases in the neck in head and neck cancer patients. *Crit. Rev. Oncol. Hematol.* **1996**, *22*, 175–82. Available online: http://www.ncbi.nlm.nih.gov/pubmed/8793273 (accessed on 11 October 2018)

10. Ahuja, A.; Ying, M. Sonography of neck lymph nodes. Part II: Abnormal lymph nodes. *Clin. Radiol.* **2003**, *58*, 359–366.

11. Khanna, R.; Sharma, A.D.; Khanna, S.; Kumar, M.; Shukla, R.C. Usefulness of ultrasonography for the evaluation of cervical lymphadenopathy. *World J. Surg. Oncol.* **2011**, *9*, 29. Available online: http://www.ncbi.nlm.nih.gov/pubmed/21356049 (accessed on 27 April 2019)

12. Hohlweg-Majert, B.; Metzger, M.C.; Voss, P.J.; Hölzle, F.; Wolff, K.-D.; Schulze, D. Preoperative cervical lymph node size evaluation in patients with malignant head/neck tumors: comparison between ultrasound and computer tomography. *J. Cancer Res. Clin. Oncol.* **2009**, *135*, 753–759. Available online: http://link.springer.com/10.1007/s00432-008-0487-y (accessed on 26 April 2019)

13. Ying, M.; Ahuja, A.; Brook, F. Repeatability of power Doppler sonography of cervical lymph nodes. *Ultrasound Med. Biol.* **2002**, *28*, 737–744. Available online: http://www.ncbi.nlm.nih.gov/pubmed/12113786 (accessed on 26 April 2019)

14. Moghaddam, M.I.; Davachi, B.; Mostaan, L.V.; Langaroodi, A.J.; Memar, B.; Azimi, S.A.; Marouzi, P. Evaluation of the Sonographic Features of Metastatic Cervical Lymph Nodes in Patients with Head and Neck Malignancy. *J. Craniofac. Surg.* **2011**, *22*, 2179–2184. Available online: http://www.ncbi.nlm.nih.gov/pubmed/22075819 (accessed on 26 April 2019)

15. Gupta, A.; Rahman, K.; Shahid, M.; Kumar, A.; Qaseem, S.M.D.; Hassan, S.A.; Siddiqui, F.A. Sonographic assessment of cervical lymphadenopathy: Role of high-resolution and color Doppler imaging. *Head Neck* **2010**, *33*, 297–302. Available online: http://doi.wiley.com/10.1002/hed.21448 (accessed on 26 April 2019)

16. Ying, M.; Bhatia, K.S.S.; Lee, Y.P.; Yuen, H.Y.; Ahuja, A.T. Review of ultrasonography of malignant neck nodes: greyscale, Doppler, contrast

enhancement and elastography. *Cancer Imaging* **2013**, *13*, 658–69. Available online: https://dx.doi.org/10.1102%2F1470-7330.2013.0056 (accessed on 25 April 2019).

17. Moritz, J.D.; Ludwig, A.; Oestmann, J.W. Contrast-enhanced color Doppler sonography for evaluation of enlarged cervical lymph nodes in head and neck tumors. *AJR Am. J. Roentgenol*. **2000**, *174*, 1279–84. Available online: https://pubmed.ncbi.nlm.nih.gov/10789776/ (accessed on 30 September 2021)

18. Wang, S.; Yang, W.; Fu, J.-J.; Sun, Y.; Zhang, H.; Bai, J.; Chen, M.-H.; Yan, K. Microflow imaging of contrast-enhanced ultrasound for evaluation of neovascularization in peripheral lung cancer. *Medicine* **2016**, *95*, e4361. Available online: http://www.ncbi.nlm.nih.gov/pubmed/27512847 (accessed on 16 December 2018)

19. Bae, J.S.; Lee, J.M.; Jeon, S.K.; Jang, S. Comparison of MicroFlow Imaging with color and power Doppler imaging for detecting and characterizing blood flow signals in hepatocellular carcinoma. *Ultrasonography* **2020**, *39*, 85–93. Available online: https://doi.org/10.14366/usg.19033 (accessed on 30 October 2020)

20. Hwang, S.; Lee, H.J.; Ahn, H.W.; Kim, Y.G. Comparison of ultrasonographic MicroFlow Imaging with contrast enhanced CT in the evaluation of renal mass. *Ultrasound Med. Biol.* **2019**, *45*, S41. Available online: http://www.umbjournal.org/article/S0301562919312542/fulltext (accessed on 28 October 2020)

21. Van Den Brekel, M.W.M.; Castelijns, J.A.; Snow, G.B. The size of lymph nodes in the neck on sonograms as a radiologic criterion for metastasis: How reliable is it? *Am. J. Neuroradiol.* **1998**, *19*, 695–700.

22. Efron, B. Better bootstrap confidence intervals. *J. Am. Stat. Assoc.* **1987**, *82*, 171–185.

23. Ahuja, A.T.; Ying, M.; Ho, S.Y.; Antonio, G.; Lee, Y.P.; King, A.D.; Wong, K.T. Ultrasound of malignant cervical lymph nodes. *Cancer Imaging* **2008**, *8*, 48–56, Available online: https://doi.org/10.1102/1470-7330.2008.0006 (accessed on 25 April 2020)

24. Souren, C.; Kloss-Brandstätter, A.; Stadler, A.; Kross, K.; Yamauchi, K.; Ketelsen, D.; Kessler, P.; Lethaus, B. Ultrasound-guided fine-needle aspiration cytology as a diagnostic tool in comparison to ultrasound and MRI for staging in oral- and oropharyngeal squamous cell tumors. *J. Cranio-Maxillofac. Surg.* **2016**, *44*, 197–201.

25. Liao, L.-J.; Lo, W.-C.; Hsu, W.-L.; Wang, C.-T.; Lai, M.-S. Detection of cervical lymph node metastasis in head and neck cancer patients with clinically N0 neck-a meta-analysis comparing different imaging modalities. 2012. Available online:

26. http://www.biomedcentral.com/1471-2407/12/236 (accessed on 26 April 2019)

27. Borgemeester, M.C.; Brekel, M.W.M.V.D.; Van Tinteren, H.; Smeele, L.E.; Pameijer, F.A.; van Velthuysen, M.-L.; Balm, A.J.M. Ultrasound-guided aspiration cytology for the assessment of the clinically N0 neck: Factors influencing its accuracy. *Head Neck* **2008**, *30*, 1505–1513. Available online: https://doi.org/10.1002/hed.20903 (accessed on 11 October 2018)

28. van den Brekel, M.W.; van der Waal, I.; Meijer, C.J.; Freeman, J.L.; Castelijns, J.A.; Snow, G.B. The incidence of micrometastases in neck dissection specimens obtained from elective neck dissections. *Laryngoscope* **1996**, *106*, 987–991. Available online: http://www.ncbi.nlm.nih.gov/pubmed/8699914 (accessed on 11 April 2019)

29. Okumuş, Ö.; Dönmez, M.; Pekiner, F.N. Ultrasonographic Appearances of Cervical Lymph Nodes in Healthy Turkish Adults Subpopulation: Preliminary Study. *Open Dent. J.* **2017**, *11*, 404–412. Available online: http://www.ncbi.nlm.nih.gov/pubmed/28839488 (accessed on 27 April 2019)

30. Ghafoori, M.; Azizian, A.; Pourrajabi, Z.; Vaseghi, H. Sonographic Evaluation of Cervical Lymphadenopathy; Comparison of Metastatic and Reactive Lymph Nodes in Patients with Head and Neck Squamous Cell Carcinoma Using Gray Scale and Doppler Techniques. *Iran J. Radiol.* **2015**, *12*, e11044. Available online: http://www.ncbi.nlm.nih.gov/pubmed/26528381 (accessed on 26 April 2019)

31. Revzin, M.V.; Imanzadeh, A.; Menias, C.; Pourjabbar, S.; Mustafa, A.; Nezami, N.; Spektor, M.; Pellerito, J.S. Optimizing image quality when evaluating blood

flow at doppler US: A Tutorial. *Radiographics* **2019**, *39*, 1501–23. Available online: https://doi.org/10.1148/rg.2019180055 (accessed on 1 February 2021)

32. Richards, P.S.; Peacock, T.E. The role of ultrasound in the detection of cervical lymph node metastases in clinically NO squamous cell carcinoma of the head and neck. *Cancer Imaging* **2007**, *7*, 167–178. Available online: https://doi.org/10.1102/1470-7330.2007.0024 (accessed on 4 August 2020)

33. Ahuja, A.T.; Ying, M.; Ho, S.S.Y.; Metreweli, C. Distribution of Intranodal Vessels in Differentiating Benign from Metastatic Neck Nodes. *Clin. Radiol.* **2001**, *56*, 197–201. Available online:

34. https://linkinghub.elsevier.com/retrieve/pii/S0009926000905749 (accessed on 26 April 2019)

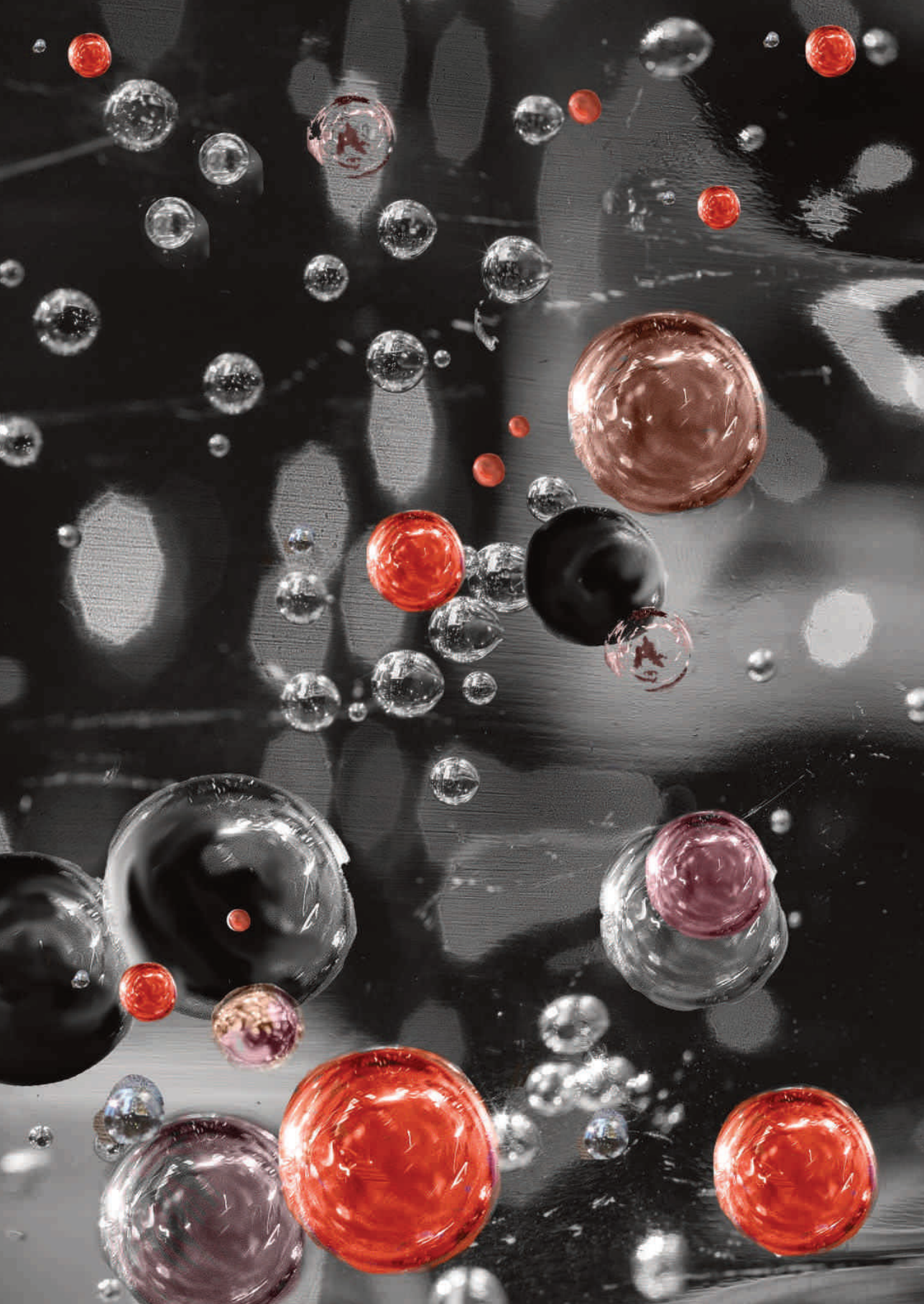

Chapter 6

General Discussion

Future perspectives

Conclusion

General discussion

Accurate TNM staging in HNSCC is crucial for treatment planning and outcome prediction. If cervical lymph node metastases are present survival is reduced with approximately 50%, especially in HPV-negative patients [1]. Clinical evaluation of the neck has a sensitivity of around 60% -70% which means that 30- 40% of the metastases are not detected [2]. Treatment morbidity should be minimalized. If the risk of occult metastases is considered to be very low, watchful waiting with close follow-up can be considered [3]. Although there is still a lot of debate about the optimal management strategy, watchful waiting is often employed in low risk superficial oral cancer and for the contralateral neck in many HNSCCs.

In oral cancer, there is a tendency to either perform elective selective neck dissection or sentinel node biopsies[4]. However, the extent of selective elective neck dissection (ND) and radiotherapy (RT) as well as the dose of RT also depend on TNM-stage which means that accurate staging is very important [5,6]. FDG PET-CT and USgFNAC are commonly used to detect nodal metastases in HNSCC. Detection of metastatic lymph nodes by CT and MRI mainly depends on size criteria (minimum axial diameter). Both imaging techniques have a moderate sensitivity (74-78%) and specificity (76-80%) [7]. Functional imaging techniques such as PET-CT, perfusion MRI, diffusion-weighted magnetic resonance imaging (DW- MRI) and Power Doppler sonography also depict metabolic parameters. For nodal staging DW-MRI has been shown to have a better performance than turbo spin-echo MRI with a higher sensitivity (76% vs 7%), but a slightly lower specificity (94% vs 99.5%), in detecting sub-centimeter nodal metastases [8]. PET-CT has been reported with a significantly higher accuracy in node-staging than MRI and CT [9] but nevertheless in small nodes it can be difficult to distinguish between reactive and malignant PET-positive nodes. Although a high sensitivity of USgFNAC has been reported [10] sensitivity drops in the palpatory negative (cN0) neck [11]. Small PET-positive nodes can have a normal morphological appearance on ultrasound and differentiation between reactivity and malignancy in small PET-positive nodes can be challenging. Real time image fusion of PET-CT and ultrasound could help to localize and to distinguish these nodes. Although real time image fusion and fused guided biopsy has been already used clinically in liver and prostate [12], [13], no research for real time image fusion in the head and neck region is available. We were able to show that real time image fusion of PET-CT and ultrasound is feasible. Fusion enables better detection of small PET-positive nodes for node selection by fused

ultrasound guided FNAC (fused-USgFNAC) [14]. However , puncture of all small PET-positive nodes to improve the sensitivity of PET-CT will lead to a high rate of unnecessary punctures. SUV_{max} cut of values should help to diminish these unnecessary punctures. In HNSCC nodes a SUVmax values of around 4.5 is proposed to predict malignancy [15]. We found that at a SUV_{max} cut of value of 2.87 and lower no malignant nodes could be detected with fused-USgFNAC. Consequently, there would be no need to puncture nodes with a SUV_{max} value lower than 2.87. Mainly in small nodes with a low FDG uptake and SUV_{max} values between 2.87 and 4.5 it is difficult to distinguish between reactive and metastatic nodes and those nodes form a major problem to be selected for puncture. To avoid node selection errors for nodes with this cut off values fused-USgFNAC can be performed as a problem solving tool. To avoid false negatives, USgFNAC should be repeated in nodes with a benign cytological result and a SUV_{max} values >= 2.87. All nodes between a SUVmax value of 2.87 to 4.5 but also nodes up to a SUV_{max} value of 10 have to be punctured because in these range of SUVmax values malignant and reactive nodes were present. To avoid sampling errors UsgFNAC should be repeated in nodes with a benign cytological result and a SUV_{max} values of >/= 2.87. Above a SUV_{max} value of 10.7 all nodes were malignant and theoretically there is no need for puncture in those nodes.

SUV_{max} values were reported to be significantly higher in non-HPV related nodes. In our study we found a higher mean SUV_{max} value in malignant HPV-negative nodes than in malignant HPV-positive nodes, but this was statistically not significant.

Metastases have an increased cellularity which leads to a restricted diffusion, and quantitative analyses by apparent diffusion coefficient (ADC) map lead consequently to a lower ADC. They also have a higher metabolism which leads to a higher FDG-uptake on PET-CT. An inverse correlation between FDG-uptake and ADC has been reported [16], [17]. ADC could therefore be helpful to distinguish between reactive and malignant PET-positive nodes. We demonstrated a slight inverse correlation between FDG-uptake and ADC values. Malignant and benign PET-positive nodes had a significantly lower ADC than PET-negative reference nodes but generally we were not able to distinguish between malignant and benign PET-positive nodes. A possible explanation could be that also reactive lymph nodes also have a higher cell proliferation [18]. Interestingly, we found a significantly lower ADC in the subgroup of non-HPV related malignant PET-positive nodes compared to benign PET-positive nodes [19].

SUV_{max} values were reported significantly higher in non-HPV related nodes compared to HPV-related nodes. In a meta-analysis higher SUVmax values in non-HPV related tumors were found but SUV_{max} scores differentiation between HPV-positive and HPV- negative tumors was not possible [20],[21]. The results of our study also emphasize a higher SUV_{max} value in non-HPV- related metastatic lymph nodes compared to HPV-related nodes, although this was not statistically significant.

Next to MRI, DW-MRI and PET-CT, ultrasound by itself can be an important imaging modality to select nodes to be punctured. Next to node size, necrosis, and extracapsular spread, absent hilum sign, peripheral vascularization and elasticity are important ultrasound features to predict metastatic lymph nodes. [22],[23],[24],[25],[26],[27]. Power Doppler imaging (PDI) enables detection of macro-vascularization in lymph nodes. Changes in vascularization in small nodes are often not detected [28]. Micro flow imaging (MFI) is a new modality to detect small vessel flow with high resolution. It has been shown that MFI has a higher sensitivity in detecting tumor vascularity than PDI [29],[30],[31]. Peripheral vascularization to predict malignancy of lymph nodes detected by MFI has not be investigated until now. Using MFI we were able to show that peripheral vascularization combined with the absent hilum are important imaging features to predict malignancy in USgFNAC. We also demonstrated that in cN0 necks the presence of peripheral vascularization has a remarkable higher PPV (94%) than absent fatty hilum sign (82%) and minimal axial diameters at a threshold of 5.5mm and 4mm (22% and 19%, respectively).

Our study workflow followed the routine clinical work flow used in most hospitals where PET-CT, MRI and USgFNAC are used for tumor and nodal staging and treatment decisions. Because most of the patients were treated with organ preservation we did not have histopathological findings as reference standard but only cytological results. Therefore sampling errors leading to false negative results cannot be excluded and we could not calculate sensitivity and specificity. However, using the features described in this thesis, we improved the selection criteria for nodes to be punctured. One should realize though, that micro-metastases will not be detectable with any imaging tool and a certain limit of accuracy has to be accepted.

Real time image fusion of PET-CT and ultrasound needs, even in hands of a well-trained radiologist, at least 10 minutes extra time. Therefore it should only be used

as a problem solving tool for small PET-positive nodes which are not clearly recognized on ultrasound.

In this study, all ultrasound examinations using MFI and fused-USgFNAC were performed by one radiologist specialized in Head and Neck cancer imaging. Therefore, the inter-observer variability is yet unknown and results should be confirmed in larger studies.

Future perspectives

For optimal treatment with less morbidity, treatment has to develop towards a more and more individualized treatment strategy.

Accurate nodal-staging is an essential parameter for individualized treatment planning. Distinguishing small malignant nodes from small reactive nodes is challenging and a high accuracy in nodal staging still means a high rate of nodal punctures. Anatomical and metabolic features of nodes should be compared and combined to select nodes to be punctured. Machine-learning texture analysis of images (radiomics) and artificial intelligence (AI) are promising tools in head and neck cancer [32]. Imaging protocols should be standardized to be able to develop reliable AI models supporting imaging tools in clinical practice. Real time image fusion with ultrasound and MRI of PET-CT could help to detect nodes on ultrasound to perform ultrasound guided punctures.

Ultrasound and ultrasound guided FNAC are commonly used for nodal-staging in HNC. Besides anatomical imaging new functional imaging techniques such as MFI and Elastography care potentially valuable imaging techniques that could improve the prediction of malignant lymph node metastases and the selection of nodes to be punctured [33], [34].

PET-CT is now the gold standard for noninvasive functional imaging in oncology. However, in HNSCC it still has his limitations. New digital PET-CT scanners have increased effective sensitivity and improved spatial resolution and therefore improved visibility of small lesions which is important to detect nodal metastases [35].

New oncological tracers are being developed. Hypoxia is a feature of human tumors and is also present in HNSCC nodal metastases. Hypoxic cells can be resistant to

radiotherapy and several chemotherapeutic drugs [36]. 18F-fluoromisonidazole (18 F-MISO), a nitro-imidazole PET-tracer, is used for the detection of hypoxia in HNSCC. In a recent study it has been shown that patients with hypoxic tumors will most likely benefit from tirapazamine-containing chemo-radiotherapy while patients without hypoxic tumors will not benefit [37].

Poly(ADP-ribose) polymerases (PARP) are DNA-damage repair enzymes. Novel cancer therapies such as PRAP inhibitors inhibit the cell repair in cancer cells which will potentiate the cytotoxic effect of chemotherapy. The first clinically approved and most studied PARP inhibitor is olaparib. It has been reported that 30%–70% of patients with mutations in DNA damage repair machinery do not respond to therapies including PARP inhibitors [38]. ^{18}F-olaparib PET is a promising noninvasive tumor imaging technique to measure PARP expression in vivo and to monitor radiation damage [39].

An increased specificity and visibility of tracer uptake should lead to a higher specificity of detection of nodal involvement and to less unnecessary punctures.

For staging MRI and PET-CT are common used. MRI has a higher resolution to detect tumor involvement of anatomical structures and perfusion and DWI detect metabolic alterations. PET-CT has the advantage to detect metabolic changes in small tumors and lymph nodes. Integrated PET/MRI combines anatomically imaging and functional imaging and these scanners can combine the information of PET and MRI and might be useful in preoperative staging of HNC [40]. Integrated parametric imaging of tumor anatomy, function and metabolism can also serve further development of multimodality imaging empowered by AI.

Sentinel lymph node (SN) biopsy is the most sensitive detection technique in the N0 neck [41]. However, it is an invasive, expensive and complicated staging technique, that should be reserved for necks that are negative at staging with modern staging techniques.

Conclusion and recommendations

The criteria of an absent fatty hilum sign and peripheral vascularization applied in USgFNAC show high PPVs for prediction of malignant nodes and should be added as selection criteria for fine needle aspiration in lymph nodes

Real time image fusion of PET-CT and ultrasound is feasible and can improve the detection rate of subclinical metastases in HNSSC. Because it is time consuming it should not be used routinely but as a problem-solving tool.

Small PET-positive reactive nodes are difficult to distinguish from small PET-positive malignant nodes. Using SUV_{max} cut of values of 2.87 and higher can improve the detection rate of malignant PET-positive nodes but this low cut off value will lead to a high rate of unnecessary punctures.

With DW-MRI we were able to show a mild inverse correlation between FDG-uptake and ADC values but we were not able to distinguish between malignant and benign/reactive PET-positive nodes in general. However, in the subgroup of non-HPV related nodes lower ADC values in cytologically malignant PET-positive nodes were observed as compared to the cytologically benign nodes , which should help inform the node selection procedure for puncture.

REFERENCES

1. Kelly HR, Curtin HD. Chapter 2 Squamous Cell Carcinoma of the Head and Neck—Imaging Evaluation of Regional Lymph Nodes and Implications for Management. Semin Ultrasound, CT MRI 2017; 38:466–478.

2. van den Brekel MWM, Castelijns JA. What the clinician wants to know: surgical perspective and ultrasound for lymph node imaging of the neck. Cancer Imaging 2005; 5 Spec No:0–16.

3. Koyama LKS, Matos LL, Kulcsar MAV, de Araújo Filho VJF, Cernea CR. Oral Cancer Treatment: Still an Indication for Elective Neck Dissection? ORL 2018; 80:96–102.

4. Schilling C, Stoeckli SJ, Vigili MG, de Bree R, Lai SY, Alvarez J, Christensen A, Cognetti DM, D'Cruz AK, Frerich B, Garrel R, Kohno N, Klop WM, Kerawala C, Lawson G, McMahon J, Sassoon I, Shaw RJ, Tvedskov JF, von Buchwald C, McGurk M. Surgical consensus guidelines on sentinel node biopsy (SNB) in patients with oral cancer. Head Neck 2019; 41:2655–2664.

5. Al-Mamgani A, Verheij M, van den Brekel MWM. Elective unilateral nodal irradiation in head and neck squamous cell carcinoma: A paradigm shift. Eur J Cancer 2017; 82:1–5.

6. Nieuwenhuis EJC, Castelijns JA, Pijpers R, van den Brekel MWM, Brakenhoff RH, van der Waal I, Snow GB, Leemans CR. Wait-and-see policy for the N0 neck in early-stage oral and oropharyngeal squamous cell carcinoma using ultrasonography-guided cytology: is there a role for identification of the sentinel node? Head Neck 2002; 24:282–9.

7. Kyzas PA, Evangelou E, Denaxa-Kyza D, Ioannidis JPA. 18F-Fluorodeoxyglucose Positron Emission Tomography to Evaluate Cervical Node Metastases in Patients With Head and Neck Squamous Cell Carcinoma: A Meta-analysis. JNCI J Natl Cancer Inst 2008; 100:712–720.

8. Vandecaveye V, De Keyzer F, Poorten V Vander, Dirix P, Verbeken E, Nuyts S, Hermans R. Head and Neck Squamous Cell Carcinoma: Value of Diffusion-weighted MR Imaging for Nodal Staging 1. Radiol ▪ Radiol 2009; 251:.

9. Roh JL, Yeo NK, Kim JS, Lee JH, Cho KJ, Choi SH, Nam SY, Kim SY. Utility of 2-[18F] fluoro-2-deoxy-D-glucose positron emission tomography and positron emission tomography/computed tomography imaging in the preoperative staging of head and neck squamous cell carcinoma. Oral Oncol 2007; 43:887–893.

10. Ostermann K, Asanau A, Lang FJW. Cervical staging by head and neck surgeon-performed ultrasound and FNAC in N + head and neck cancer. 2018; 7–15.

11. Borgemeester MC, van den Brekel MWM, van Tinteren H, Smeele LE, Pameijer FA, van Velthuysen M-LF, Balm AJM. Ultrasound-guided aspiration cytology for the assessment of the clinically N0 neck: Factors influencing its accuracy. Head Neck 2008; 30:1505–1513.

12. Shoji S. Magnetic resonance imaging-transrectal ultrasound fusion image-guided prostate biopsy: Current status of the cancer detection and the prospects of tailor-made medicine of the prostate cancer. Investig Clin Urol 2019; 60:4–13.

13. Li C, Zhu A. Application of Image Fusion in Diagnosis and Treatment of Liver Cancer. no date; .

14. de Koekkoek-Doll PK, Maas M, Vogel W, Castelijns J, Smit L, Zavrakidis I, Beets-Tan R, van den Brekel M. Real-Time Ultrasound Image Fusion with FDG-PET/CT to Perform Fused Image-Guided Fine-Needle Aspiration in Neck Nodes: Feasibility and Diagnostic Value. Am J Neuroradiol 2021; .

15. Dequanter D, Shahla M, Aubert C, Deniz Y, Lothaire P. Prognostic value of FDG PET/CT in head and neck squamous cell carcinomas. Onco Targets Ther 2015; 8:2279–2283.

16. Schaarschmidt BM, Buchbender C, Nensa F, Grueneien J, Gomez B, Köhler J, Reis H, Ruhlmann V, Umutlu L, Heusch P. Correlation of the apparent diffusion coefficient (ADC) with the standardized uptake value (SUV) in lymph node metastases of non-small cell lung cancer (NSCLC) patients using hybrid 8F-FDG PET/MRI. PLoS One 2015; 10:.

17. Heusch P, Buchbender C, Köhler J, Nensa F, Beiderwellen K, Kühl H, Lanzman RS, Wittsack HJ, Gomez B, Gauler T, Schuler M, Forsting M, Bockisch A, Antoch G, Heusner TA. Correlation of the apparent diffusion coefficient (ADC) with the standardized uptake value (SUV) in hybrid 18F-FDG PET/MRI in non-small cell lung cancer (NSCLC) lesions: Initial results. RoFo Fortschritte Auf Dem Gebiet Der Rontgenstrahlen Und Der Bildgeb Verfahren 2013; 185:1056–1062.

18. L; IHMJ. LYMPH NODE PATHOLOGY IOACHIM. no date.

19. De Koekkoek-Doll PK, Roberti S, Smit L, Vogel W V, Beets-Tan R, Van Den Brekel MW, Castelijns J. ADC Values of Cytologically Benign and Cytologically Malignant 18 F-FDG PET-Positive Lymph Nodes of Head and

Neck Squamous Cell Carcinoma. Cancers (Basel) 2022; 2022:4019.

20. Tahari AK, Alluri K, Quon H, Koch W, Wahl RL, Subramaniam RM, Subramaniam R, Morgan RH. FDG PET/CT imaging of Oropharyngeal SCC: Characteristics of HPV positive and negative tumors. Clin Nucl Med 2014; 39:225–231.

21. Fleming JC, Woo J, Moutasim K, Mellone M, Frampton SJ, Mead A, Ahmed W, Wood O, Robinson H, Ward M, Woelk CH, Ottensmeier CH, King E, Kim D, Blaydes JP, Thomas GJ. HPV, tumour metabolism and novel target identification in head and neck squamous cell carcinoma. Br J Cancer 2019; 120.

22. Ahuja AT, Ying M, Ho SY, Antonio G, Lee YP, King AD, Wong KT. Ultrasound of malignant cervical lymph nodes. Cancer Imaging 2008; 8:48–56.

23. Ahuja A, Ying M, Yuen YH, Metreweli C. Power Doppler sonography of cervical lymphadenopathy. Clin Radiol 2001; 56:965–9.

24. Ying M, Ahuja A, Brook F, Metreweli C. Vascularity and Grey-Scale Sonographic Features of Normal Cervical Lymph Nodes: Variations with Nodal Size. Clin Radiol 2001; 56:416–419.

25. Ying M, Bhatia KSS, Lee YP, Yuen HY, Ahuja AT. Review of ultrasonography of malignant neck nodes: greyscale, Doppler, contrast enhancement and elastography. Cancer Imaging 2013; 13:658–669.

26. van den Brekel MWM, Castelijns JA. What the clinician wants to know: surgical perspective and ultrasound for lymph node imaging of the neck. Cancer Imaging 2005; 5 Spec No:S41-9.

27. Pehlivan M, Kezban Gurbuz M, Cingi C, Adapinar B, De˘ Girmenci C AN, Acikalin FM, Özgür M, Pinarbas¸li P, Colak E. Brazilian Journal of OTORHINOLARYNGOLOGY Diagnostic role of ultrasound elastography on lymph node metastases in patients with head and neck cancer. Braz J Otorhinolaryngol 2019; 85:297–302.

28. JD M, A L, JW O. Contrast-enhanced color Doppler sonography for evaluation of enlarged cervical lymph nodes in head and neck tumors. AJR Am J Roentgenol 2000; 174:1279–1284.

29. Wang S, Yang W, Fu J-J, Sun Y, Zhang H, Bai J, Chen M-H, Yan K. Microflow imaging of contrast-enhanced ultrasound for evaluation of neovascularization in peripheral lung cancer. Medicine (Baltimore) 2016; 95:e4361.

30. Bae JS, Lee JM, Jeon SK, Jang S. Comparison of microflow imaging with color and power doppler imaging for detecting and characterizing blood flow signals in hepatocellular carcinoma. Ultrasonography 2019; 39:85–93.

31. Hwang S Il, Lee HJ, Ahn HW, Kim YG. Comparison of ultrasonographic MicroFlow Imaging with contrast enhanced CT in the evaluation of renal mass. Ultrasound Med Biol 2019; 45:S41.

32. van Dijk L V, Fuller CD. Artificial Intelligence and Radiomics in Head and Neck Cancer Care: Opportunities, Mechanics, and Challenges. Am Soc Clin Oncol Educ Book Am Soc Clin Oncol Annu Meet 2021; 41:1–11.

33. Vineela E, Kumar Sakalecha A, Narayanrao Suresh T. Role of Sonoelastography in Differentiating Benign From Malignant Cervical Lymph Nodes and Correlating With Pathology. 2022; .

34. Suh CH, Choi YJ, Baek JH, Lee JH. The diagnostic performance of shear wave elastography for malignant cervical lymph nodes: A systematic review and meta-analysis. Eur Radiol 2017; 27:222–230.

35. Van Der Vos CS, Koopman D, Rijnsdorp S, Arends AJ, Boellaard R, Van Dalen JA, Lubberink M, Antoon &, Willemsen TM, Visser EP. Quantification, improvement, and harmonization of small lesion detection with state-of-the-art PET. no date; .

36. Brown JM. Tumor hypoxia in cancer therapy. Methods Enzymol 2007; 435:.

37. Rischin D, Hicks RJ, Fisher R, Binns D, Corry J, Porceddu S, Peters LJ. Prognostic significance of [18F]-misonidazole positron emission tomography-detected tumor hypoxia in patients with advanced head and neck cancer randomly assigned to chemoradiation with or without tirapazamine: A substudy of Trans-Tasman Radiation Oncology Group study 98.02. J Clin Oncol 2006; 24:2098–2104.

38. Livraghi L, Garber JE. PARP inhibitors in the management of breast cancer: current data and future prospects. BMC Med 2015; 13:.

39. Wilson TC, Xavier MA, Knight J, Verhoog S, Torres JB, Mosley M, Hopkins SL, Wallington S, Allen PD, Kersemans V, Hueting R, Smart S, Gouverneur V, Cornelissen B. PET Imaging of PARP Expression Using 18F-Olaparib. J Nucl Med 2019; 60:504–510.

40. Samolyk-Kogaczewska N, Sierko E, Dziemianczyk-Pakiela D, Nowaszewska KB, Lukasik M, Reszec J. Usefulness of hybrid PET/MRI in clinical evaluation of head and neck cancer patients. Cancers (Basel) 2020; 12:.

41. De Bree R, Bart De Keizer ·, Civantos FJ, Robert ·, Takes P, Rodrigo JP, Juan ·, Hernandez-Prera C, Gyorgy ·, Halmos B, Rinaldo A, Ferlito A. What is the role of sentinel lymph node biopsy in the management of oral cancer in 2020? Eur Arch Oto-Rhino-Laryngology 2021; 278:3181–3191.

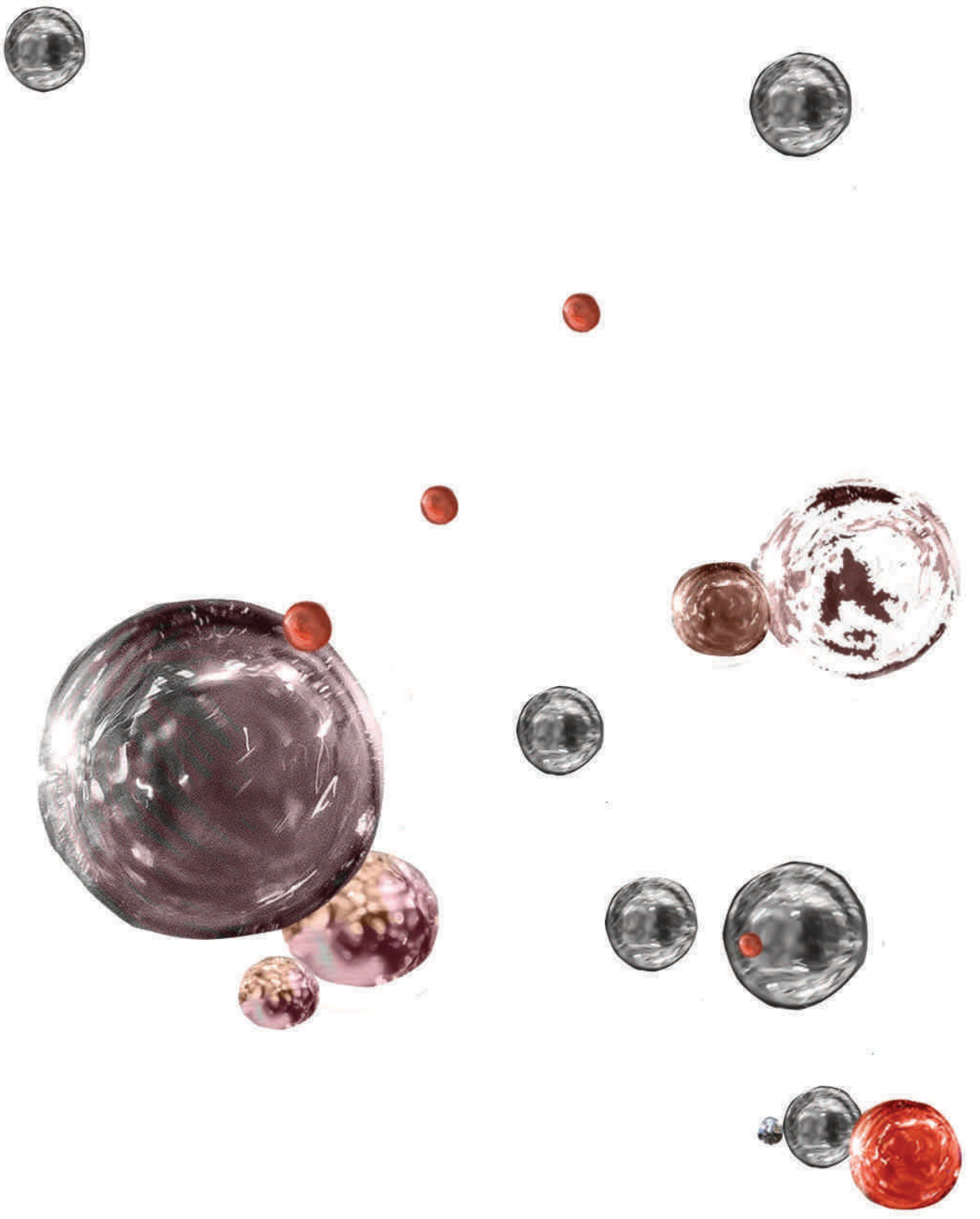

CHAPTER 7

English Summary

Nederlandse samenvatting

Impact paragraph

English Summary

Summary per Chapter

Chapter 1 (Introduction of the Thesis): Squamous cell carcinoma of the head and neck is globally the seventh most common malignancy. The presence of cervical lymph nodes is one of the most important predictors for survival. Exact N-staging is most important for prediction of survival and individualised treatment planning. Clinically examination generally overlooks 30-40% of the metastatic lymph nodes. Interpretation of anatomical images is mainly based on lymph node size and shape and signs of infiltration of surrounding tissues. CT and MRI have a moderate sensitivity and specificity. US and USgFNAC are generally used and especially USgFNAC has a high specificity. Clinically node-negative necks are challenging. 30% of lymph nodes with micro-metastases have a minimal axial diameter below 3 mm. Nodes with a minimal axial diameter of 2-3 mm and larger should be aspirated to get a high sensitivity. Functional imaging techniques enable detection of metabolic alterations and are an important modality for oncological imaging. With Power Doppler ultrasound (PDUS) on ultrasound macro-vascular flow pattern of tumours can be visualized. PET is a very sensitive functional imaging technique to assess metabolic changes in tumours and an important imaging tool for staging in head and neck cancer but in small PET-positive lymph nodes it is very difficult to distinguish between reactive and malignant nodes. Diffusion weighted magnetic resonance imaging (DW-MRI) has an increasing importance in head and neck imaging. It has been shown that it has a better diagnostic performance in detecting lymph node metastases than turbo spine-echo MRI. Micro flow imaging (MFI) is a new imaging technique for ultrasound to visualize micro flow patterns in tumour vascularisation.

New fusion technologies technology enables real time image fusion (MRI, CT or PET-CT) with live ultrasound. Fusion enables detection of the location of lesions on ultrasound and provides the possibility to guide the needle route for percutaneous interventional procedures.

Aim of the scientific work in this thesis was assessment of the diagnostic performance of new imaging tools in N-staging of HNSCC and its possible added diagnostic and therapeutic value.

Chapter 2: We investigated the feasibility of real time ultrasound image fusion with FDG PET-CT. We were able to show that real time image fusion of FDG PET-CT and ultrasound with head and neck nodes is feasible and allows accurate US identification of FDG PET positive nodes. Due to fusion additional PET positive nodes were recognized on ultrasound. Fused USgFNAC enabled a higher detection rate of malignancy in nodes. N-stage was upgraded in 9% of the patients. Although a higher rate of malignant PET positive nodes was found, the detection rate from malignant PET-positive nodes increased only from 51% to 53%, which was not significant. This may largely be explained by the small size of the additional Fused USgFNAC nodes indicating an increase in sensitivity in small nodes. In small PET-positive nodes with low SUVmax uptake it is difficult to distinguish between reactive and malignant nodes. Ultrasound of these PET-positive nodes may well show a normal anatomy. Image fusion can help to detect this PET- positive nodes to perform Fused USgFNAC and therefore increase sensitivity of USgFNAC.. Because image fusion of the head and neck is time consuming it mainly should be used as a problem solving tool in small borderline FDG PET-positive nodes which are difficult to identify on routine USgFNAC.

Chapter 3: For treatment decisions exact nodal stage (N-stage) of HNSCC is most important. If the risk of occult lymph node metastases is very low elective treatment will not be necessary. FDG-PET CT and ultrasound guided fine needle aspiration cytology (USgFNAC) are commonly used for nodal staging in HNSSC. Distinction between malignant small PET-positive nodes with low FDG uptake and reactive nodes can be difficult. Real time image fusion helps to identify these borderline nodes for guided FNAC (Fused-USgFNAC). The aim of chapter 3 was to determine optimal SUV_{max} values to select nodes for USgFNAC to improve USgFNAC sensitivity. In our study only 7% of the aspirated nodes were PET-negative and none of these nodes was malignant at cytology.

Generally a node with a SUVmax value above 4.5 may be considered to be metastatic. In our study all nodes below a SUV_{max} value of 2.87 were benign and all nodes above a SUV_{max} value of 10.6 were malignant. A SUV_{max} value between 2.87 and 4.5 will provide the major clinically problem in this cases and also up to a SUV_{max} value of 10.6 Fused-USgFNAC might be a helpful problem-solving imaging tool. Nodes with a SUV_{max} below 2.87 could be considered to be benign and with a SUV_{max} above 10.6 to be malignant and puncture would not be necessary.

In HPV related nodes the mean SUVmax values were slightly lower but this was statistically not significant.

Chapter 4: Diffusion-weighted magnetic resonance imaging (DW-MRI), 18F-fluordeoxyglucose positron emission tomography (FDG-PET) and ultrasound guided fine needle aspiration cytology (USgFNAC) are commonly used for nodal staging (N-staging) in head and neck squamous cell carcinoma (HNSCC). The specificity of USgFNAC is always in the order of 100% as false positive cytology is rare. The differences in sensitivity mainly depend on the selection of nodes to aspirate and aspiration technique. PET-CT has a good performance in nodal staging for HNSCC but differentiation of small PET- positive malignant from small PET-positive reactive nodes is still a problem. Therefore node selection especially for these nodes to be aspirated is still challenging. The aim of this chapter is, to examine if DW-MRI may be helpful to detect nodal metastases. An inverse relationship between the apparent diffusion coefficient (ADC) (=quantitative analyses of DWI) and FDG uptake has been shown. Aim of this study was to investigate if ADC will be helpful to distinguish PET-positive malignant from PET-positive reactive nodes and so improve node selection for puncture. We found a negative correlation between SUVmax and ADC values. ADC was significantly higher in PET-negative reference nodes than in PET-positive nodes. Generally ADC values of PET-positive malignant nodes did not differ significantly from PET-positive benign (reactive) nodes, but in the subgroup of non-HPV related nodes PET-positive malignant nodes had significantly lower ADC values than PET-positive benign nodes. These significant findings indicate that the measurement of ADC might be helpful to differentiate between small malignant non-HPV-related PET-positive and reactive non-HPV-related PET-positive nodes, and this implies that if a node is PET-positive, then DW-MRI will improve node selection for puncture.

Chapter 5: Ultrasound-guided fine needle aspiration cytology (USgFNAC) has a high specificity in the order of 100% as false positive cytology is rare. It is commonly used for N-staging in HNSCC-patients. We investigated different ultrasound futures as size, hilum sign, restive index (RI) and peripheral vascularization obtained by micro-flow imaging as a predictor of malignancy in lymph nodes of HNSCC. Micro-flow

imaging is a new technique to visualize not only macro-flow but also micro-flow vascular patterns. Aim of this study was to improve the selection criteria for nodes to be aspirated. We demonstrated that the positive predictive value (PPV) for malignancy at cytology was 83% if peripheral vascularization was present as assessed by MFI and 82% if an absent hilum sign was present. If both features were present the PPV proved to be 94%. We concluded that next to size, the combination of a absent fatty hilum sign and present peripheral vascularization should be used as an additionally criteria to select neck nodes for fine needle aspiration in HNSCC-patients .

Chapter 6: For treatment planning in HNSCC exact nodal staging is essential and still, mainly in cN0 necks, very challenging. Treatment should be as effective as possible but treatment damages should be minimized. FNAC is generally used for nodal-staging in HNSSC but node selection for nodes to be punctured is challenging. In our research we wanted to observe if available new imaging techniques such as MFI and real time image fusion of ultrasound and PET-CT are available, will help to improve node selection criteria of nodal staging and will improve sensitivity.

Using MFI we were able to show that peripheral vascularization combined with absent hilum has a high PPV for malignancy in USgFNAC nodes. In cN0 necks the presence of peripheral vascularization has a remarkable higher PPV (94%) than absent fatty hilum sign (82%) and minimal axial diameters at a threshold of 5.5mm and 4mm (22% and19%, respectively).

We were able to show that real time image fusion of PET-CT and ultrasound is feasible in HNSCC and image fused guided FNAC improves the detection rate of malignant PET-positive nodes which should improve sensitivity. We established cut-off values for nodes to be punctured and found that nodes with a SUVmax value lower than 2.87 were all benign and higher than 10.6 were all malignant. Nodes between a SUVmax of 2.87 and 10.6 must be punctured.

We found a mild inverse relationship between ADC values and SUVmax values and significant lower ADC values in PET-positive than in PET-negative nodes but in generally we were not able to distinguish between malignant and reactive PET-positive nodes. Remarkable, in the subgroup of non HPV-related nodes, we found

lower ADC values in malignant PET-positive nodes compared to benign PET-positive nodes.

We conclude that peripheral vascularization in cN0 can has a high PPV for malignancy in cN0 nodes and should be helpful in node selection for punctures, and it can easily can be added to the routine-work-up.

Real time image fusion is feasible in HNSCCC and fused guided FNAC can be used as a problem-solving tool to puncture small PET-positive nodes with normal anatomically features. Using SUVmax- cut off values can help to limit unnecessary node punctures. In non HPV-related nodes we found a significant lower ADC values in malignant PET-positive than in benign PET-positive nodes,. This indicates that ADC could be added to node selection criteria's for puncture of PET-positive nodes. As the non HPV-related group was performed in a small group of patients research in a larger group should be performed in future.

Nederlandse samenvatting

Samenvatting per hoofdstuk

Hoofdstuk 1 (Introductie van de Thesis): Plaveiselcelcarcinoom van het hoofd-halsgebied is wereldwijd de zevende meest voorkomende maligniteit. De aanwezigheid van cervicale lymfeklieren is een van de belangrijkste voorspellers voor overleving. Exacte N-stadiëring is het belangrijkst voor het voorspellen van overleving en geïndividualiseerde behandelplanning.

Bij klinisch onderzoek wordt over het algemeen 30-40% van de metastasen over het hoofd gezien. Interpretatie van anatomische beeldvorming is voornamelijk gebaseerd op grootte, vorm van de klieren, centrale necrose in klieren en tekenen van infiltratie van het omringende weefsel. CT en MRI hebben een matige sensitiviteit en specificiteit. Echografie (US) en in het bijzonder echogeleide punctie cytologische punctie (USgFNAC) worden over het algemeen gebruikt voor diagnostiek en hebben een hoge specificiteit. Diagnostiek van halzen die bij klinische onderzoek geen palpabele klieren tonen is problematisch. De minimale axiale diameter van 30% van de klieren met micro-metastasen is kleiner dan 3 mm. Om een hoge sensitiviteit te krijgen moeten klieren met een minimale axiale diameter van groter/ gelijk dan 2-3 mm geaspireerd worden.

Functionele beeldvormingstechnieken kunnen metabole veranderingen weergeven en zijn een belangrijk hulpmiddel voor oncologische beeldvorming. Met Doppler-echografie kan het macro-vasculaire stroompatroon van tumoren worden gevisualiseerd.

PET is een zeer gevoelige functionele beeldvormingstechniek om metabole veranderingen in tumoren te beoordelen en een belangrijk beeldvormend hulpmiddel voor stadiëring bij hoofd-hals carcinomen, maar in kleine PET-positieve lymfeklieren is het erg moeilijk om onderscheid te maken tussen reactieve en maligne klieren.

Diffusie gewogen MRI-beeldvorming wordt steeds belangrijker bij beeldvorming van hoofd en hals. Er werd aangetoond dat het betere diagnostische mogelijkheden

heeft voor detectie van lymfekliermetastasen dan MRI-beeldvorming met de turbo-Spin Echo techniek.

Microflow-beeldvorming is een nieuwe beeldvormingstechniek om middels ultrasound micro-vasculaire patronen in tumorvaten te visualiseren.

Nieuwe technologie voor beeldfusie maakt real-time beeldfusie met MRI, CT of PET-CT enerzijds met real-time echografie anderzijds mogelijk. Fusie kan helpen om locatie van klieren op echografie te detecteren en biedt de mogelijkheid om de naaldroute voor percutane interventionele procedures te begeleiden.

Het doel van het wetenschappelijk werk in dit proefschrift was het beoordelen van de diagnostische mogelijkheden van nieuwe beeldvormende modaliteiten in N-stadiëring van HNSCC en de mogelijke toegevoegde diagnostische en therapeutische waarde ervan.

Hoofdstuk 2: In dit hoofdstuk hebben we de haalbaarheid van real-time ultrasound beeldfusie met FDG PET-CT onderzocht. We konden aantonen dat real-time beeldfusie van FDG PET-CT en echografie van klieren in de hals mogelijk is en een nauwkeurige identificatie van FDG PET-positieve klieren mogelijk maakt. Door fusie werden extra PET-positieve klieren op echografie herkend en kan een Fusie-geleide USgFNAC (Fusie-USgFNAC) plaatsvinden, wat tot een hoger aantal detecteerde maligne klieren leidde. N-stadium werd bij 9% van de patiënten opgewaardeerd. Hoewel een hoger percentage maligne PET-positieve klieren werd gevonden nam het detectiepercentage van maligne PET-positieve klieren slechts toe van 51% tot 53% wat niet statistisch significant is. Dit kan grotendeels worden verklaard door de geringe afmeting van de extra Fused-USgFNAC-klieren, wat op een toename in sensitiviteit in kleine klieren wijst. In kleine PET-positieve klieren met een lage SUVmax-opname is het moeilijk om middels echografie onderscheid te maken tussen reactieve klieren en maligne klieren; deze tonen op echografie meestal een normale anatomie. Beeldfusie kan helpen om deze PET-positieve klieren te detecteren en om een Fused-USgFNAC uit te voeren. Middels Fused-USgFNAC kan de sensitiviteit van USgFNAC verhoogd worden. Omdat beeldfusie van hals klieren tijdrovend is, moet het vooral als een probleemoplossend hulpmiddel in kleine

borderline FDG PET-positieve klieren, die moeilijk te identificeren zijn op routine USgFNAC, worden gebruikt.

Hoofdstuk 3: Voor therapeutische beslissingen is het exacte klier stadium (N-stadium) van HNSCC het belangrijkst. Als de kans op occulte lymfekliermetastasen erg laag is, is een electieve behandeling niet (altijd) nodig. FDG-PET CT en echogeleide cytologische aspiratie (USgFNAC) worden vaak gebruikt voor lymfklier stadiëring in de hals bij patiënten met HNSSC. Het differentiëren tussen kleine maligne PET-positieve klieren met lage FDG-PET-opname enerzijds en kleine reactieve PET-positieve klieren anderzijds kan moeilijk zijn. Real-time beeldfusie helpt bij het identificeren van deze klieren voor Fused-USgFNAC. Het doel van hoofdstuk 3 was om optimale SUVmax-waarden te bepalen om klieren voor USgFNAC te selecteren en de sensitiviteit voor USgFNAC te verbeteren. In onze studie was slechts 7% van de geaspireerde klieren PET-negatief en geen van de PET-negatieve klieren was cytologisch maligne. We konden aantonen dat onder een SUVmax-waarde van 2,87 geen van de geaspireerde PET-positieve klieren maligne was en boven een SUVmax-waarde van 10,6 geen van de klieren benigne was.

In HPV-gerelateerde klieren waren de gemiddelde SUVmax-waarden iets lager, maar dit was statistisch niet relevant.

Over het algemeen wordt een klier met een SUVmax-waarde boven 4,5 als en mogelijke kliermetastase beschouwd. In ons studie waren onder een SUVmax waarde van 2,87 waren alle klieren benigne en boven een SUV max waarde van 10,6 alle klieren maligne. Een SUVmax-waarde tussen 2,87 en 4,5 vormt in deze gevallen het belangrijkste diagnostische probleem en ook tot een SUVmax-waarde van 10,6 kan een Fused-USgFNAC een nuttig hulpmiddel zijn om problemen op te lossen. Klieren met een SUVmax-waarde lager dan 2,87 zouden als benigne en boven 10,6 als maligne beschouwd kunnen worden en derhalve zou er geen punctie gedaan hoeven worden.

Hoofdstuk 4: Diffusie-gewogen magnetische resonantie beeldvorming (DW-MRI), 18F-fluordeoxyglucose positron emissie tomografie (FDG-PET) en echogeleide (fijne naald) aspiratie cytologie (USgFNAC) zijn belangrijke vaak gebruikte beeldvormingen voor het stadiëring van lymfeklier metastasen (N-stadiëring) in

plaveiselcelcarcinoom in het hoofd en halsgebied (HNSCC). De specificiteit van USgFNAC is altijd in de orde van 100%, aangezien vals-positieve cytologie zeldzaam is. Het verschil in sensitiviteit hangt voornamelijk van de selectie van de te aspireren klieren en de aspiratie-techniek af. . PET-CT heeft een goede diagnostische mogelijkheden voor N-statging bij HNSCC, maar het onderscheid tussen kleine PET-positieve maligne enerzijds en kleine PET-positieve reactieve klieren anderzijds is nog steeds een probleem. Daarom is selectie van de aan te prikken klieren nog steeds een probleem . DW-MRI kan bij selectie van aan te prikken klieren helpen. Er is een omgekeerde relatie tussen de apparente diffusie coëfficiënt (ADC) (=kwantitatieve analyses van DWI) en FDG-opname aangetoond. Het doel van deze studie was om te onderzoeken of het bepalen van ADC-waardes kan helpen om PET-positieve maligne van PET-positieve reactieve klieren te onderscheiden en daarmee de selectie van aan-te-prikken klieren voor te verbeteren. We vonden een negatieve correlatie tussen SUVmax en ADC-waarden. ADC was significant hoger in PET-negatieve klieren dan in PET-positieve klieren. Over het algemeen verschilden de ADC-waarden van PET-positieve maligne klieren niet significant van PET-positieve goedaardige (reactieve) klieren, maar in de subgroep van niet-HPV-gerelateerde klieren hadden PET-positieve maligne klieren significant lagere ADC-waarden dan PET-positieve goedaardige klieren. Deze significante bevindingen geven aan dat de meting van ADC nuttig kan zijn om onderscheid te maken tussen kleine kwaadaardige niet-HPV-gerelateerde PET-positieve en kleine reactieve PET-positieve klieren, en dit impliceert dat als bij deze subgroep een klier PET-positief is, DW-MRI de klierselectie voor punctie zal verbeteren.

Hoofdstuk 5: Echogeleide fijne naald aspiratie cytologie (USgFNAC) heeft een hoge specificiteit in de orde van 100% aangezien vals-positieve cytologie zeldzaam is. Het wordt vaak gebruikt voor N-stadiëring in hoofd-hals plaveiselcelcarcinoom (HNSCC). In hoofdstuk 5 onderzochten we verschillende echografisch detectie criteria van klieren, zoals grootte, aanwezige of afwezige hilus, resistieve index (RI) en perifere vascularisatie verkregen door micro-flow imaging (MFI) als een voorspeller van maligniteit in lymfeklieren van HNSCC. MFI is een nieuwe techniek om niet alleen macroflow patronen maar ook microflow patronen te visualiseren. Het doel van het onderzoek was om de selectiecriteria voor de aspiratie van klieren te verbeteren. We toonden aan dat de positieve voorspellende waarde (PPV) voor

maligniteit bij aanwezigheid van perifere vascularisatie 83% is, bij een afwezig hilus-teken 82% is en de combinatie van beide kenmerken 94% is. We concludeerden dat naast de grootte van klieren het afwezige hilus-teken en aanwezige perifere vascularisatie, aanvullende criteria zijn voor selectie van aan-te-prikken hals klieren bij patiënten met een HNSCC.

Hoofdstuk 6: Voor behandel planning in HNSCC is een exacte nodale stadiëring essentieel en vooral in cN0-halzen, zeer uitdagend. De behandeling moet zo effectief mogelijk zijn, maar de schade door de behandeling moet tot een minimum worden beperkt. FNAC wordt over het algemeen voor stadiëring gebruikt maar de selectie of klieren voor punctie is een probleem. In ons onderzoek wilden we onderzoeken of beschikbare nieuwe beeldvormingen als realtime-imagefusie van PET-CT en echografie en nieuwe echografie technieken, zoals MFI kunnen helpen om de selectie criteria voor te puncteren klieren om te puncteren kunnen verbeteren en helpen om de sensitiviteit voor stadiëring te verbeteren.

Met behulp van MFI konden we aantonen dat perifere vascularisatie in combinatie met de afwezige hilus een hoge PPV voor maligniteit in USgFNAC-klieren heeft. In cN0-halzen heeft de aanwezigheid van perifere vascularisatie een opmerkelijk hogere PPV (94%) dan de afwezige vette hilus (82%) en minimale axiale diameters bij een drempel van 5,5 mm en 4 mm (respectievelijk 22% en 19%).

We konden aantonen dat real-time beeldfusie van PET-CT en echografie in HNC haalbaar is en dat real time image fused-geleide FNAC de detecties van kwaadaardige PET-positieve klieren verbetert, wat de sensitiviteit zou moeten verbeteren. Wij konden SUV_{max} afkapwaarden voor het puncteren van klieren definiëren en alle klieren met een SUVmax-waarde lager dan 2,87 waren benigne en alle klieren met en SUVmax warde hoger dan 10,6 waren maligne. Klieren tussen een SUVmax van 2,87 en 10,6 moeten worden gepuncteerd.

We vonden een milde omgekeerde relatie tussen ADC-waarden en SUVmax-waarden en significant lagere ADC-waarden in PET-negatieve dan in PET-positieve klieren, maar in het algemeen waren we niet in staat om tussen maligne en reactieve PET-positieve klieren te onderscheiden. Opmerkelijk is dat we in de subgroep van niet HPV-gerelateerde PET-positieve maligne klieren significant lagere ADC-waarden vonden dan benigne PET-positieve klieren.

We concluderen dat perifere vascularisatie in cN0 een hoge PPV heeft voor maligniteit en een hulp rijke selectie criteria is. Het kan gemakkelijk routinematig worden toegevoegd.

Real-time image fusie in HNC is mogelijk en fused-geleide FNAC kan als een probleemoplossend hulpmiddel om kleine PET-positieve klieren voor punctie te selecteren gebruikt. Het gebruik van SUVmax-cut-off-waarden kan helpen om onnodige klier puncties te beperken. Wij vonden in de groep van niet HPV-gerelateerde klieren significant lagere ADC-waarden van maligne PET-positieve dan in benigne PET-positieve klieren, dit geeft aan dat ADC als selectie criteria voor punctie van PET-positieve klieren kan worden toegevoegd. Aangezien de subgroep of niet HPV gerelateerde klieren klein was, dient onderzoek in een grotere groep te worden uitgevoerd.

Impact paragraph

Research (aim and conclusion)

Squamous cell carcinoma (SCC) of the head and neck (HN) are derived from mucosal epithelium in the oral cavity, pharynx and larynx. Tobacco consumption, alcohol abuse or both will increase the risk for oral cavity and larynx cancer. HNSSC of the pharynx can be associated with human papillomavirus infection (HPV) and HNSCC can be separated into HPV-related and non HPV-related tumors.

Before treatment, the origin of the tumor and histopathology of the tumor as well as tumor size and tumor spreading have to be defined. Tumor stage (TNM) is reported as tumor size(T), nodal metastases (N) and distant metastases (M).

The presence of cervical lymph node metastases next to tumor volume, is one of the most important predictors for survival.

For nodal staging computer tomography (CT), ^{18}Fluordeoxyglucose positron emission tomography (PET), Magnetic resonance imaging (MRI) ultrasound (US) and ultrasound guided fine needle aspiration cytology (FNAC) are commonly used.

PET-CT has a very good performance to detect lymph node metastases but in small nodes it is still difficult to distinguish between reactive (benign) nodes and small metastases, therefore node selection for FNAC is still very challenging and nodes with small metastases can be missed and remain as occult metastases.

Real time image fusion with CT, PET-CT or MRI on one hand and ultrasound on the other hand, is a relatively new imaging technique. Although image fusion to guide biopsies and therapeutic interventional procedures is widely used, real time image fusion of PET-CT and ultrasound in head and neck imaging is rarely used and no literature on this topic has been published before.

With Power Doppler ultrasound vascularization of tissue can be shown. In malignant tissue de vascularization pattern will change. Micro flow imaging with ultrasound is a new method to depict micro flow in small vessels.

In our thesis we wanted to investigate if these new imaging methods will help to improve the detection rate of lymph node metastases and improve sensitivity.

In **chapter 2** we were able to show that real time image fusion of PET-CT with ultrasound is feasible. This implicates that fused-USgFNAC of PET-positive nodes can be performed with more confidence and the detection rate of lymph node metastases will be improved.

In **chapter 3** we defined SUVmax cut-off values for nodes which have to be punctured to minimize unnecessary punctures in PET-positive reactive nodes. We found that all nodes with a SUVmax below 2.87 were benign and all nodes with SUVmax above 10.6 were malignant at USgFNAC. Consequently punctures could be avoided in those nodes but still we have to deal with the group of nodes between 2.87 and 10.6, in this group malignant as well as reactive (benign) nodes were present.

In **chapter 4** we investigated if DW-MRI would help to distinguish between malignant PET-positive lymph nodes and reactive PET-positive lymph nodes. DW is a method to measure the diffusion of water molecules in tissue. Tumor tissue has generally a higher cellularity than normal tissue and diffusion is therefore restricted. The apparent diffusion coefficient (ADC) reflects the quantitatively analyses of this restricted perfusion, and tissue with a higher cellular density has a lower ADC. We found significantly lower ADC values in PET-positive lymph nodes than in PET-negative nodes but only in the subgroup of non HPV-related nodes we were able to distinguish between malignant PET-positive and reactive/benign PET-positive nodes. This might be helpful for node selection of PET-positive nodes to be punctured.

In **chapter 5** we investigated the positive predictive value (PPV) of peripheral vascularization of lymph nodes using MFI and compared it with the PPV of nodal size and the absence of a fatty hilum of a lymph node. We were able to show that peripheral vascularization and hilum sign have a high predictive value to predict metastases and in cN0 PPV of peripheral vascularization is remarkable higher than in other ultrasound features . Because it is not time consuming and can easily be added to routine ultrasound work-up, it can be used routinely.

Relevance

The treatment of HNSSC is complex, it includes tumor surgery and surgery of the neck nodes (neck dissection (ND)), radiotherapy, chemo radiotherapy and immunotherapy.

Treatment planning is a balancing act between sufficiently radical treatment and preservation of functional structures. To preserve quality of life and to reduce treatment morbidity, treatment should be individualized. Next to tumor evaluation exact N-staging is essential to individualize treatment, which is improved with new imaging techniques.

If the probability of occult metastases is low enough, often 20% is mentioned, a watchful-waiting policy instead of elective neck treatment can be considered. With image fusion of PET-CT and ultrasound the detection rate of malignant nodes can be improved. Unnecessary Neck Dissection can be reduced which will lead to a higher life quality.

For sufficient radiotherapy planning and to reduce side effects of RT, nodal involvement per neck level has to be determined. Exact staging will help to limit RT fields to the neck levels of nodal involvement.

A higher detection rate of occult micro-metastases can lead to a lower recurrence of metastases with all the consequences for the patient and the public health costs.

Target population

The results of this thesis are relevant to several groups.

First the radiologist will be able to stage HNSSC tumors more exactly and with more confidence. Second, the treating health care professionals can plan treatment with more confidence. And thirdly the patient will be provided a more personalized treatment with less side effects and a higher quality of life. A higher detection rate of occult metastases will lead to a lower rate of tumor recurrence and will improve survival.

Scientific results are shared with the scientific community and provide new knowledge and inspiration for further investigations. Users of real time image fusion techniques and other new image techniques can share their experience and problems can be solved together with the industry.

Activities

The results of this thesis have been presented on the European congress of radiology (ECR) and published in peer-reviewed international journals. Results of this thesis can be implemented into the clinical practice and follow up projects can be performed in our Institute.

This thesis shows that the investigated new imaging techniques will help to improve nodal staging in HNSSC. But still there are many questions to be answered. Image fusion techniques for HNSSC nodal staging should be used more widely and to improve nodal staging of HNSSC research results should be shared nationally and internationally.

Curriculum Vitae

Petra de Koekkoek-Doll was born on the 28th of December 1960 in Breitenwang, Tirol, Austria. After graduating high school she attended the University of Medizin in Innsbruck. Austria, where she recived her medical degree in in July 1985. From 1984 till April 1986 she was working on a research project at the Hormone and High Blood Pressure Laboratory with Prof. Dr. F. Dep. of Internal Medicine, Univ. Hospital of Innsbruck. Between January 1986 till may 1991 she became mother of 2 children and was working in the general hospital of Reutte and at the University hospital of Innsbuck, where she degrade as a general practitioner in May 1991. In October 1991 she started with scientific work on ultrasound and doppler in prenatal diagnostik at the Department of Gynecology. From October 1992 till august 1993 she worked as a researcher at the Univ. Hospital Dijkzigt Erasmus University of Rotterdam.

From August 1993 till December 1993 she worked as assistant doctor at the Department of Vascular Surgery and there-after as an assistant doctor for Radiology at the Department of Radiology at the Universal Hospital of Innsbruck, were she graduated as Consultant of radiology in December 1998. She continues there her work as a Consultant of Radiology till January 2009 and with a leading position as Breast radiologist from 2005 till 2009. In 2009 she moved to the Netherlands and worked for one year as a general Radiologist in the dept. of Radiology, Westfries Gasthuis, Hoorn. In 2010 and 2011 she did a Fellowship in Head and Neck and Neuroradiology at Erasmus MC Rotterdam, were she graduated as a Neuroradiologist in January 2012. Since September 2011 she works as a breast and neuroradiologist in the Department of Radiology in the Netherlands Cancer Institute/ Antoni van Leeuwenhoek Hospital in Amsterdam. Her currently research interests are in the field of head and neck - and neuroradiology,. She is member of ESR, ESNR, ESHNR and EUSOBI.

List of own Publications

P. K. De Koekkoek-Doll *et al.*, "ADC Values of Cytologically Benign and Cytologically Malignant 18 F-FDG PET-Positive Lymph Nodes of Head and Neck Squamous Cell Carcinoma," *Cancers (Basel).*, vol. 2022, p. 4019, 2022, doi: 10.3390/cancers14164019.

P. K. de Koekkoek-Doll *et al.*, "Value of assessing peripheral vascularization with micro-flow imaging, resistive index and absent hilum sign as predictor for malignancy in lymph nodes in head and neck squamous cell carcinoma," *Cancers*, vol. 13, no. 20. 2021, doi: 10.3390/cancers13205071.

H. A. Geuzinge *et al.*, "Cost-Effectiveness of Magnetic Resonance Imaging Screening for Women With Extremely Dense Breast Tissue," *J. Natl. Cancer Inst.*, vol. 113, no. 11, pp. 1476–1483, Nov. 2021, doi: 10.1093/JNCI/DJAB119.

B. M. den Dekker *et al.*, "Reducing false-positive screening MRI rate in women with extremely dense breasts using prediction models based on data from the DENSE trial," *Radiology*, vol. 301, no. 2, pp. 283–292, Nov. 2021, doi: 10.1148/RADIOL.2021210325.

N. M. Bekedam *et al.*, "Intra-operative resection margin model of tongue carcinoma using 3D reconstructed ultrasound," *Adv. Oral Maxillofac. Surg.*, vol. 4, p. 100154, Oct. 2021, doi: 10.1016/J.ADOMS.2021.100154.

P. K. de Koekkoek-Doll *et al.*, "SUVmax values at FDG PET-CT to predict malignancy in lymph nodes aspirated by real time image fused USgFNAC in head and neck squamous cell carcinoma," *Am. J. Nucl. Med. Mol. Imaging*, vol. 11, no. 3, p. 178, 2021, Accessed: Jul. 13, 2021. [Online]. Available: /pmc/articles/PMC8255217/.

S. G. A. Veenhuizen *et al.*, "Supplemental breast MRI for women with extremely dense breasts: Results of the second screening round of the DENSE trial," *Radiology*, vol. 299, no. 2, pp. 278–286, 2021, doi: 10.1148/RADIOL.2021203633.

P. K. de Koekkoek-Doll *et al.*, "Real-Time Ultrasound Image Fusion with FDG-PET/CT to Perform Fused Image-Guided Fine-Needle Aspiration in Neck Nodes: Feasibility and Diagnostic Value," *Am. J. Neuroradiol.*, Jan. 2021, doi: 10.3174/ajnr.A6938.

D. Hellingman *et al.*, "Feasibility of radioguided occult lesion localization of clip-marked lymph nodes for tailored axillary treatment in breast cancer patients treated with neoadjuvant systemic therapy," *EJNMMI Res.*, vol. 9, no. 1, 2019, doi: 10.1186/S13550-019-0560-3.

S. V. de Lange *et al.*, "Reasons for (non)participation in supplemental population-based MRI breast screening for women with extremely dense breasts," *Clin. Radiol.*, vol. 73, no. 8, pp. 759.e1-759.e9, Aug. 2018, doi: 10.1016/J.CRAD.2018.04.002.

S. Heijmink, P. De Koekkoek-Doll, H. Van der Poel, and R. Beets-Tan, "MRI guided biopsy in patients with previously negative TRUS biopsy or suspicion of non-low grade disease on multiparametric MRI: High yield with predominantly intermediate to high risk prostate cancer found," *Eur. J. Cancer*, vol. 72, p. S195, Feb. 2017, doi: 10.1016/S0959-8049(17)30702-5.

L. S. Rigter *et al.*, "Neoadjuvant chemotherapy adaptation and serial MRI response monitoring in ER-positive HER2-negative breast cancer," *Br. J. Cancer*, vol. 109, no. 12, pp. 2965–2972, Dec. 2013, doi: 10.1038/BJC.2013.661.

R. Van Soest *et al.*, "217 Structured reporting of multiparametric MRI in detecting prostate cancer: Accuracy and inter-observer variability," *Eur. Urol. Suppl.*, vol. 12, no. 1, p. e217, Mar. 2013, doi: 10.1016/S1569-9056(13)60704-6.

R. van Soest *et al.*, "De accuratesse van gestandaardiseerde verslaglegging van multiparametrische MRI voor de detectie en stagering van prostaatcarcinoom door drie radiologen," *Tijdschr. voor Urol.*, vol. 2, no. 3, pp. 56–57, May 2012, doi: 10.1007/S13629-012-0018-0.

W. Buchberger, A. Niehoff, P. Obrist, P. DeKoekkoek-Doll, and M. Dünser, "Clinically and mammographically occult breast lesions: Detection and classification with high-resolution sonography," *Semin. Ultrasound CT MRI*, vol. 21, no. 4, pp. 325–336, 2000, doi: 10.1016/S0887-2171(00)90027-1.

W. Buchberger, P. DeKoekkoek-Doll, P. Springer, P. Obrist, and M. Dünser, "Incidental findings on sonography of the breast: Clinical significance and diagnostic workup," *Am. J. Roentgenol.*, vol. 173, no. 4, pp. 921–927, 1999, doi: 10.2214/AJR.173.4.10511149.

D. Fries *et al.*, “Doppler sonographic examination of the time average motion and the flow volume in the transjugular intrahepatio portosystemic shunt (TIPS),” *Ultraschall der Medizin*, vol. 19, no. 5, 1998.

S. Voelckel, G. Bodner, W. Voelckel, C. Stadlwieser, P. De Koekkoek, and P. Springer, “Doppler sonographic assessment of vascular resistance in arteriovenous shunts of the fingertip,” *Ultraschall der Medizin*, vol. 19, no. 4, pp. 181–186, 1998, doi: 10.1055/S-2007-1000486.

W. Buchberger, P. Dekoekkoek-Doll, O. Pbrist, and M. Dünser, “Der stellenwert der MR-tomographie beim unklaren Mammographiebefund,” *Radiologe*, vol. 37, no. 9, pp. 702–709, Sep. 1997, doi: 10.1007/S001170050271.

P.K. de Koekkoek-Doll, T. Stijnen, and J. W. Wladimiroff, “Behavioural state dependency of renal artery and descending aorta velocimetry and micturition in the normal term fetus,” *BJOG An Int. J. Obstet. Gynaecol.*, vol. 101, no. 11, pp. 975–978, 1994, doi: 10.1111/J.1471-0528.1994.TB13043.X.

P.K. de Koekkoek-Doll, T. Stijnen, and J. W. Wladimiroff, “Hourly fetal urinary production rate and blood velocity waveforms in the fetal renal artery relative to fetal heart rate pattern and fetal eye movements in normal pregnancies at 30-32 weeks of gestation,” *Early Hum. Dev.*, vol. 38, no. 1, pp. 27–34, 1994, doi: 10.1016/0378-3782(94)90047-7.

P. Kotanko, F. Skrabal, G. Gruber, P. Doll, and B. Meister, “Adrenergic receptors and sodium reabsorption in normotensive subjects as related to salt sensitivity,” *Clin. Exp. Hypertens.*, vol. A9, no. S1, pp. 307–318, 1987, doi: 10.3109/10641968709160181.

F. Skrabal, P. Kotanko, B. Meister, P. Doll, and G. Gruber, “Up-regulation of alpha 2 adrenoceptors and down-regulation of beta 2 adrenoceptors by high-salt diet in normotensive men: enhanced up-regulation of operative (alpha 2:beta 2) adrenoceptor ratio predicts salt sensitivity.,” *J. Hypertens. Suppl.*, vol. 4, no. 6, Dec. 1986.

F. Skrabal, L. Hamberger, G. Gruber, B. Meister, P. Doll, and E. Cerny, “Hereditäre Salzsensitivität als Ursache der essentiellen Hypertonie: Untersuchungen des Membrantransportes und der intrazellulären Elektrolyte,” *Klin. Wochenschr.*, vol. 63, no. 18, pp. 891–896, Sep. 1985, doi: 10.1007/BF01738142.

Dankwoord

De weg waar je in je leven naar toe zal gaan wordt al vroeg bepaald en je eigen beslissingen leiden van kinds af aan naar de weg die je zult gaan. Op dit pad hebben velen mij begeleid en geholpen waarvoor ik erg dankbaar ben. Het zou dus mede gezien mijn leeftijd niet mogelijk zijn iedereen in dit dankwoord te benoemen en misschien is mij van velen de belangrijke rol in mijn ontwikkeling tot wat ik geworden ben, niet eens bewust.

Toch wil ik proberen mijn diepe dank uit te spreken voor de sterkst betrokkenen.

Dank aan het AVL omdat ik een onderdeel van het team mag uitmaken. Lieve collega's ik dank jullie voor jullie steun en het mij vrij maken voor wetenschap. Ook voor het opvangen van het verdriet als het een keer niet zo lukte zoals ik het wilde. In het bijzonder dank aan alle patiënten voor hun medewerking .

Mijn promotor, Prof. Dr. Beets-Tan, beste Regina. Zonder jou zou ik de wetenschap niet opnieuw opgepakt hebben. Met jouw komst naar het AVL heb je wetenschap onderzoek op onze afdeling nieuw leven ingeblazen. Met jouw visie raakte je me bij mij de juiste snaar. Vanaf wilde ik toch nog voor de PhD gaan. Ik dank je van harte dat je mij hiervoor de mogelijkheid bood en voor al je steun hierin.

Mijn Promotor, Prof. Dr. W. Michiel van den Brekel, beste Michiel. Toen ik je vroeg of je er zin in had om mij te begeleiden bij een project aangaande real-time-image-fusie van hals klieren , had ik nog geen idee hoeveel je voor mij in dit proces zou betekenen. Je heb mij altijd met de noodzakelijke blik op de kliniek door dit project geleid en op te vingers getikt als ik te overmoedig was geworden. Ik dank je bijzonder voor de enorme steun; zonder jou zou het niet gelukt zijn.

Mijn Promotor Prof. Dr. Jonas Castelijns, beste Jonas Jij kwam er later bij, het liep nogal stroef, maar jij geloofde meteen in mijn ideeën; dank zij jou ging het dan ook snel vooruit. Je was op elk moment bereid naar mij te luisteren en te helpen. Wat mij dan ook enorm geholpen had was je positieve motivatie; je geloofde in mij. Ook al verschillen wij niet veel in leeftijd, toch ben je een soort wetenschappelijke vader voor mij geworden. Enorme dank voor je steun en je zo vriendelijke manier van hulp en begeleiding om deze promotie waar te maken.

Mijn coauteurs, Monique Maas, Sander Roberti, Laura Smit, Wouter Vogel en Ioannis Zavrakidis. Veel dank jullie voor al jullie tijd, met name Monique en Wouter. Jullie hebben mij enorm begonnen mijn schrijven weer op te starten en dat was nog veel werk voor jullie, erg bedankt. Laura en Ioannis, dank voor jullie kennis en input. Beste Sander je bent er later bij gekomen, de man van de statistiek, dank voor al ons gesprekken en het prachtige verwerken van de data en je fantastisch bijdrage als coauteur, ik bewonder je accuratesse.

Dr. Pedro Sanches en Franz Gleuwink, beste Pedro en Franz. Samen hebben wij de real-time-fusie van PET-positieve hals klieren met echografie werkbaar gemaakt. Ik dank jullie voor jullie kennis en alle geïnvesteerde tijd, het was erg leerzaam en enorm plezierig met jullie.

Prof. Dr. P. Gabriel Krestin, onwijs dank dat u mij de mogelijkheid voor een fellowship Neuro- en Hoofd Hals-radiologie aan het Erasmus MC bood. Prof. Dr. Aad van de Lugt en Dr. Herve Tanghe, Best Aad en Herve jullie waren mijn leermeesters. Aad, je was mijn groot voorbeeld voor de hoofdhals radiologie en i.h.b. hals klieren, Dat was erg belangrijk voor je. Bedankt, je was echt een mentor. Prof. Dr. Marion Smits en Prof. Dr. Meike Vernooij Beste Marion en Meike, het was enorm plezierig met jullie te werken, dank voor deze jaren.

Prof. Dr. Werner Jaschke, beste Werner, jij was het nieuwe hoofd van de radiologie aan de Universiteit Innsbruck. Jij vond meteen dat ik radioloog mocht worden. Dat was doen nog bijzonder, want als vrouw met twee kinderen kwam ik moeilijk aan de slag. Bedankt voor de prachtige opleiding en bedankt voor alle jaren die ik met jouw als baas mocht werken en bedankt dat wij nog steeds af en toe gezellige avonden hebben met lekker eten en gesprekken over verleden en heden in de radiologie.

Dank aan al mijn collega's in Innsbruck en wat fijn dat wij nog steeds met veel plezier op congressen ontmoeten.

Emiel de Koekkoek, vader van mijn kinderen, je stond enorm veel jaren aan mijn zijde en heb mij gesteund met werk en kinderen, nog eens hartelijke dank hiervoor en je liefde. Wij wandelen nu verschillende paden maar je zal mij altijd blijf je dierbaar blijven.

Mijn lieve dochter Lara, mijn geweten van kleins af aan; wat ben je toch een prachtige meid, met een enorm groot hart, je heb de weg als psycholoog gekozen

en ik heb enorm veel steun aan je slimme opmerkingen. Wat ben ik blij dat jij nu je lieve Jonathan aan je zijde heb, Dank Jonathan, dat je in onze familie bent en bedank voor taal correcties.

Mijn lieve zon Felix, degene die mij lachen maakt, je word radioloog en bent dus in mijn voetstappen getreden, dat is erg leuk. Bijzondere dank je dat je zo vroeg papa bent geworden. Lisa, mijn schoondochter, dank dat je voor mijn zoon gekozen hebt en ik nu van mijn prachtige kleinkinderen, Ben en Emilian, mijn zonnetjes, samen met jullie genieten mag.

Lara en Felix, bijzondere dank dat jullie het nooit erg vonden, dat mama zo veel werkte maar dat jullie er juist trots op waren. Bedankt jullie voor alles; zonder jullie zou ik niet willen zijn.

Mijn geliefde Ouders, Annelies en Anton Doll, jullie zijn er niet meer. Ik weet dat jullie enorm trots zouden zijn. Studeren in mijn tijd was niet zo maar gedaan. Uit een klein dorp, al met 13 jaar ver weg om het waar te kunnen maken. Jullie hebben mij laten vertrekken ook was dat voor jullie erg moeilijk. Jullie gaven mij mentale en enorme financiële steun en dat was voor jullie geen pretje. Ik geef jullie blijk , waar jullie ook mogen zijn, van mijn diepste dank toe en stuur jullie mijn liefde; zonder jullie zou ik nergens zijn.

Lieve Jacques, mijn trouwe lieve partner, dank je voor al je geduld met mij en dit proefschrift. Dank voor al die weekenden achter de PC waar je mijn hulp bood om mijn chaotisch lay-out in goede banen te leiden. Dank voor al je steun in al die jaren, voor het luisteren over mijn zorgen en de lach die je altijd weer op mijn lippen tovert. Diepe dank dat je er voor mijn kinderen bent en een oh zo lieve opa voor mijn kleinkinderen. Ik hoop ten diepste dat we oud met elkaar mogen worden